Behavior of High Strength Fiber Reinforced Concrete Beams in Shear

by

Dawood Abdulhai Pandor

B.Eng., Imperial College, University of London

Submitted to the Department of Civil and Environmental Engineering
in partial fulfillment of the requirements for the degree of

Master of Science in Civil and Environmental Engineering

at the

MASSACHUSETTS INSTITUTE OF TECHNOLOGY

February 1994

Author .....
Department of Civil and Environmental Engineering
January, 1994

Certified by .....
Oral Buyukozturk
Professor
Thesis Supervisor

Accepted by .....
Joseph Sussman
Chairman, Departmental Committee on Graduate Students

Behavior of High Strength Fiber Reinforced Concrete Beams in Shear

by

Dawood Abdulhai Pandor

Submitted to the Department of Civil and Environmental Engineering
on January, 1994, in partial fulfillment of the
requirements for the degree of
Master of Science in Civil and Environmental Engineering

Abstract

The objective of this thesis is to investigate experimentally the behavior of high strength fiber reinforced deep concrete beams in shear, in order to arrive at a working model and equation for predicting the shear strengths of these structural members .

In the experimental program, the volume fraction and aspect ratio of fibers, the shear span to depth ratio of the specimens, and the maximum aggregate size were varied in order to determine the effect of these variables on the specimen strength, on application of four point loading .

In general, it was observed that the addition of fibers led to a significant improvement in the shear strengths of the specimens .

Modification of an existing formula, proposed for the prediction of beam shear strengths, and the incorporation of a term to account for the contribution from the fibers to the specimen strength, yielded results which correspond very closely to those obtained experimentally and in other research programs .

A model for high strength fiber reinforced concrete, based on an existing shear truss model, was also developed to enable the peak deflections and strengths of these specimens to be predicted, and this model also yielded very good agreement with the observed data .

Use of this model therefore represents a useful method for investigating the behavior of high strength fiber reinforced deep concrete beams, and the proposed equation, after the inclusion of a satisfactory factor of safety, is an especially useful tool for utilisation in design practise .

Thesis Supervisor: Oral Buyukozturk
Title: Professor

Acknowledgements

I would like to thank the following :

Professor Buyukozturk, for providing the necesssary guidance to enable me to successfully complete this thesis .

Professor Leung, Thanakorn Pheeraphan, Yiping Geng and Amjad Shahbazker for providing valuable advice and assistance .

W.R. Grace and Co., for providing the materials used in the experimental program .

The American Concrete Institute, for providing partial funding for this research .

My family, for the support and guidance which they have always provided for me .

Contents

List of Figures

List of Tables

Chapter 1

Introduction

Concrete with a 28 day compressive strength of over 7 000 psi (High Strength Concrete) has, only over the last 20 years, received serious attention from Structural Engineers and, indeed, been utilised in engineering applications [1] . Therefore, compared with the research on Normal Strength Concrete(NC) which has occurred over the last century, as much is not understood about the behavior of High Strength Concrete(HSC).

One of the first misconceptions to clarify with respect to HSC, is that it is not an entirely new material [2] . Indeed, HSC can be made by simply reducing the water/cement ratio of concrete to a suitable level. This may then merit the addition of superplasticisers in order to improve the workability of the resulting mix.

In order to obtain further increases in strength (over approximately 11 000 psi), it will then be necessary to add other components, such as silica fume. Further measures, such as high temperature or pressure curing, and polymer impregnation [3], and modification of aggregate properties, can be taken to bring about an improvement in the performance of the material. The basic point, however, is that the essential components of a concrete mix need not be dramatically altered in order to create a concrete of higher strength.

A basic understanding for the differences between HSC and NC having been provided, it is now necessary to examine the advantages and disadvantages to using HSC in practise.

HSC generally has the advantages, over normal strength concrete, of providing :

1. increased stiffness,
2. reduced axial shortening of members and therefore reduced problems concerning the maintenance of horizontally supported surfaces,
3. construction time saving, as strength development occurs at an early age,
4. possibility of creating new types of structural supporting systems-an area which requires further research,
5. economic advantages - the ability to remove formwork rapidly, the increased availibility of floor area as member sizes can be reduced, and decreased foundation costs as the overall weight of the structure can be reduced.

Other advantages, such as reduced prestressing losses (due to a reduced coefficient of creep) and a reduction in the quantity of reinforcement required, can also be incurred. It should be noted that the properties of core samples, removed from structural members after seven years of service, have indicated that the properties of HSC remain excellent over time [3].

HSC, however, does have certain drawbacks to its application.

In attempting to reduce element sizes due to the increased strength, attention must be paid to ensure that the overall member stiffness (as distinct from the material stiffness) is not reduced.

Also, the tensile strength of HSC, while greater than that of NC, does not increase in proportion to the compressive strength increase. For NC the tensile strength is usually approximately 10% of the compressive strength, but for HSC, the value may be as low as 5% [4] .

The most significant drawback with HSC is its ductility, or rather, the lack of ductility.

HSC demonstrates a very brittle behavior upon reaching the ultimate load, with very limited post-peak ductility - failure of HSC specimens is usually very dramatic with little or no warning.

In structural practise it is essential that the ultimate limit state behavior be such that sufficient warning of impending failure is provided to the occupants of the structure.

It is also very important for structures to have sufficient ductility to be able to absorb impact energy, and also to prevent dramatic failure in seismically active areas, where structures are subjected not only to rapidly varying displacements, but also to large shear forces. Many of the important metropolitan areas of the world are indeed located in seismic regions and therefore this consideration must be adressed for HSC.

The use of steel tubes to provide a confining force for concrete has been applied successfully in practise, most notably in Seattle [1], to improve the ductility of HSC columns.

However, a more general method of attaining this beneficial improvement is needed; a method more easy to implement in practise, and to a wider range of element types.

One possibility is through the use of fiber reinforced HSC, the subject of this thesis.

1.1 Objectives and scope of the research program

1.1.1 Objectives

The main objectives of this research program are to try to gain a better understanding for the shear behavior of high strength fiber reinforced concrete beams subjected to shear loading, and to try to obtain a means of predicting the behavior of such members.

1.1.2 Scope

In order to satisfy these objectives, it is necessary to divide the research into an experimental and a theoretical program.

The aims of the experimental program are to investigate the influence on the shear behavior of HSC beams when the following properties are varied :

1. the volume fraction of fibers (V_f)

2. the shear span to depth ratio (a/d)

3. the aggregate size (d_a)

4. the aspect ratio (l/d) of the fibers.

The experimental program allows for an effective investigation of some of the factors influencing the shear strength of these specimens.

In the theoretical program, the results of these experiments, as well as the results from previous research studies, will be applied to try to obtain a predictive equation and model which will enable the shear strength of steel fiber reinforced HSC beams to be quantified successfully.

1.1.3 Organisation of thesis

This thesis is divided into six main sections :

Chapter 2 provides a brief review and discussion of the literature associated with this field of study,

Chapter 3 explains the model used in this thesis,

Chapter 4 outlines the experimental program,

Chapter 5 provides the observations and results from this program,

Chapter 6 contains a discussion of the results,

Chapter 7 summarises the overall conclusions from this study.

Chapter 2

Review of the shear behavior of concrete beams

2.1 Shear behavior of plain concrete

Research over the last forty years has contributed significantly to attainment of a more complete understanding of the behavior of concrete specimens.

Essentially, failure in concrete beams develops as a result of the interaction between the applied flexural and shear stresses, cracking occurring when this biaxial state of stress exceeds the capacity of the concrete.

There are generally two mechanisms for the transfer of shear forces within beams :

a) Beam action (Figure 2-1), and

b) Arch action (Figure 2-2),

the dominance of any one particular type of mechanism being determined by the a/d ratio of the specimen [5, 6] .

Beam action, dominant at large a/d values when the load cannot be transferred to the supports by the arch supporting mechanism, is generally considered to result from the resistance offerred by the uncracked concrete, the longitudinal reinforcement (dowel action) and the aggregate interlock mechanism.

Arch action, dominant at low a/d, generally results in the direct transfer of shear load from the point of application, to the supports. As the support is approached

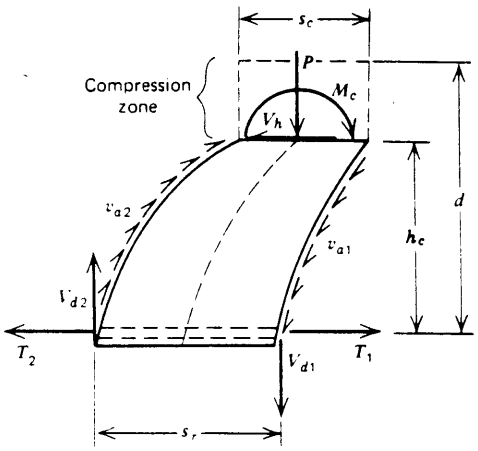

Figure 2-1: Beam action[5]

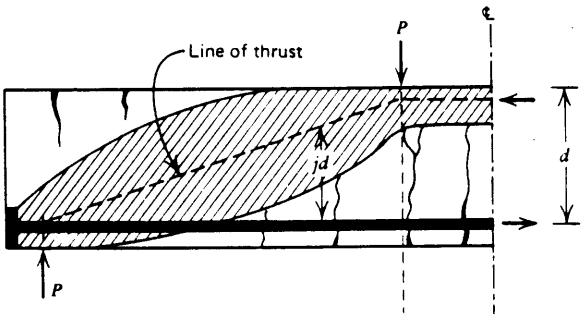

Figure 2-2: Arch action[5]

by the load, the depth of the compression zone increases, and thus the mechanism is facilitated, the horizontal resistance to the opening of the arch being provided by the longitudinal reinforcement.

2.2 Shear behavior of normal strength fiber reinforced concrete beams

In this section, the basic trends which occur when NC beams, reinforced with fibers, are subjected to shear, are presented.

The application of short, randomly distributed fibers to improve the properties of building materials is not a new concept, and indeed, its application is recorded in the scriptures [7] .

The major effect of fibers occurs in the post-cracking state, when the fibers bridge across the cracks that have propogated in the matrix, thereby influencing the ultimate strength and deformation behavior of the SFRC composite, and its mode of failure.

Fibers generally result in a more uniform redistribution of stresses in the matrix, and so when these types of specimens are tested, it is generally observed that not only are the cracks smaller, more numerous, and at a closer spacing, but also spalling of the concrete is eliminated due to the ability of the fibers to hold parts of the concrete together in the post-cracking stages [8, 9] .

Fiber addition also results in an increase in the post-cracking stiffness of the concrete, when the stress-strain behavior begins to deviate from the pseudo-linear response [10] .

In terms of the effect of fiber addition on the ultimate load capacity of fiber reinforced specimens, some researchers have noted an increase by as much as 30% [9] , but the majority of reports have shown that fibers have no significant effect on the shear strength of NC specimens [8, 12, 9] , although the first cracking strength does improve slightly, indicating an improvement in the tensile strength.

The post-peak ductility is also observed to notably increase on addition of fibers [8, 9, 12, 11, 13, 14] . This results from the ability of the strain energy to be absorbed

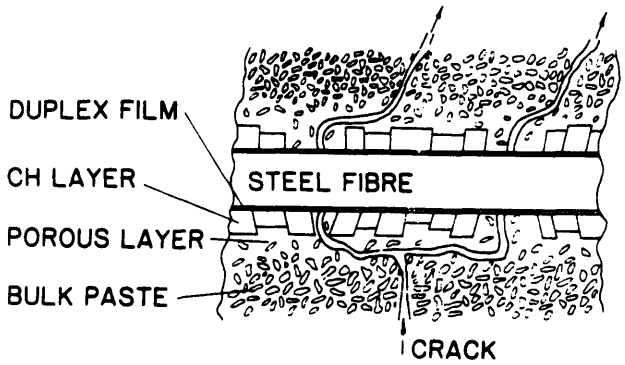

Figure 2-3: Transition layer, containing calcium-hydroxide, around a fiber[7]

during the pullout of the steel fibers from the matrix, resulting from the presence of a weak interface between fiber and matrix in normal concrete specimens, due to the accumulation of a weak calcium-hydroxide layer(see Figure 2-3) at the interface [7] .

It has also been observed that fibers also help to improve the contribution from dowel action to shear resistance, making failures more ductile [11, 15] . This occurs due to the ability of the fibers to maintain the integrity of the concrete to which the dowel forces are transferred, thereby preventing the degradation of this shear resisting mechanism.

As previously mentioned, there are primarily two transfer mechanisms responsible for shear transfer in beam specimens : beam action and arch action. However, as fibers do not significantly improve the compressive strength of NC specimens [16, 17] , the contribution of fibers to arch action is not as significant [12], and the main effectiveness of fibers is in the beam mechanism (for larger shear spans) when the fibers help bridge across the cracks which propagate in the matrix, and maintain the effectiveness of the dowel contribution.

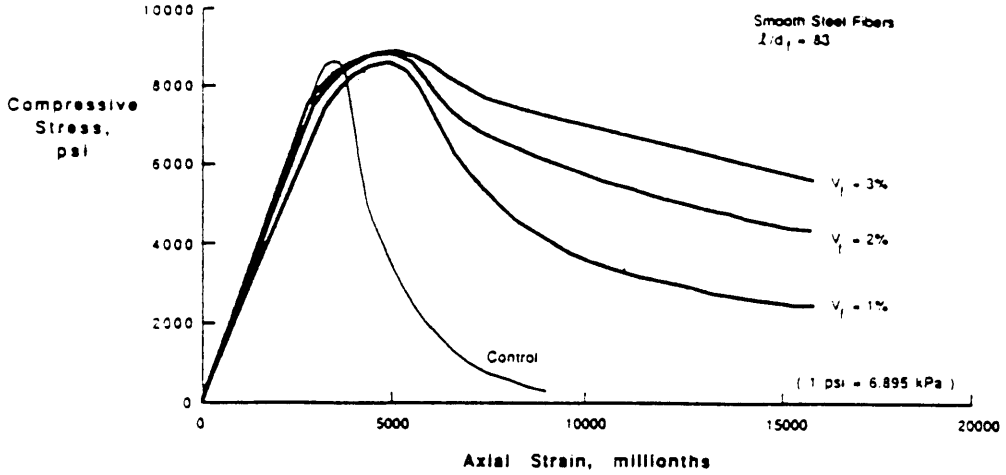

Figure 2-4: Improved post-peak ductility due to fiber addition[17]

2.3 Shear behavior of high strength fiber reinforced concrete beams

One of the directions in which the ACI suggested research into HSC be guided, was towards the incorporation of fibers in the material [18] .

Very limited research efforts have, however, been concentrated on this area of research, a brief summary of these findings being presented below.

2.3.1 General properties of high strength fiber reinforced concrete (HSFRC)

The results of tests carried out on the behavior of HSFRC specimens show that the use of fibers enables the post-peak behavior to be better investigated [16, 8], as opposed to plain HSC, where the cracks grow rapidly and unstably(Figure 2-4) .

The inclusion of silica fume in a concrete matrix, to obtain higher strengths, in-

creases the strain corresponding to the peak stress, and the inclusion of steel fibers provides further increase of this strain. While HSRFC reaches its peak stress at a compressive strain slightly higher than for lower strength concrete, the ultimate strain is lower for HSC. A value for ultimate strain of 0.003, specified by ACI committee 318, could be less conservative for HSC. The presence of steel fibers would, however, increase this ultimate strain, thereby allowing HSFRC to withstand larger deformations before failure.

It was also found that if smooth fibers were used and the V_f increased, there was not a noticeable increase in f_c', but that if deformed or hooked end fibers were used, there was a noticeable increase, thus indicating that bond improvement helps bring about this change [19] .

Change in V_f was also found to be more significant for HSC than for NC, in terms of increased strength, as fibers tend to yield in HSC as opposed to simple pullout, due to the improved matrix-fiber interface properties resulting from the addition of silica fume and the reduction in water content (silica reacts with the weak calcium-hydroxide to form a cementitious compound, and as calcium-hydroxide precipitation is initiated in areas of high water content, the reduced water content causes reduced precipitation).

It was observed (for $V_f = 1.25\%$) that an increase in f_c' of approximately 5 % was obtained [20], and that the modulus of rupture was increased by 67-82 %, compared with an increase for NC of 50-70 %.

The splitting tensile strengths were also higher than for NC with fibers, and 60 % higher than for plain HSC.

2.3.2 Behavior of plain high strength concrete beams in shear

Results from investigations on the behavior of HSC beams in shear have shown that the failure mode is indeed very brittle [21] .

Generally, for $a/d <= 2.5$, failure occurs by crushing of the arch ribs, while for

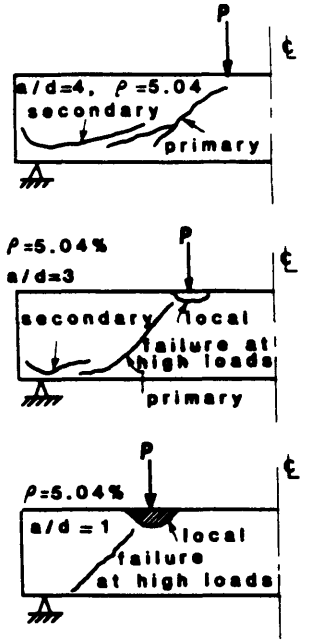

Figure 2-5: Dependancy of failure mode on shear span ratio[21]

$a/d > 2.5$, failure was by diagonal tension(Figure 2-5) .

Nilson [22] stated that for high strength beams, aggregate interlock is the first mechanism to break down, dowel action and shear in the compresion zone providing the residual shear resisting mechanisms.

If the state of stress meets the failure criterion for the concrete in the compression zone, an abrupt and sometimes explosive failure occurs. If dowel resistance is the controlling mechanism, vertical tension in the concrete around the bars causes splitting cracks along the reinforcement.

Paulay [5] also provides information for NC which is relevant to HSC.

He postulates that at advanced stages of cracking, inclined cracks propagate towards the compression zone and debilitate the cantilever action considerably, resulting in large rotations at the free end, which may result in exhaustion of the dowel capacity. When dowel cracks form, a large proportion of the load, for NC, is taken by aggregate interlock. A reduction in aggregate interlock forces due to some reason, such as widening of cracks on one side of the cantilever mechanism, causes inbalance

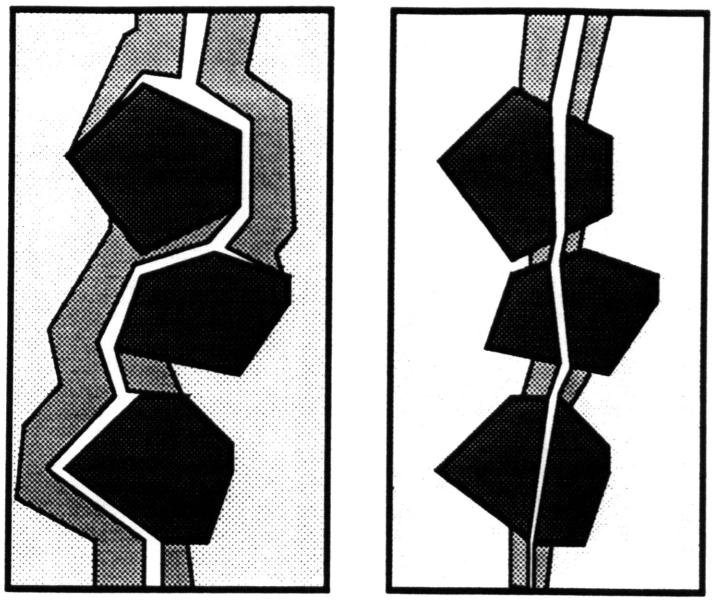

Figure 2-6: a)Crack propagation in NC b)Crack propagation in HSC

and further crack propagation, leading to diagonal tension failure, which is sudden.

Hence, as for HSC the crack surface is smooth due to crack propagation through the aggregates(Figure 2-6), aggregate interlock forces are minimised and so failure may follow the aforementioned stages, ignoring the aggregate interlock stage.

It was also observed in previous studies that the reinforcement ratio (ρ) played a significant role in controlling the type of shear failure.

This is because, not only of the contribution from dowel action to the shear resisting mechanism, but also because an important factor that affects the rate at which a flexural crack develops into an inclined one is the magnitude of stresses near the crack tip. The intensity of principle stresses above the flexural crack depends on the depth of penetration of the crack, and the greater the value of ρ, the less the penetration of the flexural crack - The less the penetration of the flexural crack, the less the principle stress for a given load, and consequently, the greater must be the shear force to cause the principle stresses that will result in diagonal tension cracking (This idea could also be extended to an increase in the a/d ratio, which results in an

increased moment at a section, and hence the increased possibility of flexural cracks with increased crack lengths. Hence, the possibility that these cracks would develop into diagonal cracks would increase, and consequently, it would be expected that for increased a/d, the specimen shear capacity would decrease) .

2.3.3 Behavior of high strength fiber reinforced concrete beams in shear

Review of Ashour

The results of this research indicated the same general relationships between the a/d ratio and the mode of failure previously discussed [21] .

The tests indicated a marked improvement in the post-peak behavior of the specimens, with a significant increase in the ductility. The effect of the fibers on beam ductility became more pronounced as the a/d ratio increased, and this supports the idea [12] that the fibers are more effective in contributing to the beam transfer mechanism, than to the arch mechanism.

Most significantly, the results confirmed those noted by Valle [8] , in that it was observed that the addition of fibers to the specimens caused a noticeable increase in the shear strength(Figure 2-7).

Two formulae (in MPa) were also proposed for the prediction of the shear capacity of HSFRC beams :

$$v_u = (0.7\sqrt{f'_c} + 7F)\frac{d}{a} + 17.2\rho\frac{d}{a}\ (I)$$

and,

$$v_u = (2.11\sqrt[3]{f'_c} + 7F)(\rho\frac{d}{a})^{0.333}\ (II)$$

($F = (l/d)V_f d_f$ and d_f is the fiber effectiveness)

When compared with the results obtained by Shahbazker [24] (see Table 2.1 (units in psi)), it was, however, observed that these give extremely conservative predictions, for deep beams, and therefore are not satisfactory for practical applications.

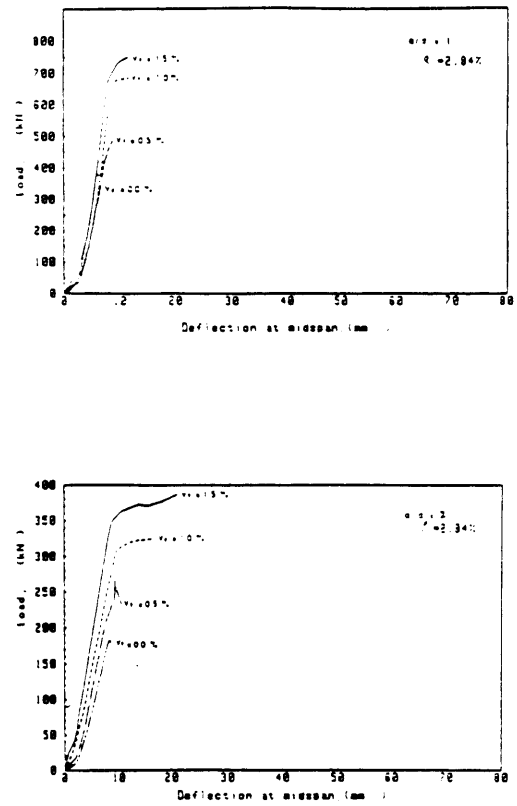

Figure 2-7: Effect of V_f on shear capacity[23]

V_f	v_c(Shabaz.)	Eqtn. I	Eqtn. II
0	1271.1	721.6	758.0
0.4	1502.2	789.4	835.0
0.8	1608.9	895.6	942.2

Table 2.1: Application of eqtns. I and II to the specimens tested by Shahbazker

Examination of the results of this research, and the methods of analysis adopted by the authors, indicate that there are two main reasons for the conservative predictions of these proposed equations :

a) In considering the contribution from the fibers, fiber pull-out was considered as the dominant mechanism, though verification of this was not provided,

b) Even though flexural failure occurred in many of the specimens, the peak loads for these specimens was taken as the shear capacity of the specimens, and these results included in the linear regression analysis used to obtain the final design equations. Thus, as the results used for the situations where flexural failure occurred are conservative estimates of the shear capacity of the specimens, it would be expected that the equations derived would likewise be conservative.

Review of Shahbazker

The results of this research confirm many of the observations made by Ashour [23] and Valle [8, 40] .

. Experiments were also performed in this program incorporating stirrups, and this was found to result in much greater improvements in ductility, as expected.

The results also seem to indicate that the contribution from fibers and stirrups to the peak shear stress is not additive, possibly due to a lack of correspondence of peak strains, the overestimate being of the order of 15 % if the contributions are added directly.

It should, however, be noted that tests were only performed for a single specimen in each case (as indeed were the tests performed by Ashour) and therefore this suggests that it would be useful to repeat several of these tests to confirm the actual quantitative results obtained.

Also, in using Bazant's equation (in psi) [25] :

$$v_u = \frac{10\sqrt[3]{\rho}}{\sqrt{1 + d/25d_a}}[\sqrt{f'_c} + 3000\sqrt{\rho/(a/d)^5}\,]$$

to predict the shear strength of plain HSC, not only is the contribution from dowel ac-

a/d	V_f	ρ	v_c(exper.)	eqtn. I	v_c(Baz.'84)	v_c(s'baz.)
1	0.5	2.84	1318.1	1394.9	1399.0	1882.0
2	0.5	2.84	698.9	548.1	468.1	951.1
1	1.0	2.84	1847.3	1703.8	1394.0	2100.1
2	1.0	2.84	878.7	662.7	462.9	1169.1
2	1.0	4.58	975.9	765.6	604.8	1432.9

Table 2.2: Application of Shahbazker's eqtn. to the results obtained by Ashour[23]

tion perhaps underestimated, but also the equation has been assumed to not account for dowel action, which it does.

Examining Table 2.2, when the equation proposed by Shahbazker,

$$v_u = \frac{10\sqrt[3]{\rho}}{\sqrt{1+d/25d_a}}[\sqrt{f'_c} + 3000\sqrt{\rho/(a/d)^5} + 70F\ ]$$

where $F = (l/d)V_f^{0.548}d_f$ is applied to the results of Ashour [23] (using only those results in which shear failure was known to have occurred), it can be seen that the shear capacities of the sections are dramatically overestimated, suggesting the need for further modifications to the proposed equation. Modifications to this equation are discussed in this thesis .

Chapter 3

Load-deformation predictions for high-strength fiber reinforced deep beams

In attempting to model the behavior of the beams in this program of study, it is essential to account for their deep nature, as this significantly effects the mode of shear transfer .

The model adopted in this study is based on the deep beam shear transfer model proposed by Hsu and Mau [27], as a review of the existing literature confirms the effectiveness of this model in accurately predicting the shear transfer response of specimens [8, 28, 29, 30] .

The aim in utilising this model was to enable :

- the peak load capacity for HSFRC beams to be predicted,
- the central span deflection behavior to be predicted, and
- to validate the application of the softened truss model to HSFRC beams .

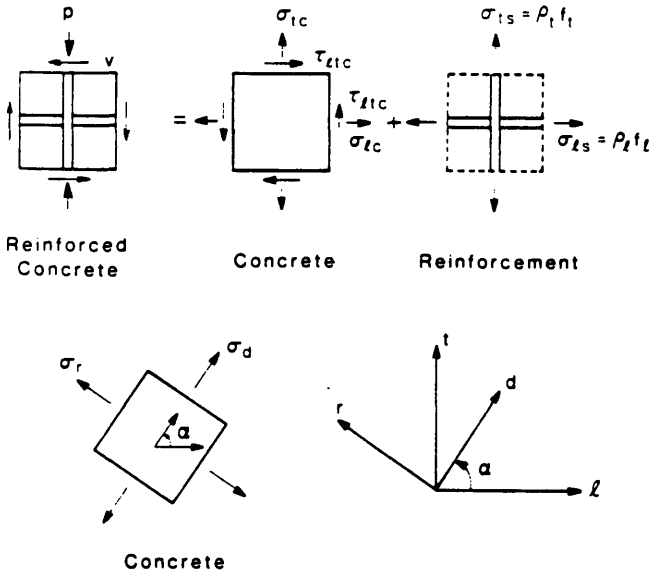

Figure 3-1: Truss model for reinforced concrete element[29]

3.1 Deep beam shear model

The deep beam shear model has developed from the softened truss approach (which relies on the ability to characterise the softening behavior of concrete), and the Modified Compression Field Theory [31, 32] .

The principle attraction of this model is that, in addition to not relying on the assumption of a pre-existing failure plane, it also introduces an effective transverse compression in the beam web, thus accounting for the arch transfer mechanism .

It is assumed that when the concrete cracks on application of load, the concrete struts so formed act in conjunction with the longitudinal and transverse reinforcement to form a truss-like mechanism (Figure 3-1) which resists the shear loading (It should therefore be noted that for small loadings, when the concrete is uncracked, the predictions of this model will be inappropriate) .

A key to the variables is provided below :

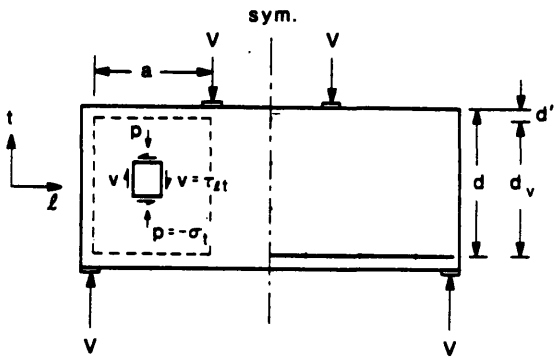

Figure 3-2: Deep beam stress condition[27]

σ = normal stress

τ = shear stress

f = stress in steel

ρ = reinforcement ratio

α = the angle of inclination of the d axis with respect to the x axis (positive counterclockwise

The subscripts x, y, d, and r correspond to the chosen axis .

Though no transverse reinforcement (stirrups) have been provided in this research program, the truss mechanism is still valid as it is expected that the fibers will be effective in performing the role of stirrups .

It is assumed that the moment in the concrete section is taken by the couple formed by the steel reinforcement and an equivalent depth of concrete d' (where d' = half the depth needed to provide a compressive force in concrete to balance the tension in the bottom steel at yield (see Figure 3-2)) .

The shear load is then resisted by the concrete depth d_v, where :

$$d_v = d - d'$$

Essentially the truss mechanism formed must satisfy the laws of compatibility and equilibrium, and the material laws .

3.1.1 Equilibrium equations

After cracking, the principle stress directions are denoted by d and r (compressive and tensile respectively - see Figure 3-1) and the angle of inclination of the principle axis, α .

Hence, using the Mohr's circle stress transformations, and assuming that the steel reinforcement can take only longitudinal stresses, the following equilibrium equations are obtained :

$$\sigma_x = \sigma_d \cos^2 \alpha + \sigma_r \sin^2 \alpha + \rho_x f_x \tag{3.1}$$

$$\sigma_y = \sigma_d \sin^2 \alpha + \sigma_r \cos^2 \alpha + \rho_y f_y \tag{3.2}$$

$$\tau_{xy} = (\sigma_d - \sigma_r) \sin \alpha \cos \alpha \tag{3.3}$$

(ρ_y is the equivalent area of fiber steel across the shear plane and it should be noted that the fibers are considered to be only effective in the y-axis direction as the contribution to the x-axis direction is negligible compared to the area of longitudinal steel)

3.1.2 Compatibility equations

Again using the Mohr's circle stress transformations, and utilising the result from the Modified Compression Field Theory that the principle stress and strain inclinations correspond to the inclination of the concrete struts formed, the following equilibrium results are obtained :

$$\epsilon_x = \epsilon_d \cos^2 \alpha + \epsilon_r \sin^2 \alpha \tag{3.4}$$

$$\epsilon_y = \epsilon_d \sin^2 \alpha + \epsilon_r \cos^2 \alpha \tag{3.5}$$

$$\gamma_{xy} = 2(\epsilon_d - \epsilon_r) \sin \alpha \ \cos \alpha \tag{3.6}$$

where :

ϵ_x, ϵ_y = average normal strains in the x and y directions (tension positive), respectively,

γ_{xy} = average shear strain,

ϵ_d, ϵ_r = average principle compressive and tensile strains respectively

3.1.3 Material laws

Steel reinforcement

The longitudinal bars, and the steel fibers, are assumed to demonstrate elastic-perfectly plastic stress-strain characteristics, as shown in Figure 3-3 (the high bond strength for steel fibers in HSC allows this assumption to be made for the fibers, even though in reality some fiber debonding will occur before the yield strength is reached) .

$$f_s = E_s \epsilon_s \ \leq \ f_y \tag{3.7}$$

where E_s and f_y are the Young's Modulus and the yield stress of the steel reinforcement respectively .

Concrete

The principle compressive stress-strain curve for HSFRC, which incorporates the softening effect due to the biaxial state of stress, is shown in Figure 3-4 :

The ascending portion is represented by :

$$\sigma_d = f_c'[\ 2(\frac{\epsilon_d}{\epsilon_0}) - \lambda(\frac{\epsilon_d}{\epsilon_0})^2\ ] \tag{3.8}$$

for $\epsilon_d \leq \epsilon_p$,

and is the same as for NC, as there is essentially no sigificant change when fibers are added .

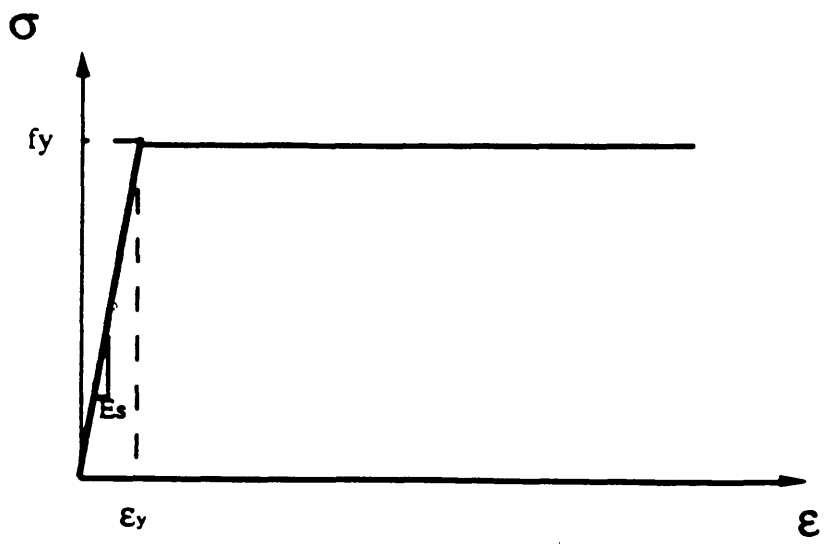

Figure 3-3: Stress-strain relationship for steel

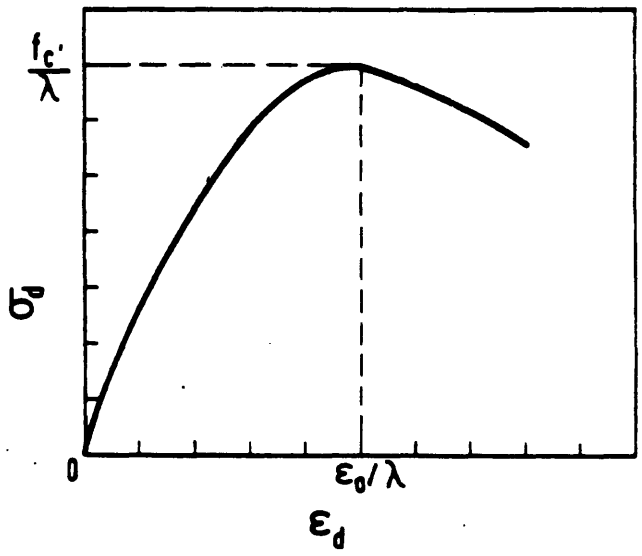

Figure 3-4: Compressive stress-strain relationship for concrete

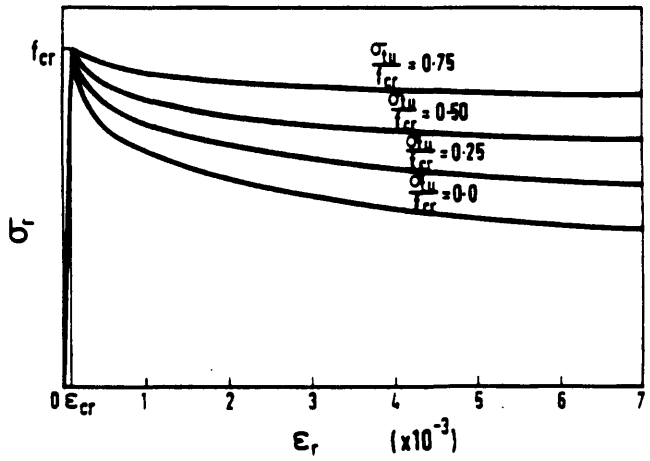

Figure 3-5: Tensile stress-strain relationship for concrete

For the descending portion :

$$\sigma_d = \frac{f_c'}{\lambda}[\,1 - (\frac{\frac{\epsilon_d}{\epsilon_0} - \frac{1}{\lambda}}{2 - \lambda})^2\,] \tag{3.9}$$

for $\epsilon_d \geq \epsilon_p$

where $\epsilon_p = \epsilon_0/\lambda$, and lambda is a coefficient to account for the softening phenomenon, where :

$$\lambda = \sqrt{0.7 - \frac{\epsilon_r}{\epsilon_d}} \tag{3.10}$$

This is again the same relation as used for NC because, due to the addition of fibers, it is expected that the post-peak behavior for HSC would be improved only to the extent that the ductility would be comparable to that for NC .

The assumed principle tensile stress-strain relation was also taken to consist of two portions : a pre- and a post-cracking behavior (Figure 3-5) :

Before cracking, the ascending portion is given by :

$$\sigma_r = \epsilon_r E_c \tag{3.11}$$

for $\epsilon_r \leq \epsilon_{cr}$

where E_c is the Young's Modulus of concrete and ϵ_{cr} is the cracking strain of fiber concrete,

$$f_{cr} = 7.5\sqrt{f_c'}$$

$$E_c = 40000\sqrt{f_c'} + 1.0 \times 10^6$$

ACI 363[35] notes that for, curing conditions followed by air drying, the use of $7.5\sqrt{f_c'}$ is probably fairly close to the full strength range for high strength concrete .

The post-cracking behavior is given by :

$$\sigma_r = \frac{f_{cr} + (\beta \sigma_{tu})}{1 + \beta} \tag{3.12}$$

$$\beta = \sqrt{\frac{\epsilon_r - \epsilon_{cr}}{0.005}} \tag{3.13}$$

for $\epsilon_r > \epsilon_{cr}$

This post-cracking behavior occurs because, after cracking, the stress across the cracks is still quite significant due to the presence of fibers . This stress across the cracks is denoted by σ_{tu}, where,

$$\sigma_{tu} = \frac{\eta_l \, \eta_0^{'} \, V_f \, l_f \, \tau_u}{2r'}$$

r' is the ratio of the area of cross section to the perimeter of the fiber .

The ultimate bond strength of the fibers, τ_u, has been calculated to be the bond stress at yielding of the fibers, to account for the higher bond properties of HSC .

3.1.4 Simplifying assumptions

At this stage, there exist 14 unknowns but only 11 equations, and therefore it is necessary to make several simplifying assumptions to enable a solution to be obtained .

As the depth d_v is assumed not to carry any flexure, then it can be assumed that :

$$\sigma_y = 0$$

Also, Hsu and Mau [29] have shown that :

$$\sigma_t = K \cdot \tau_{lt}$$

where K is the ratio of maximum transverse stress to maximum shear stress, and is given by :

$$K = \frac{d_v}{h} [\frac{h}{a} (\frac{4}{3} - \frac{2}{3} \frac{a}{h})]$$

for $0.5 < a/h \leq 2$

This value takes into account the variation in the distribution of the stresses within the shear span, when the magnitude of the shear span is varied, as shown in Figure 3-6 .

Hence, making these two assumptions, for a given value of ϵ_d (chosen because it is expected to increase monotonically), the 14 unknowns can be obtained, as outlined in Section 3.1.6 .

3.1.5 Modifications to existing shear model

Dowel contribution

As the proposed model by Hsu [29] does not account for the dowel contribution from the longitudinal steel, and does not account for aggregate interlock, it is necessary to modify the modify the model to attain a higher degree of accuracy .

For HSC, when cracks propagate, they generally pass through the aggregate, as this offers the path of least resistance . Thus the crack surface is generally quite

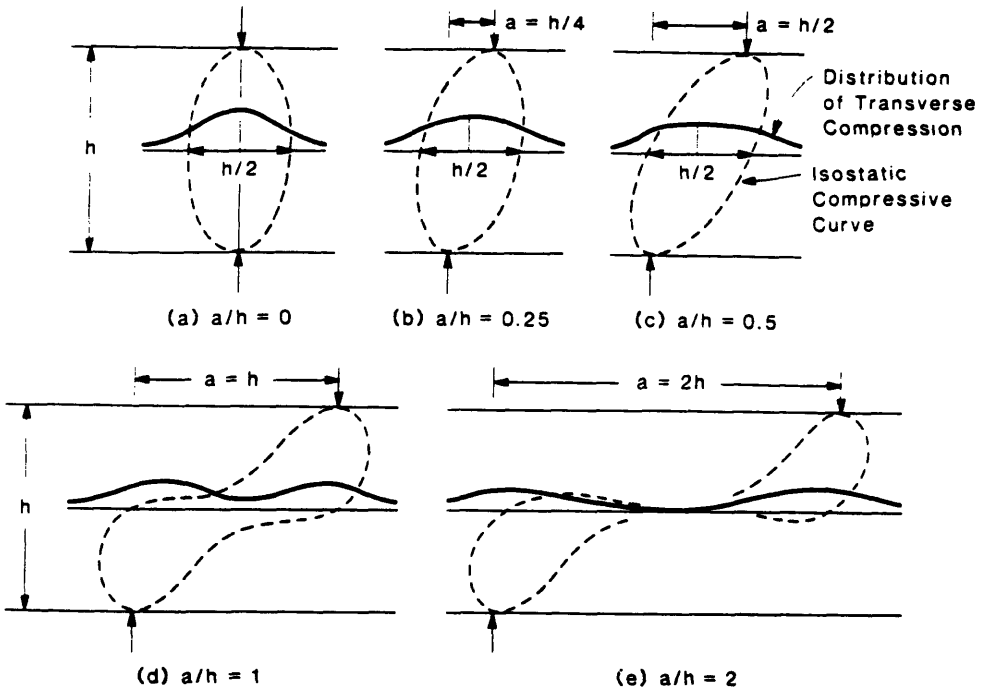

Figure 3-6: Distribution of compressive stresses for different values of a/d[27]

smooth as there are no protruding aggregate particles .

Thus, aggregate interlock shear transfer is nominal [35], and so will be ignored in this study .

It is, however, expected that the dowel contribution will be an important shear transfer process as the area of longitudinal steel is quite high, and so will be incorporated in this model .

The formulation [33] used to calculate the dowel contribution is based on the 'beam on elastic foundation theory' (Figure 3-7) .

Failure, in this model, is assumed to occur when a plastic hinge is developed at the section of maximum moment in the bar, by which point a crushed zone of length c has developed from the crack face under the longitudinal bars .

It should be noted that this approach has been developed for typical beam-column joints, as shown in Figure 3-8, but is nevertheless valid for this experimental study, as at failure the shear crack propagates close to the support, which in turn performs the function of the column (Figure 3-9) .

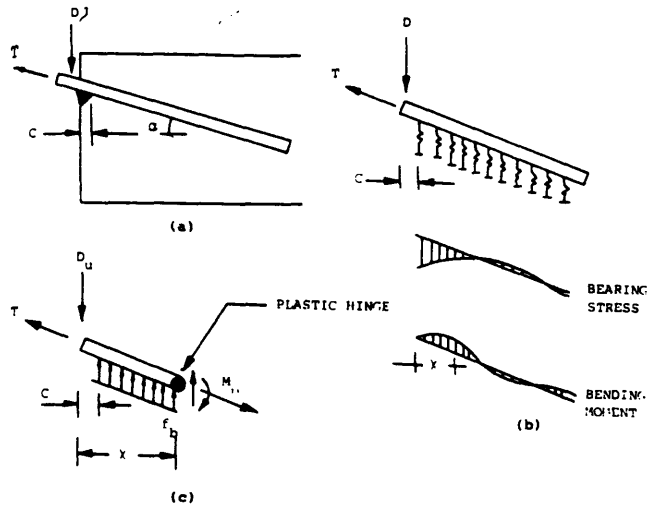

Figure 3-7: Dowel action idealization: (a)dowel bar, (b) beam on an elastic foundation model, (c)failure condition[33]

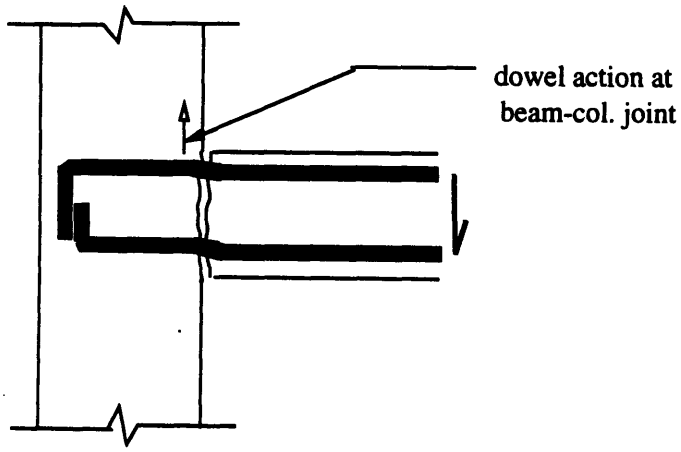

Figure 3-8: Dowel action at beam-column joint[33]

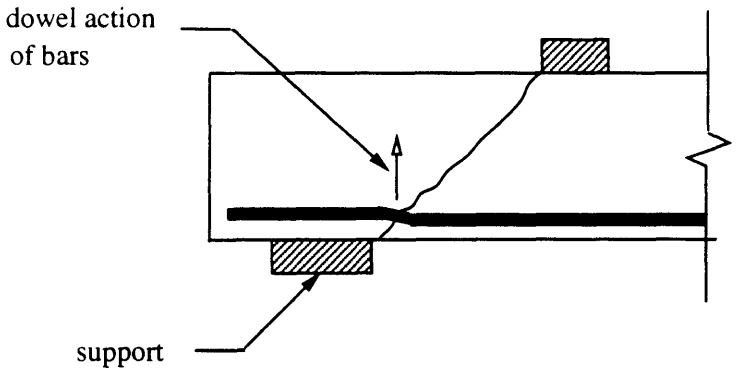

Figure 3-9: Dowel action at beam support

The theory would not therefore be as appropriate for cracks developed away from the supports of a beam .

Taking moment equilibrium about the plastic hinge (see Figure 3-7) results in the following expression for the ultimate dowel contribution :

$$D_u = 0.5\, f_b\, (0.37\, \gamma\, d_b - c)^2 + 0.45\, f_y\, d_b^2\, (1 - T^2/T_y^2)/\gamma$$

where f_b, the bearing strength of the concrete underneath the dowel bar, is given by :

$$f_b = 154\, \sqrt{f_c'}/\, \sqrt[3]{d_b}$$

and,

d_b = dowel bar diameter,

K_f = concrete foundation modulus ($1 \times 10^6 psi$),

γ = $\sqrt[4]{E_s/K_f d_b}$,

T = dowel bar axial force,

T_y = dowel bar yield axial force

It is then necessary to use emperical relations in order to calculate the dowel load for a given shear displacement .

The deflection at ultimate load is given by :

$$S_u = 4.26 \times 10^{-6}\ D_u + 0.00945$$

and the load D for a given deflection S, is given by :

$$D = D_u \sqrt{S/S_u} \tag{3.14}$$

for $S \leq S_u$, and :

$$D = D_u - D_u \frac{S - S_u}{0.4/d_b - S_u} \geq 0.4 D_u \tag{3.15}$$

for S S_u

Flexural deflections

By virtual work, the central deflection of the beam is given by :

$$\delta_f = \frac{601.6\ P}{6\ E_c I_e}$$

where P is the load applied at each of the four load points (Figure 3-10), and I_e, the effective moment of inertia, is given by :

$$I_e = (\frac{M_{cr}}{M_a})^3\ I_g + [1 - (\frac{M_{cr}}{M_a})^3]\ I_{cr}$$

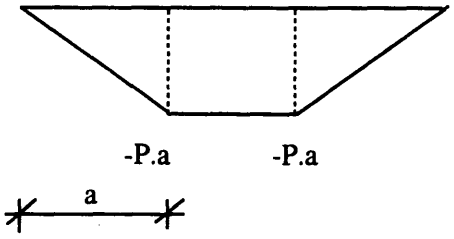

a) Bending moment diagram

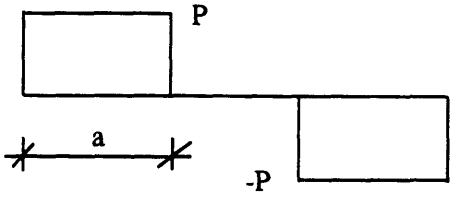

b) Shear force diagram

Figure 3-10: (a) Bending moment diagram (b) Shear force diagram

M_{cr} = moment at first cracking,

M_a = applied moment at the section,

I_g = gross moment of inertia of the section,

I_{cr} = moment of inertia of the cracked transformed section

It should be noted that the stiffening effect of the fibers has not been included in the calculation of I_e and therefore the predicted deflections are expected to be higher than the practical values obtained, for larger loads, when the fibers are effective in bridging the cracks which are developing .

The model used in this study therefore differs from the one used by Valle[8] in that the greater shear span ratio used has led to the inclusion of a term to account for the variation in stress within the shear span .

Also, this model includes a contribution from dowel action , as a much greater area fraction of longitudinal steel has been used . Central deflections have also been

predicted, as opposed to shear strains in the study by Valle .

In addition, for the contribution from the fibers in the material laws, alternative expressions have been used in some cases in order to try to improve the predictions of peak strength, which in the case of Valle's work, tended to be overpredicted slightly . The fibers have also been taken as having a contributing effect to the transverse steel, and thereby effecting an increase in the shear strength of the beams .

3.1.6 Solution procedure

It is necessary to use an iterative procedure in order to solve for the required unknowns, and this iterative procedure is outlined below :

1. Choose avalue of ϵ_d,
2. Assume a value for ϵ_r,
3. Find σ_d and σ_r from the stress-strain relations,
4. Solve for α from eqtn. ,
5. Solve for the updated value of σ_r from the equilibrium eqtns.,
6. Compare the values of σ_r calculated from steps 3 and 5; if there is a significant difference, repeat steps 2-6,
7. Calculate the other desired unknowns - for this case τ_{xy} and γ_{xy} .

A simple flow chart may be used to illustrate the solution procedure, as shown in Figure 3-11 .

Hence, in this manner, for different values of ϵ_d, the shear behavior of the beam can be traced .

The shear deflection of the beam can then be calculated,

$$\delta_s = \gamma_{xy}\, d\,,$$

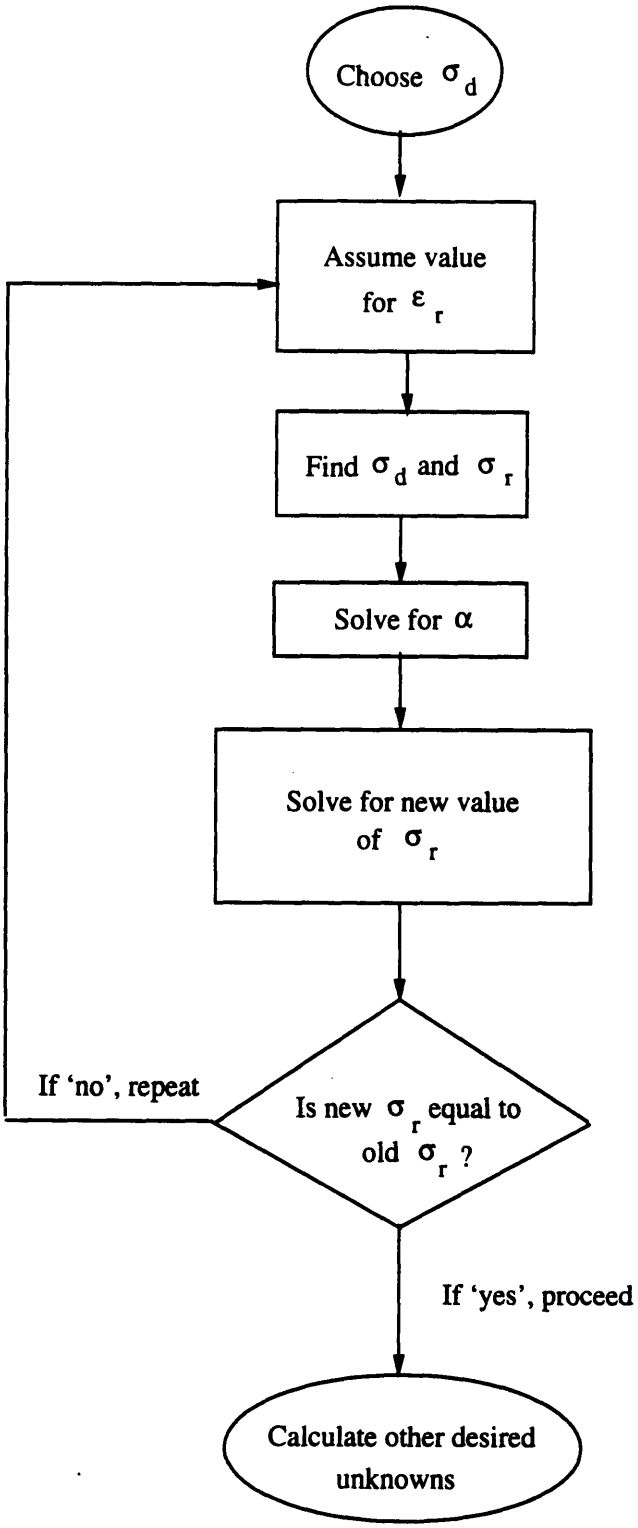

Figure 3-11: Flow chart illustrating model solution procedure

and consequently, from eqtns. 3.14 and 3.15, the dowel contribution is obtained, enabling the total load acting on the specimen to be calculated :

$$Total\ load = \tau_{xy}\ d_v\ b + D$$

Finally, the overall deflection is simply the sum of the flexural and shear deflections,

$$\delta_T = \delta_s + \delta_f\ ,$$

and hence the overall load-deflection behavior is obtained .

A computer program to perform these operations was written in the 'C' programming language, and is provided in the appendix .

Chapter 4

Experimental work

4.1 Scope

The variables investigated in this program were :

1. V_f of fibers,
2. l/d ratio of fibers,
3. a/d ratio of the specimens,
4. size effect of the aggregate,
5. fiber effectiveness .

A total of 22 laboratory size specimens were cast, and the compressive strength developed was approximately 10 000 psi .

In the remainder of this thesis, the following key will be used to represent the specimens :

$$V_f - (a/d) - (l_f/d) - d_a \ ,$$

where d_a = maximum aggregate size, and the other terms are as defined previously .

A summary of the specimen types is provided in Table 4.1 .

Specimen	Specimen type	No. cast
a1	0.0-1.46-28.1-0.375	2
a2	0.4-1.46-28.1-0.375	3
a3	0.8-1.46-28.1-0.375	3
a4	1.2-1.46-28.1-0.375	2
b1	0.8-0.93-28.1-0.375	2
b2	0.8-1.73-28.1-0.375	2
c1	0.8-1.46-61.5-0.375	2
c2	0.8-1.46-50.0-0.375	2
d1	0.8-1.46-28.1-0.250	2
d2	0.8-1.46-28.1-0.090	2

Table 4.1: Specimen types investigated

4.2 Tests specimens

Figure 4-1 indicates the dimensions of the beams which have been used in this investigation .

The formwork used allowed two beams to be cast simultaneously, and was made from plexiglass (Figure 4-1) .

Only tension steel was provided (See Section 4.3), and this consisted of 2 No. 5 and 1 No. 4 bars .

Stirrups were provided outside of the loaded span(Figure 4-1) in order to maintain the rebars in the correct location with the appropriate nominal cover requirement .

They therefore played no part in the shear transfer process, as it was felt necessary to first try to understand, and predict, the behavior of specimens without transverse reinforcement .

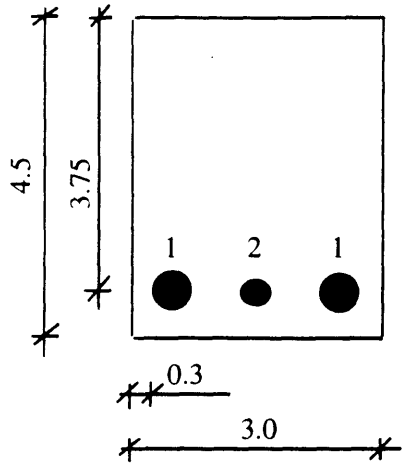

Bar No.	Size	Length
1	5	20
2	4	20

Section A-A

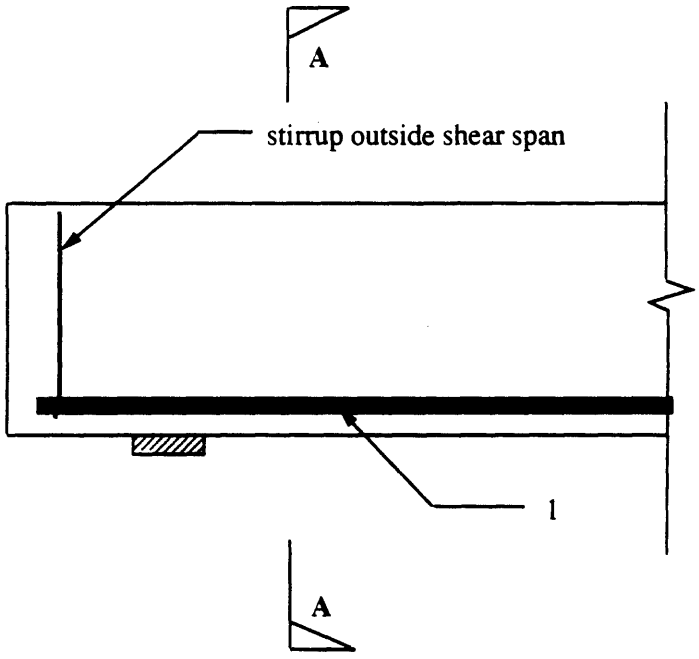

Side elevation

Notes :

a) All dimensions in inches

b) Drawings not to scale

c) Cover to main reinforcement equals 0.44"

Figure 4-1: Sectional drawings

4.3 Design of HSFRC beams

4.3.1 Flexural analysis

The first stage in the flexural design of the beams, is the calculation of the balanced steel ratio, ρ_b :

$$Effective\ section\ size = 3'' \times 3.75''$$

$$A_s = (\pi/4)\,[2\,(5/8)^2 + (4/8)^2)] = 0.810\ in.^2$$

$$\rho = \frac{0.810}{3 \times 3.75} = 0.073$$

So,

$$\rho_b = 0.65 \times 0.85 \times \frac{10000}{60000} \times \frac{0.003\ E_s}{0.003\ E_s + f_y} = 0.0708$$

Hence, as the beams are over-reinforced, only the balanced steel ratio will be used in the flexural calculations .

It is also advisable to provide this additional steel, because shear stresses will cause longitudinal stresses to develop in the steel, and so part of the steel area provided will not be available to resist flexure .

For the principle fibers used in this study, of square cross section,

fiber length, l_f = 1"

breadth = 0.045"

depth = 0.011"

Therefore, the effective diameter of the fiber, d_f, may be calculated :

$$\pi \times d_f = 2 \times\ (0.045 + 0.011)$$

hence,

$$d_f(effective) = 0.0357$$

and,

$$l_f/d_f = 1/0.0357 = 28.1$$

Figure 4-2 summarises the simplifications made in estimating the flexural capacity

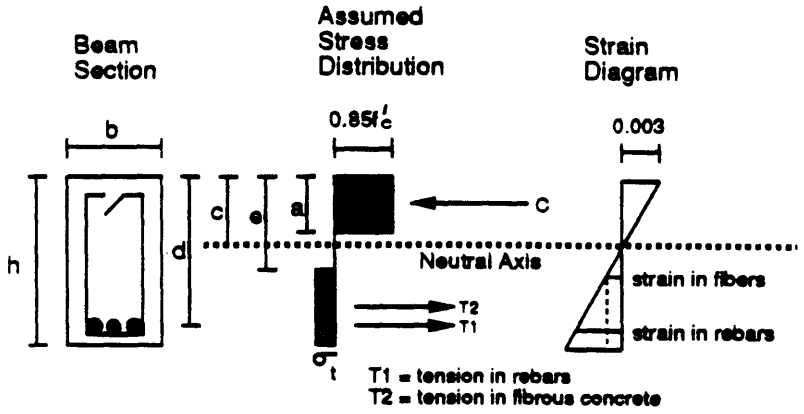

Figure 4-2: Stress-strain diagrams for beam cross-section[24]

of the beams .

The flexural capacity of a normal fiber reinforced beam is given by [17, 34] :

$$M_u = A_s.f_y\,(d - \frac{a}{2}) + \sigma_{ft}.b\,(\frac{h}{2} + \frac{e}{2} - \frac{a}{2})$$

where σ_{ft} is the tensile strength of the fiber concrete, and is given by :

$$\sigma_{ft} = 0.41 \times 0.82 \times \tau_d\,(l/d_f)\,V_f\,F_{be}$$

where F_{be} is the fiber efficiency factor, taken as 1.2 for crimped fibers, and τ_d is the dynamic bond stress of the fibers .

This equation has also been assumed to be valid for HSC [35], the improved bond strength being accounted for in the value of τ_d used $(600\,psi)$.

Now :

$$e = \frac{(\epsilon_f + 0.003)}{0.003}\,c\,,$$

where ϵ_f is the strain in the fiber .

Hence,

$$e = \frac{(\frac{\sigma_f}{E_s} + 0.003)}{0.003} c$$

σ_f is the tensile stress in the fibers during pullout (for normal concrete), and is obtained by equating the tensile stress in the fibers to the bond stress :

$$\sigma_f = \frac{\tau_d \, F_{be} \, l_f \, (b_f + w_f)}{b_f \, w_f}$$

(Note that the fibers are of square cross section, the dimensions being given by w_f and b_f .)

This value is independent of the volume fraction of the fibers and may be calculated at this stage :

$$\sigma_f = \frac{600 \times 1.2 \times 1 \times (0.045 + 0.011)}{0.045 \times 0.011} = 81455 \, psi$$

As the yield strength of the fibers is 60 000 psi, then the above result would tend to indicate that the fibers will actually yield before pull-out occurs .

Thus $\sigma_f = 60\,000 \, psi$.

Now,

$$\epsilon_f = \frac{\sigma_f}{E_s} = \frac{60\,000}{29 \times 10^6} = 2.069 \times 10^{-3}$$

therefore,

$$e = \frac{0.002069 + 0.003}{0.003} c = 1.69 \, c$$

but $a = 0.65 \, c$, so :

$$e = 2.60 \, a$$

The value of a (see Figure 4-2) is determined by equating the compression in the concrete section to the tension, and the resulting expression may be expressed as :

$$a = \frac{A_s \, f_y + \sigma_{ft} \, b \, h}{0.85 \, f'_c \, b + 2.6 \, \sigma_{ft} \, b}$$

Specimen	Moment capacity($lb\,in$)	Total load($kips$)
0.0-1.46-28.1-0.375	134374	48.80
0.4-1.46-28.1-0.375	134918	49.06
0.8-1.46-28.1-0.375	135224	49.16
1.2-1.46-28.1-0.375	135529	51.28
0.8-0.93-28.1-0.375	135224	77.27
0.8-1.73-28.1-0.375	135224	41.60
0.8-1.46-61.5-0.375	135952	49.44
0.8-1.46-50.0-0.375	135339	49.21
0.8-1.46-28.1-0.250	135224	49.16
0.8-1.46-28.1-0.090	135224	49.16

Table 4.2: Summary of flexural calculations

The flexural capacity may then be determined using the aforementioned expression for M_u, and consequently the ultimate load capacity obtained .

A summary of the results of the calculations for the different specimen types is provided in Table 4.2 .

4.3.2 Shear strength estimation

As the shear capacity of the members is the focus of this study, it is essential that the shear capacity be less than the flexural capacity of the members .

Even though the formula proposed by Shahbazker [24] needs further modification, it is nevertheless used to obtain an estimate of the shear capacity of the members .

$$v_c = \frac{10\sqrt[3]{\rho}}{\sqrt{1 + d/25d_a}}[\sqrt{f_c'} + 3000\sqrt{\rho/(a/d)^5} + 70\ F\ ]$$

and,

$$v_u = v_c + v_d$$

where :

$$v_d \approx 0.25\ v_u$$

A summary of the estimated shear capacities for the different specimens is pre-

Specimen	V_c (lbs)	V_u (lbs)	Total load (lbs)
0.0-1.46-28.1-0.375	16.12	21.49	42.98
0.4-1.46-28.1-0.375	18.94	25.25	50.50
0.8-1.46-28.1-0.375	20.24	26.99	53.98
1.2-1.46-28.1-0.375	21.26	28.34	56.68
0.8-0.93-28.1-0.375	45.69	60.92	121.84
0.8-1.73-28.1-0.375	16.03	21.37	42.74
0.8-1.46-61.5-0.375	25.13	33.51	67.02
0.8-1.46-50.0-0.375	21.01	28.01	56.02
0.8-1.46-28.1-0.250	18.93	25.24	50.48
0.8-1.46-28.1-0.090	14.67	19.56	39.12

Table 4.3: Estimated shear capacities

sented in Table 4.3 (all loads in *kips*):

Hence, it is expected that shear failure will occur before flexural failure for the specimens under investigation as the flexural calculations are very conservative .

4.4 Batch design and material selection

The materials used in the experimental program are outlined below :

- Type I Portland Cement,
- Fine aggregate (mortar sand),
- Coarse aggregate (pea gravel - 3/8"max. size),
- Condensed silica fume (Force 10 000 - 50% water by weight) to enable a stronger between fiber and matrix and a satisfactorily high strength to be obtained,
- Superplasticizer (WRDA-19, ASTM C-494, type A & F), used to increase the workability of the mix with no loss in strength,
- Steel fibers ($f_y = 60000\ psi$) - 3 types were used (Figure 4-3) :

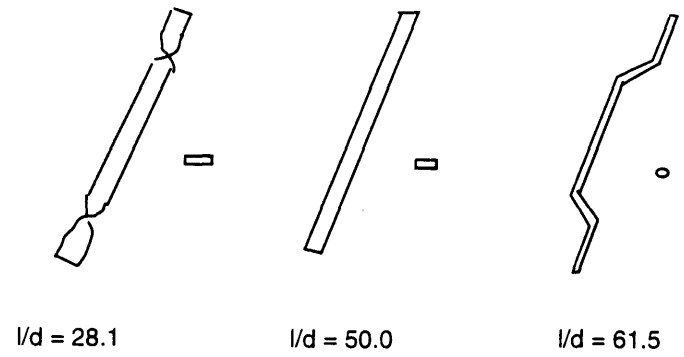

Figure 4-3: Fiber types used

1. deformed fibers, $l/d = 28.1$,$1'' \times 0.011'' \times 0.044''$,
2. hooked end fibers, $l/d = 61.5$, $1.2'' \times \phi = 0.0195''$,
3. straigth fibers, $l/d = 50.0$, $1'' \times 0.022'' \times 0.01''$.

The mixing proportions used to prepare the specimens are given in Table 4.4 , the mix being designed to obtain a strength of 10 000 psi at 28 days .

The quantities used in a typical mixing operation are provided below in Table 4.5 .

Variable	Proportions
sand/cement	2.0
gravel/cement	2.0
silica	10%
superplasticiser	3%
water/(cement + silica)	0.36

Table 4.4: Mix proportions used

Material	Quantity (*lbs*)
cement	13
sand	26
gravel	26
silica fume	2.6
water	3.9
superplasticiser	0.39
fibers	1.75

Table 4.5: Quantities used in typical casting operation

4.5 Preparation and casting of specimens

The rebars were first assembled into a reinforcing cage utilising stirrups (outside the shear span), and these were all held together with steel wire .

The plexiglass formwork was then coated with bondbreaker, and the reinforcing cages placed inside the formwork .

The concrete was then prepared following the procedure outlined below :

1. The sand, cement and gravel were placed in a rotating-drum mixer(Figure 4-4) and mixed for 30 seconds,

2. At this stage, the water, silica fume and superplasticizer (which had all been previously mixed together) were then gradually added to the mixer,

3. If fibers were used, these were 'sprinkled' into the mixer, ensuring that they did not ball together as they were added,

4. The mixing was then discontinued 5 minutes after step 2 had been completed .

The concrete was then placed in the formwork and, in addition, 4 test cylinders were cast .

The concrete was cast according to ACI code requirements [36, 37] and the specimens were then vibrated for 3 minutes .

The specimens were then covered in plastic sheeting, and left in this state for 24

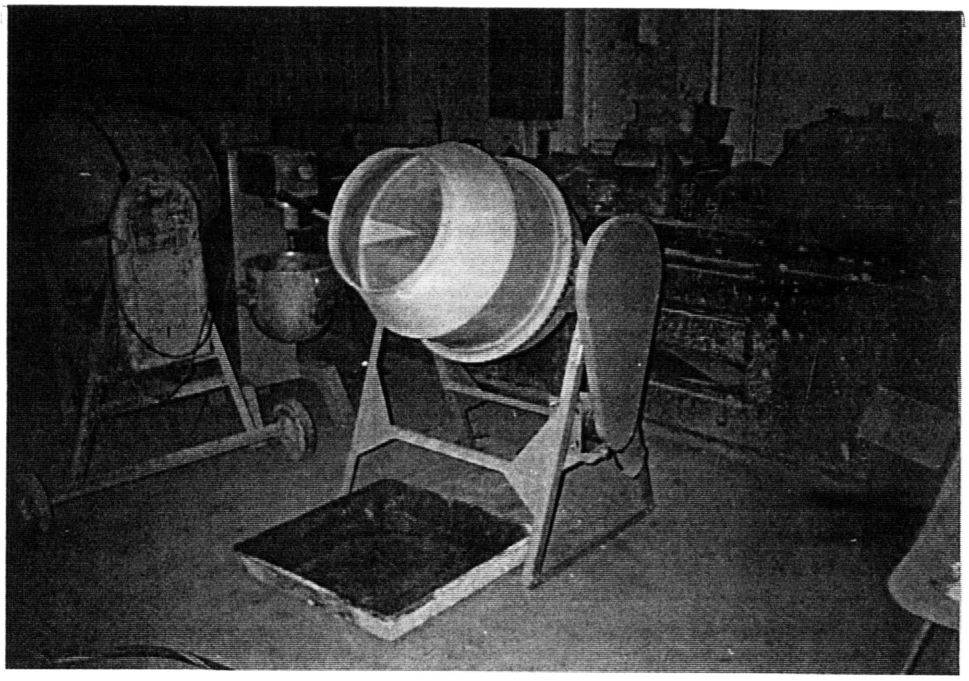

Figure 4-4: Laboratory cement mixer

hours in order to allow setting of the concrete to occur . They were then demoulded and cured in water for 28 days [35] .

4.6 Testing procedure

A 200 kip capacity 'Baldwin Testing Machine' was used for all the tests performed in this experimental program, and the signals from this machine were recorded using an IBM AT computer (see Figure 4-5) .

4.6.1 Compression and splitting tensile tests

Of the four cylinders prepared during each casting sequence, two were used for for compression tests, and two for splitting tensile tests .

Prior to testing, the cylinders for the compression tests were capped using hydrostone, in order to ensure an even contact surface with the loading platens of the testing machine (Figure 4-6).

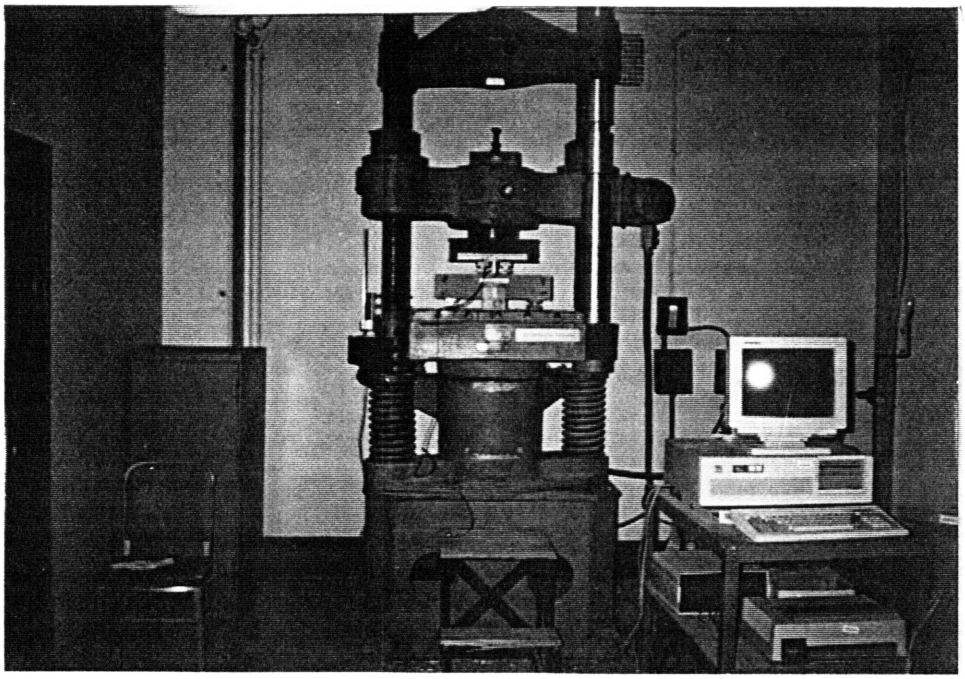

Figure 4-5: Testing machine

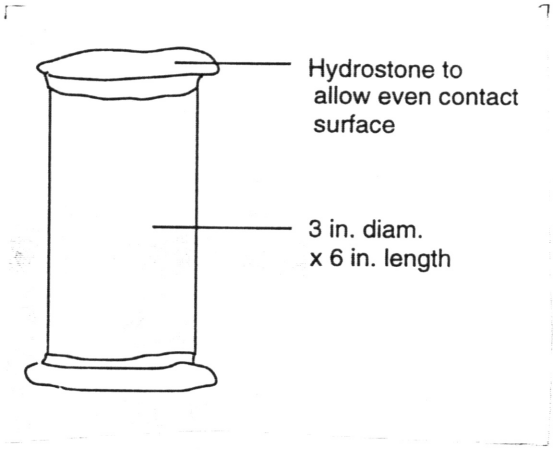

Figure 4-6: Testing cylinders capped with hydrostone

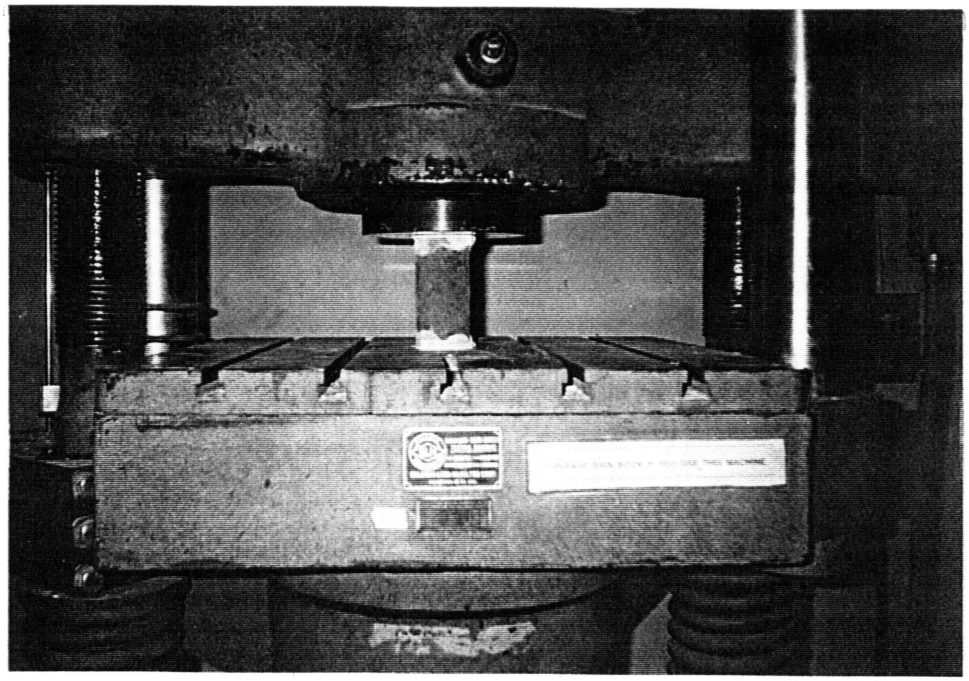

Figure 4-7: Compressive strength determination

The compression test program consisted of two main stages :

1. The Young's Modulus of the cylinders were measured by placing two Linear Voltage Displacement Transducers (LVDT) on diametrically opposite sides of the cylinders being tested, and then loading the cylinders up to approximately 40% of the expected ultimate capacity, at a displacement rate of 0.016 in/min. .

2. The LVDT's were then removed, and the cylinders reloaded at a displacement rate of 0.016 in/min. to enable the ultimate compressive strength, f_c', to be determined (Figure 4-7).

In performing the splitting tensile tests, the cylinders were placed flat on their longitudinal axis (Figure 4-8), and loaded until the occurrence of vertical cracking, which was readily determined from the load-displacement plot, as loading occurred . The displacement control rate used was 0.016 in/min. .

The results from these splittimg tensile tests were not utilised in this experimental program, but were only performed in order to provide a measure of the tensile strength

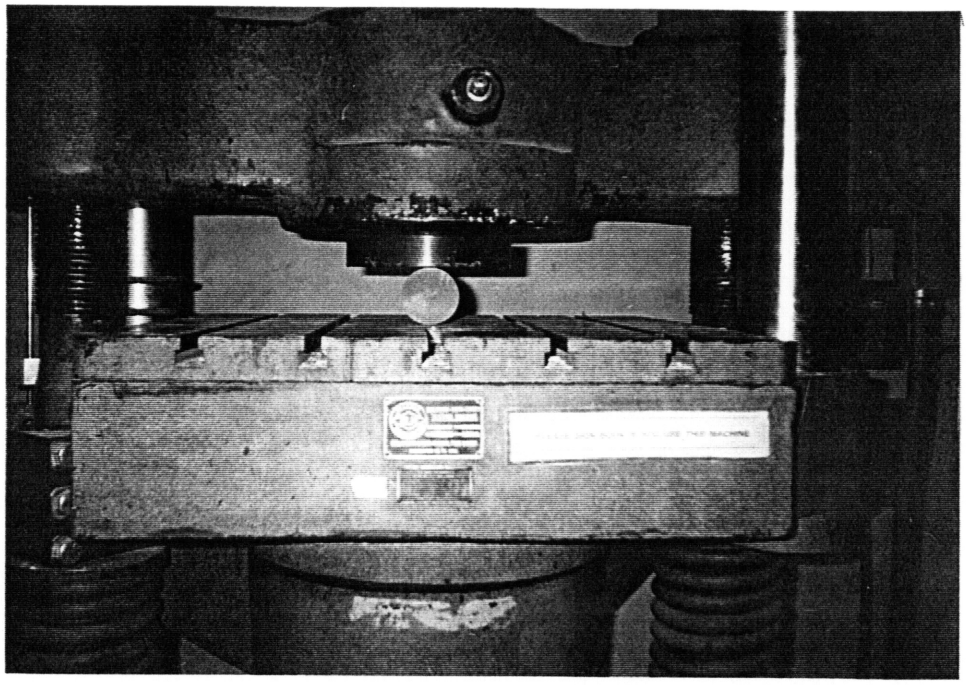

Figure 4-8: Tensile splitting test set-up

and its variation for the specimens .

4.6.2 Beam shear tests

The beam shear tests were performed using four point loading . For shear tests on beams, ACI 318 [36] recommends that the beams be tested soon after removal from water, to avoid the development of shrinkage cracks and a consequent reduction in the tensile strength of the specimens . Therefore, all the tests performed on the specimens (including the cylinders) were performed on the same day of removal from water .

In order to measure the central deflection of the specimens, an LVDT was used, located as indicated in Figure 4-9 .

The supports used were designed to allow for rotation at the support points and thereby maintain a simply supported configuration .

The displacement control rate used was 0.04 in/min., and loading was continued

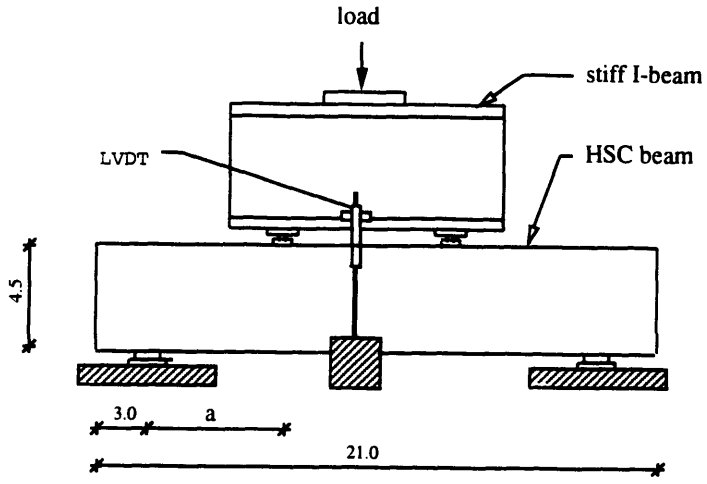

Figure 4-9: Beam shear test set-up

beyond the ultimate capacity in order for the post-peak behavior to be observed .

Chapter 5

Observations and Results

5.1 Experimental results

5.1.1 Production

Initially, concrete with a strength in the range of 13 000 psi was attempted to be produced, however, when the mix design used by Shahbazker [24] to achieve such a strength was utilised, satisfactory workability was not achieved .

The probable reason for this was that the mixer used by Shahbazker was more effective in terms of the way in which the concrete was mixed, and also because the concrete could be pressurised, allowing for a more homogeneous mix .

In this program, the mixer available for use was of the rotating drum, gravity induced type (Figure 4-4), which is not as effective, and therefore it was necessary to use a higher water/cement ratio in order to achieve a satisfactory workability . This resulted in a concrete compressive strength of approximately 10 000 psi .

Addition of fibers to the mix did not have an adverse effect on the mix, the reduction in workability not being very significant .

The cement used, however, provided some mixing problems . This was because, on using different bags of cement, it was found that there was a noticeable change in workability . For the cases with diminished workability, mixing was allowed to continue for longer period of time .

5.1.2 Compression tests

Table 5.1 summarises the results from the compression tests on the cylinders . It is seen that the values of Young's Modulus are greater than those expected for NC, confirming the trend of increased stiffness when using HSC .

It was also observed that when the V_f of fibers is increased there is a coresponding increase, not only in the Young's Modulus, but also in the compressive strength of the specimens, and this confirms the beneficial effects of the fibers when added to the mixture .

5.1.3 Splitting tensile tests

The results from the splitting tensile tests (Table 5.1) indicate that, as the V_f increases, so also does the tensile splitting strength, and this is due to the inherent ability of the steel fibers to carry tensile stress .

It was observed for the case with $V_f = 0.0$ that the cylinders split completely into two halves at failure (Figure 5-1) .

Figure 5-1 also indicates that the resulting surfaces were also very smooth and this is because generally in HSC, the cracks propagate directly through the aggregate due to the improved aggregate/matrix bond .

When fibers were added, the occurrence of failure was not directly observable, as the specimens remained intact . Failure in those cases was determined by careful observation of the load/displacement plot as loading was continued .

5.1.4 Beam shear tests

As loading progressed, it was observed that there were no visible flexural cracks formed at the midspan of the beams .

Diagonal cracking began at approximately $20000\,lbs$ for the specimens with $a/d = 1.46$. These cracks began at mid-depth of the beams, as shown in Figure 5-2, and then propagated towards the supports .

As the cracks approached the supports, they did not continue towards the center

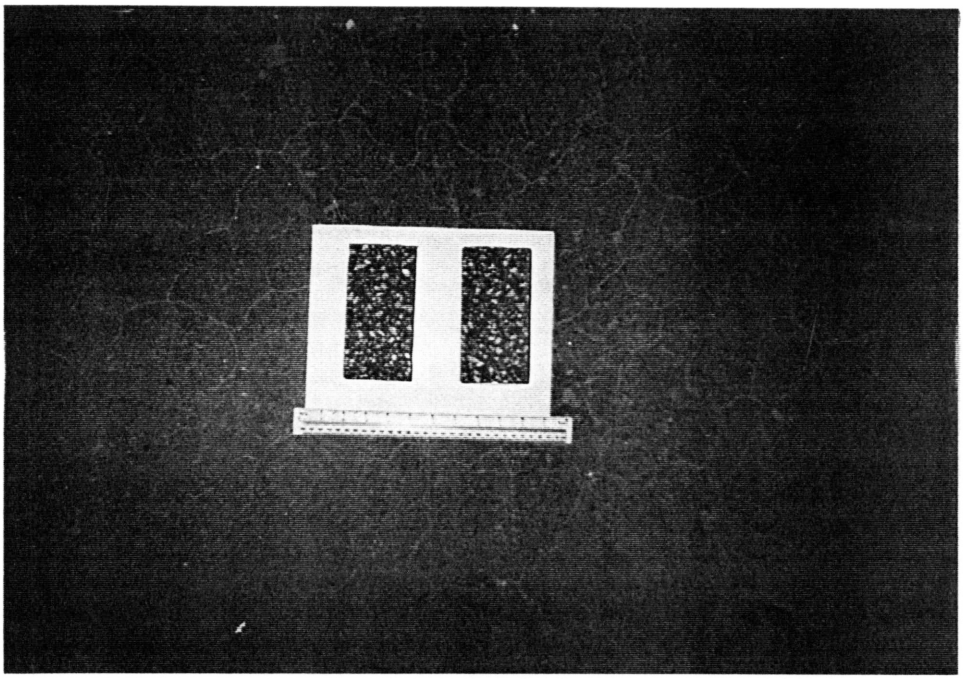

Figure 5-1: Split cylinder test for $V_f = 0.0$

Specimen	$f_c^{'}(psi)$	$f_{st}(psi)$	Estimated $2V_u$	$2V_u(lbs)$	$E_c(ksi)$
a1	9720.9	406.4	42980	37585.5	3655.97
a2	10157.9	564.0	50500	40993.4	3706.20
a3	10387.4	592.3	53980	42377.8	4368.07
a4	10774.5	725.8	56680	49225.7	3818.03
b1	9052.6	658.1	121840	74443.6	3858.30
b2	10258.9	612.4	42740	35953.9	4470.64
c1	11695.3	697.6	67020	50691.1	4555.66
c2	7859.6	615.0	56020	38237.1	4006.31
d1	9587.1	690.9	50480	40379.1	3890.88
d2	7154.5	640.5	39120	30980.6	30549.87

Table 5.1: Table of experimental results

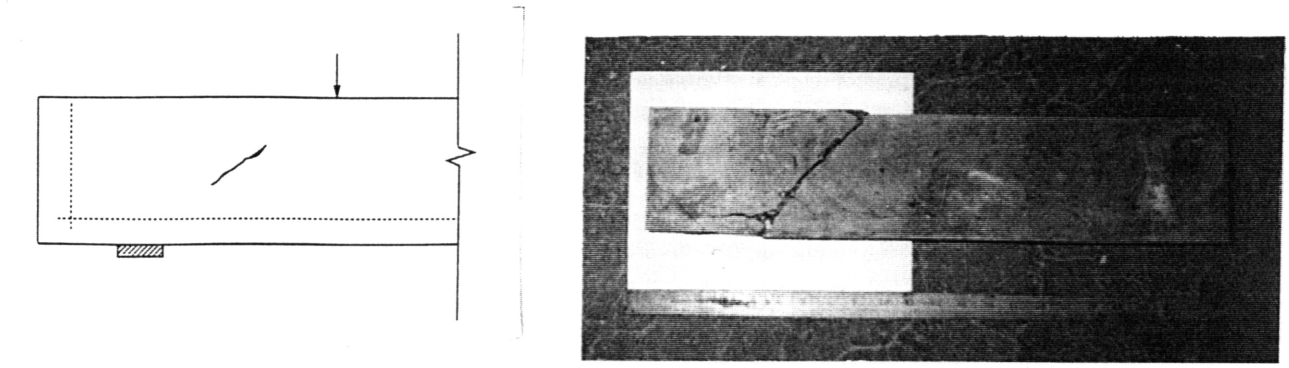

Figure 5-2: (a)Initial crack location in specimens (b)Failed specimen

of the supports, but instead towards the closer edges of the supports, as this allowed for large shear displacements (Figure 3-9) .

It should also be noted that, as observed from the load-deflection diagrams, there is not a significant decrease in stiffness upon the occurrence of first cracking at approximately 20000 *lbs* . This is because the system under study involves deep beam behavior, with the diagonal cracks initiating close to the neutral axis, and therefore the cracking has nominal effect on the deflection of the specimens .

If the study had involved slender beam behavior, the occurrence of first cracking would have probably been more evident from the load-deflection curves . This is because, for slender beams, shear diagonal cracks generally develop as extensions of flexural cracks[5] i.e. they develop at the outer tensile fiber (at the bottom of the specimens in four point loading) . Thus, the reduction in total effective moment of inertia on first cracking of the specimenns would lead to a reduced overall flexural rigidity of the specimen, and, therefore, a more noticeable increase in the deflection of the beam . The fibers present would, however, help to limit the increase in deflection .

As loading continued beyond the peak load, longitudinal cracks developed along the main reinforcement, indicating that the dowel capacity was being reached .

Also, as the tests progressed into the post-peak range, the relative displacement between the sides separated by the crack (Figure 3-9) noticeably increased .

The plots for the specimens tested are given in Figure 5-3, Figure 5-4, Figure 5-5, Figure 5-6, Figure 5-7, Figure 5-8, Figure 5-9, Figure 5-10, and Figure 5-11 .

It should be noted that for the specimens with $V_f = 0.0$, on reaching the peak load, failure was brittle (Figure 5-3), with little post-peak ductility, and failure was accompanied by the emission of a loud noise .

For the specimens with fibers, there was a noticeable increase in the post-peak ductility (Figure 5-4 to Figure 5-11), however, for $V_f = 1.2\%$, the increase in ductility was not as significant as was expected (refer to Chapter 6) .

The results also confirm the beneficial effects of adding fibers to the concrete, because as seen in Table 5.1, as the V_f is increased, there is a corresponding increase in shear strength of the specimens .

The fibers also helped the specimens to maintain their integrity as the tests progressed (after reaching the peak load), wheras, in the cases with $V_f = 0.0$, pieces of concrete tended to spall off .

For the specimens tested with various shear spans, it is seen that the smaller the a/d ratio, the greater is the increase in shear strength, as expected .

For the specimens tested with hook ended fibers, it should be noted that after the ultimate load was reached, continual 'clicking' sounds were heard, a phenomemon which was not experienced in the other tests, and this was probably the result of the fibers being pulled out .

It should also be noted that, of the fibers tested, these hooked ended fibers, with the greatest aspect ratio, caused the greatest increase in shear strength .

In all cases it was noted that for large displacements, the load-displacement plots eventually levelled out (Figure 5-3 to Figure 5-11), and this load corresponded to the residual dowel capacity of the specimens .

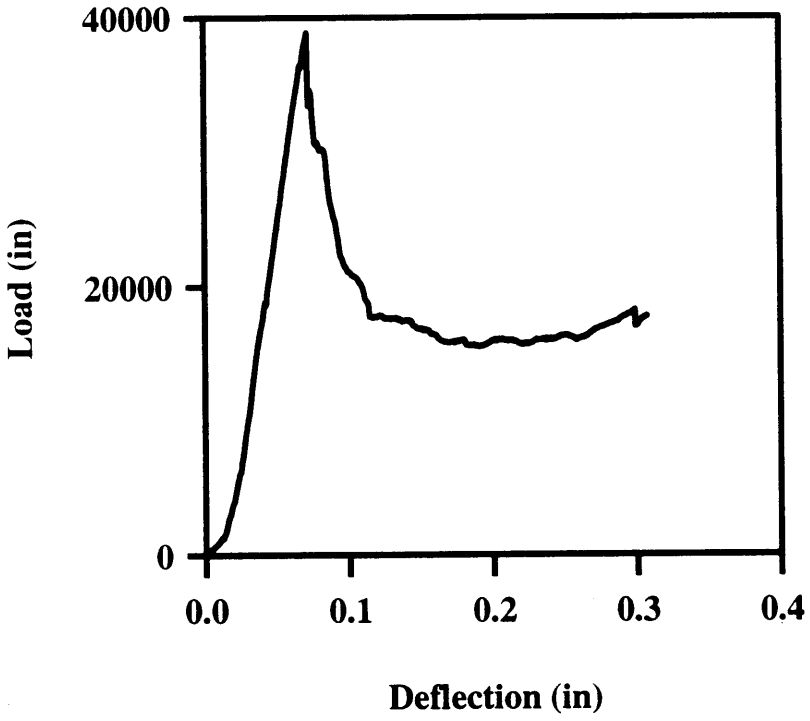

Figure 5-3: Beam tests for $V_f = 0.0$ (a1)

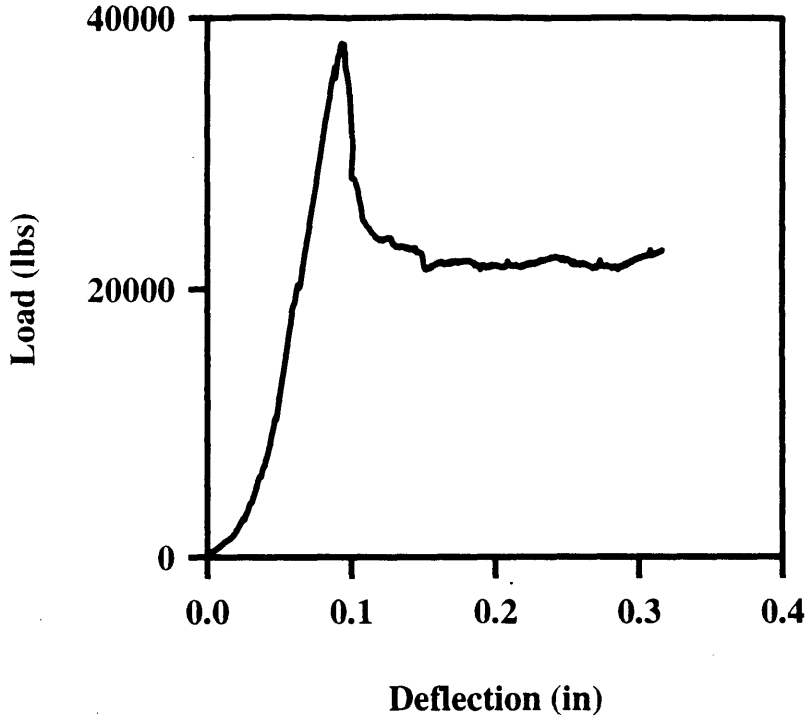

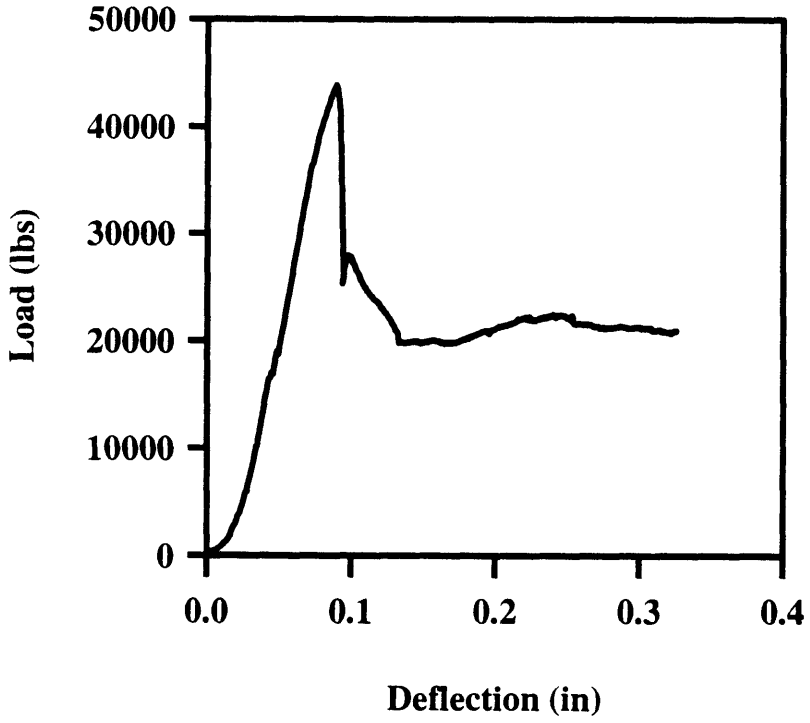

Figure 5-4: Beam tests for $V_f = 0.4$ (a2)

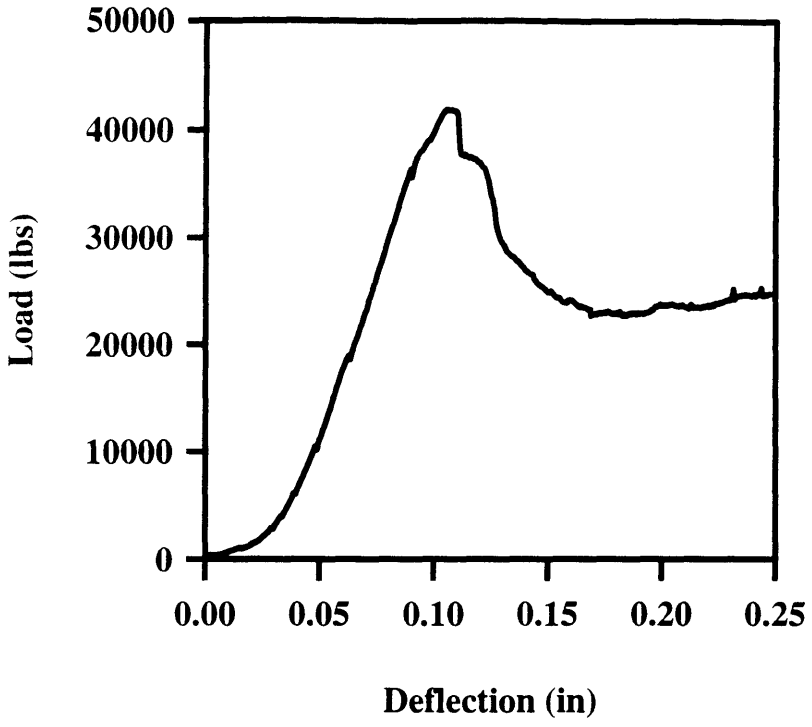

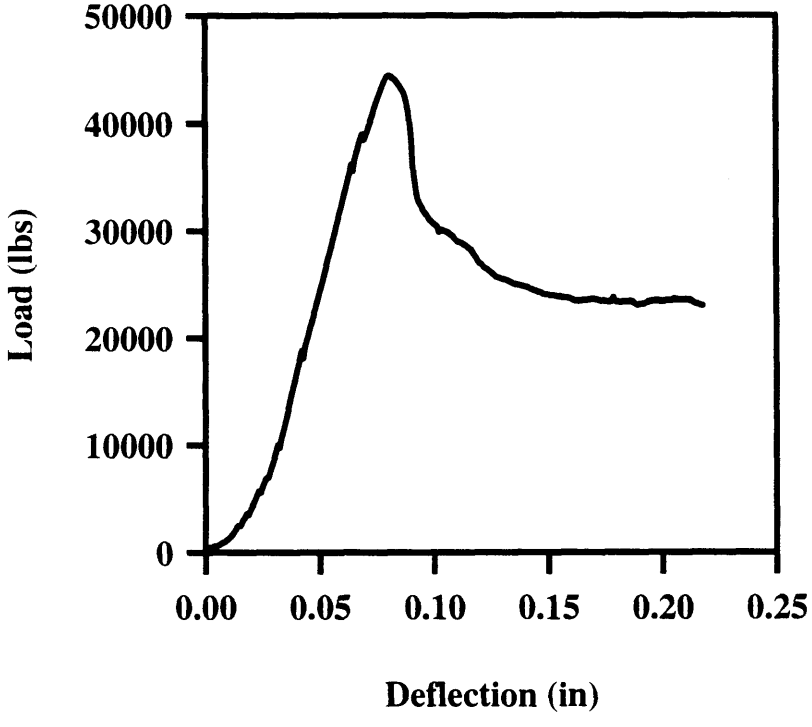

Figure 5-5: Beam tests for $V_f = 0.8$(a3)

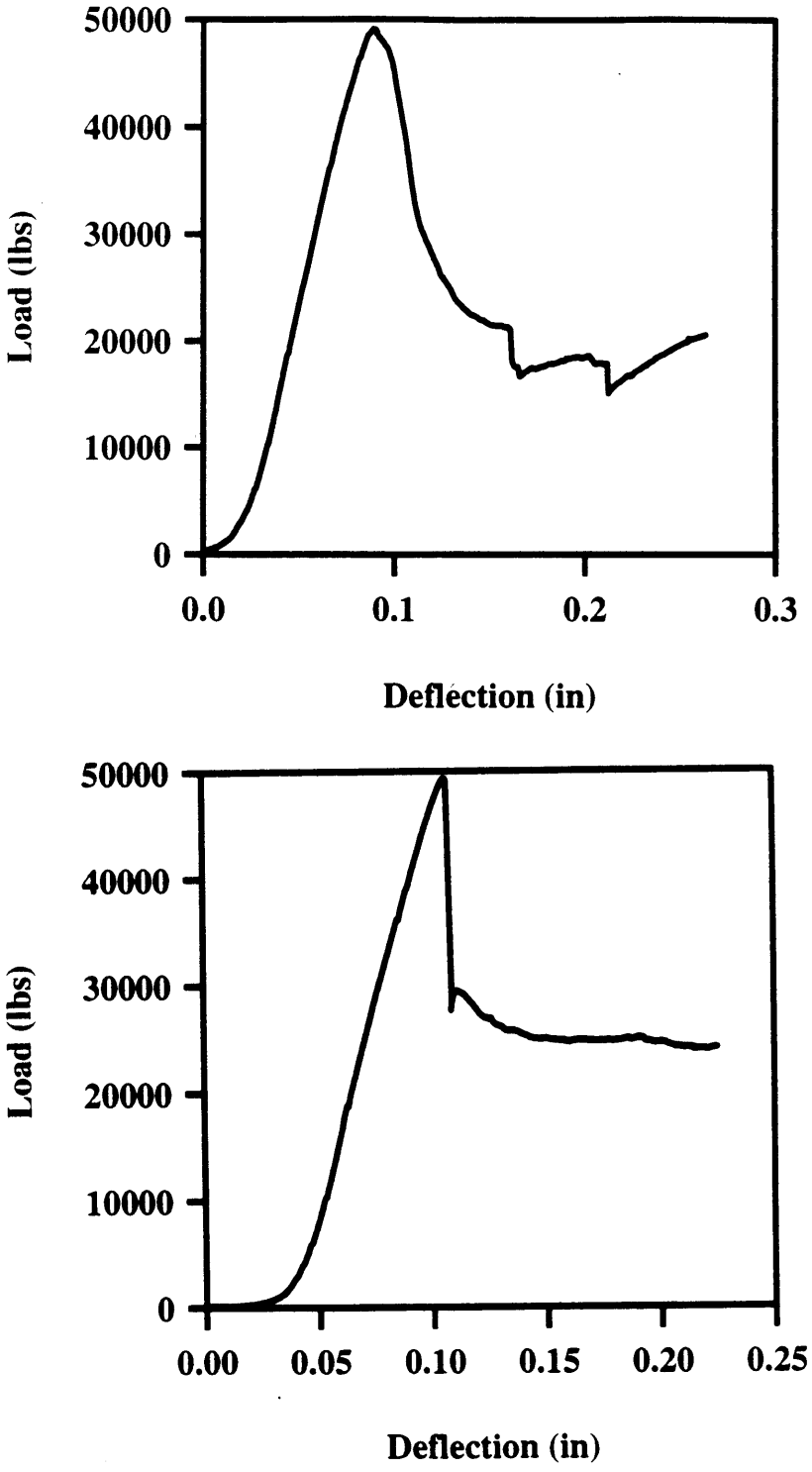

Figure 5-6: Beam tests for $V_f = 1.2$ (a4)

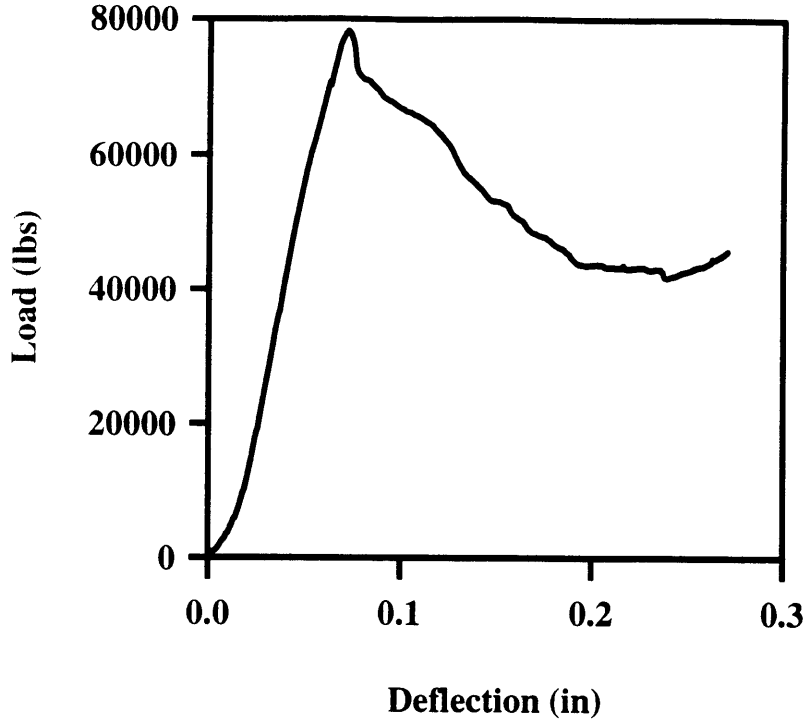

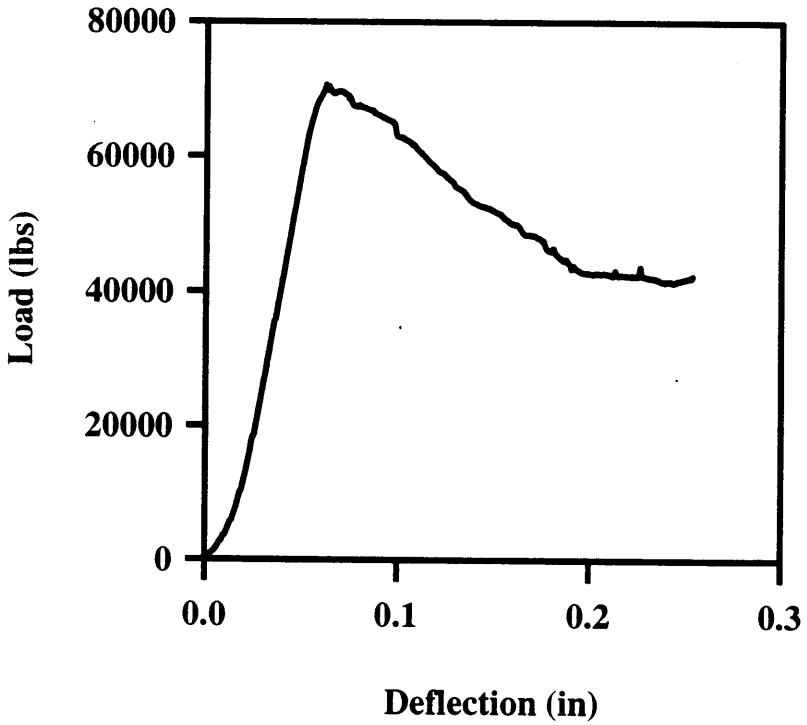

Figure 5-7: Beam tests for $a/d = 0.88$ (b1)

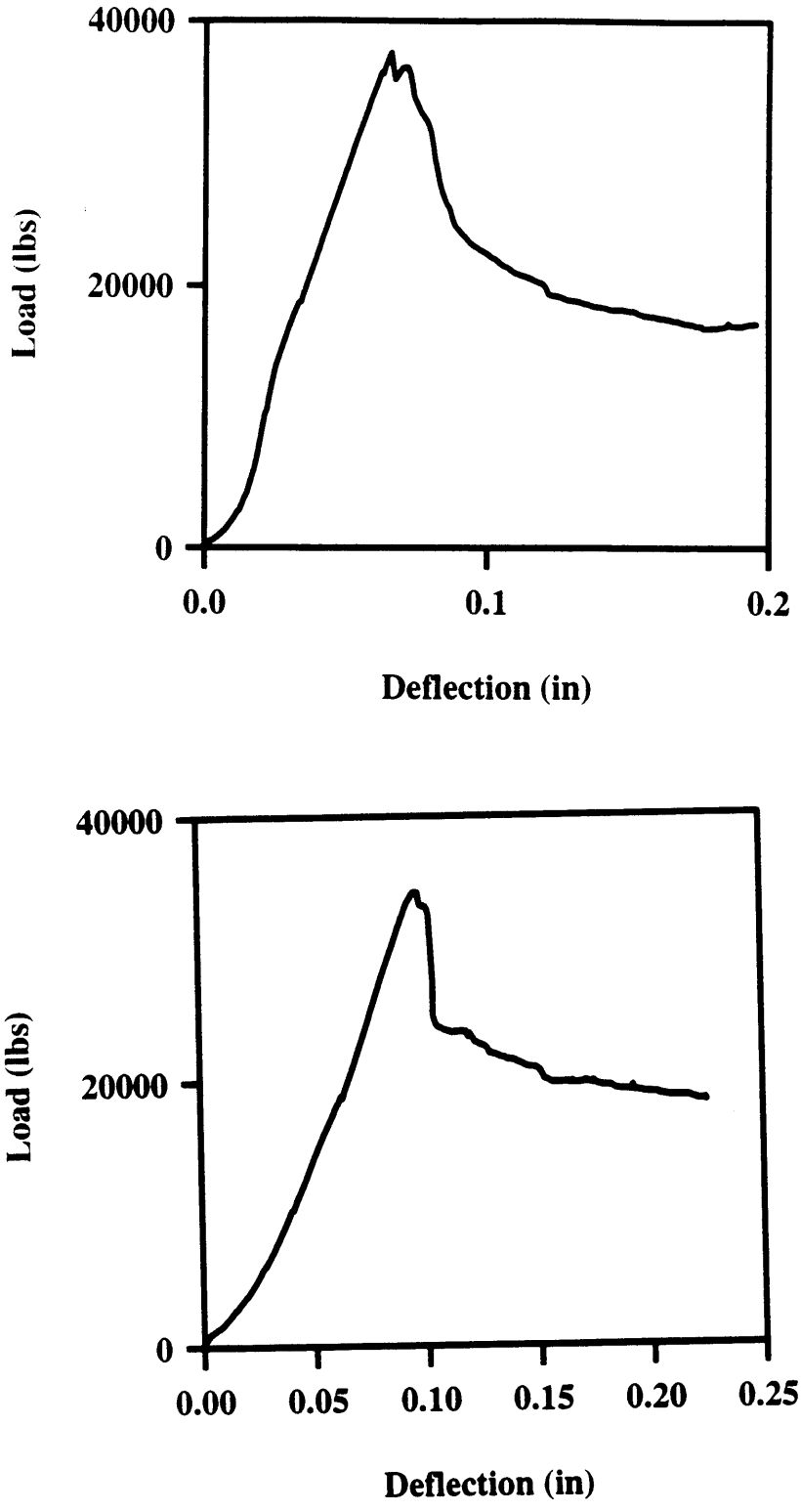

Figure 5-8: Beam tests for $a/d = 1.73$ (b2)

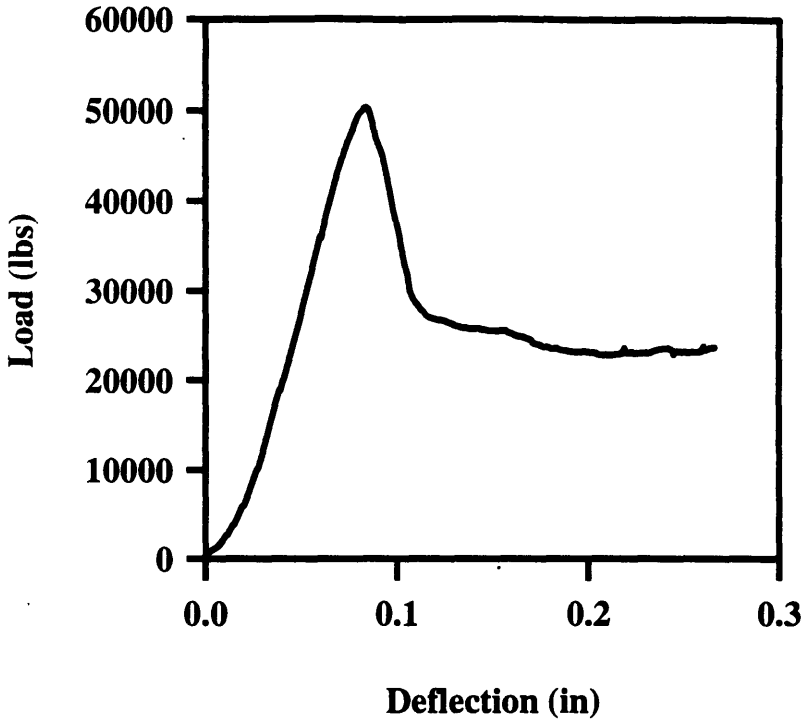

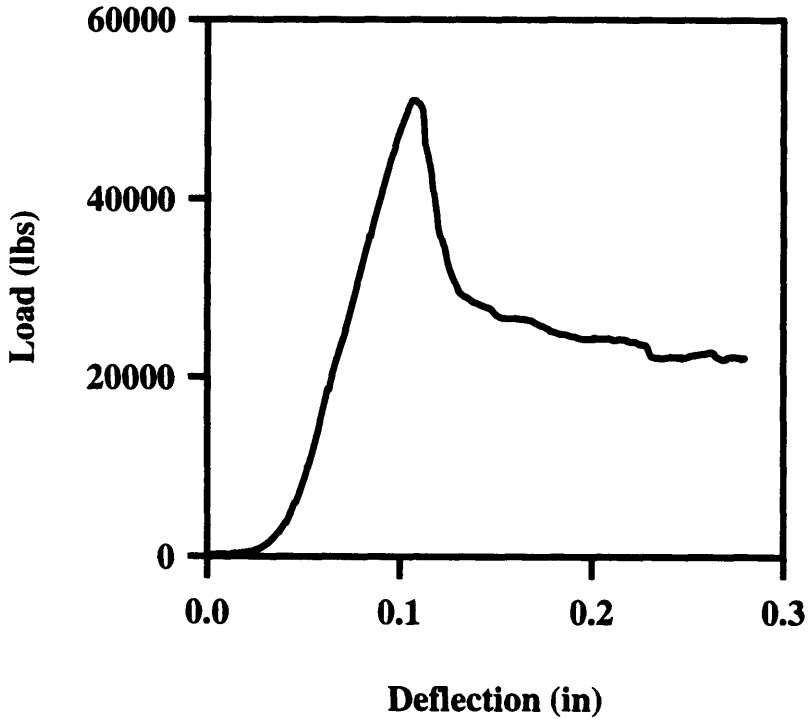

Figure 5-9: Beam tests for hooked end fibers (c1)

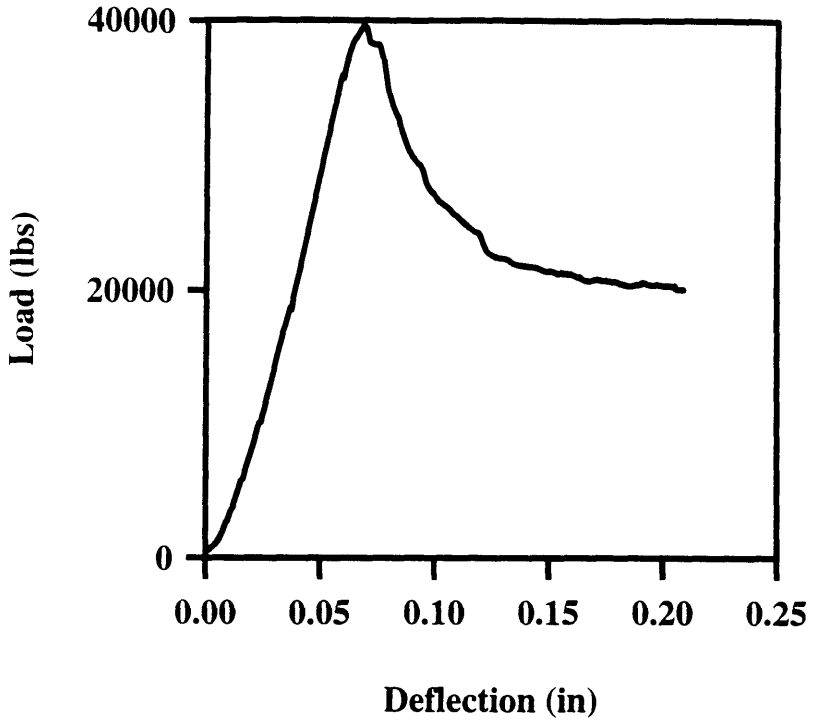

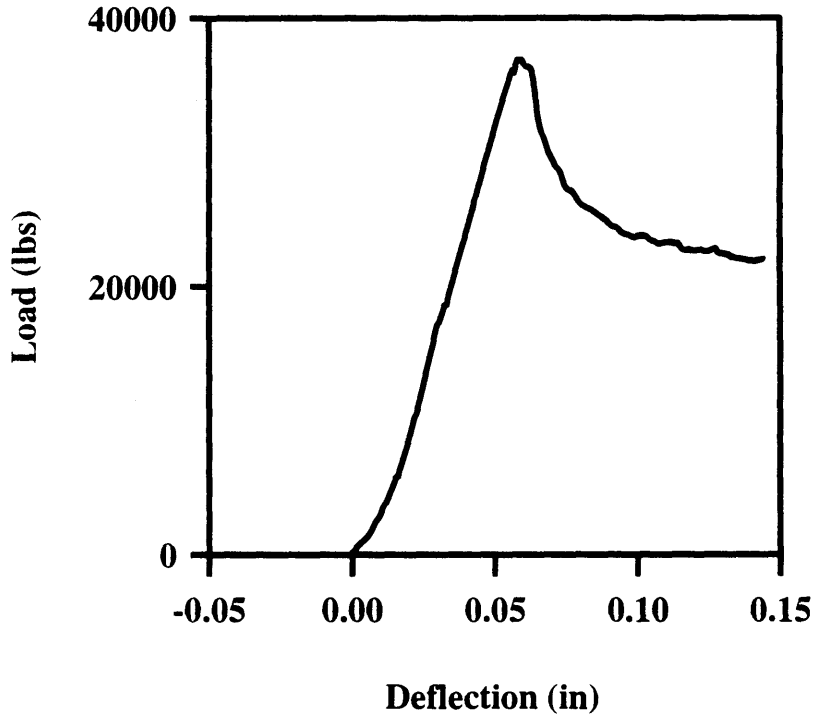

Figure 5-10: Beam tests for straight fibers (c2)

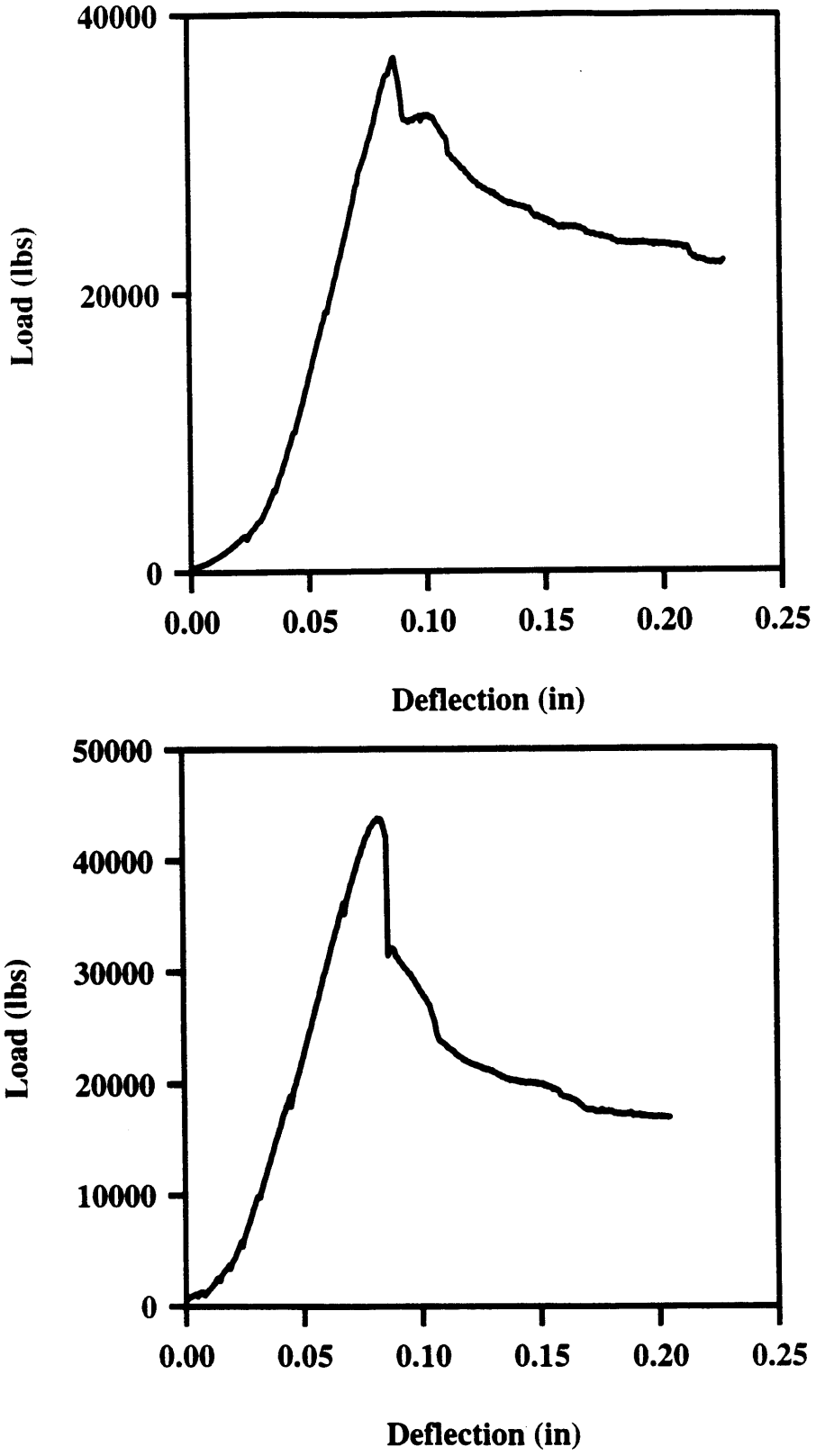

Figure 5-11: Beam tests for maximum $d_a = 0.25\ in$ (d1)

Chapter 6

Discussion of results

6.1 Deep beam shear model

In order to account for the noticeable increase in the shear capacity for the HSFRC specimens in the deep beam shear model, it was first necessary to make two reasonsble assumptions regarding the contribution from the steel fibers :

1. The fibers help to improve the inherent strength of the concrete in resisting shear loading, by applying a confining effect to crack propagation, thereby improving the stress-strain properties of the concrete (Figure 6-1 (a)),

2. The fibers perform the role of transverse steel reinforcement (stirrups) and in the process act to support some of the shear load acting on the concrete (see Figure 6-1 (b)) .

As previously discussed in Chapter 3, the effect of assumption 1 has already been accounted for in the stress-strain relations for the HSFRC .

In order to account for assumption 2, values for ρ_y (the equivalent fiber contribution to the transverse reinforcement) were chosen which best fit the observations from the experimental program .

A table of the results from the application of this model, as well as the values of ρ_y used, is presented below (Table 6.1):

Figure 6-1: Action of fibers to (a)improve concrete properties, and (b)perform the role of stirrups

Specimen type	Observed (lbs)	Predicted (lbs)	A_s (in^2)
(a1) 0.0-1.46-28.1-0.375	37585.5	37740	0.000
(a2) 0.4-1.46-28.1-0.375	40993.4	40503	0.027
(a3) 0.8-1.46-28.1-0.375	42377.8	42769	0.053
(a4) 1.2-1.46-28.1-0.375	49225.7	44934	0.081
(b1) 0.8-0.93-28.1-0.375	74443.6	50519	0.053
(b2) 0.8-1.73-28.1-0.375	35953.9	38510	0.053
(c1) 0.8-1.46-61.5-0.375	50691.1	48968	0.150
(c2) 0.8-1.46-50.0-0.375	38237.1	436860	0.027

Table 6.1: Results from deep beam shear model

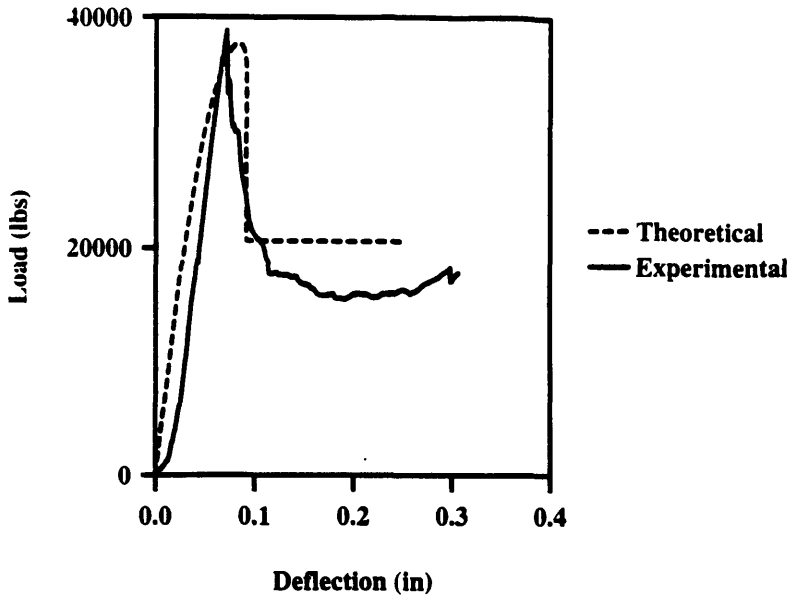

Figure 6-2: Model comparison for $V_f = 0.0\%$

Comparison of the experimental and theoretical plots are shown in Figure 6-2, Figure 6-3, Figure 6-4, Figure 6-5, Figure 6-6, Figure 6-7, Figure 6-8, and Figure 6-9 .

It should be noted from the plots, that as the peak load capacity is appproached, the theoretical prediction indicates a decreasing stiffening behavior of the specimens, wheras, with the experimental results, this decrease in stiffness is not as dramatic .

This arises because, as previously discussed in Chapter 3, in the model study, the ability of the fibers to preserve the concrete flexural rigidity, after cracking is initiated, is not accounted for in terms of the value of I_e used .

Ashour[38] , proposed a modification to the formula for I_e to account for this stiffening effect, and so one of the directions for future study could be the implementation of this stiffening behavior in the model .

The post-peak slopes, indicated in the plots, have been obtained using a simple empirical analysis (see Chapter 3) .

This was obtained by analysing the results from this experimental program, as well as those due to Shahbazker[24] .

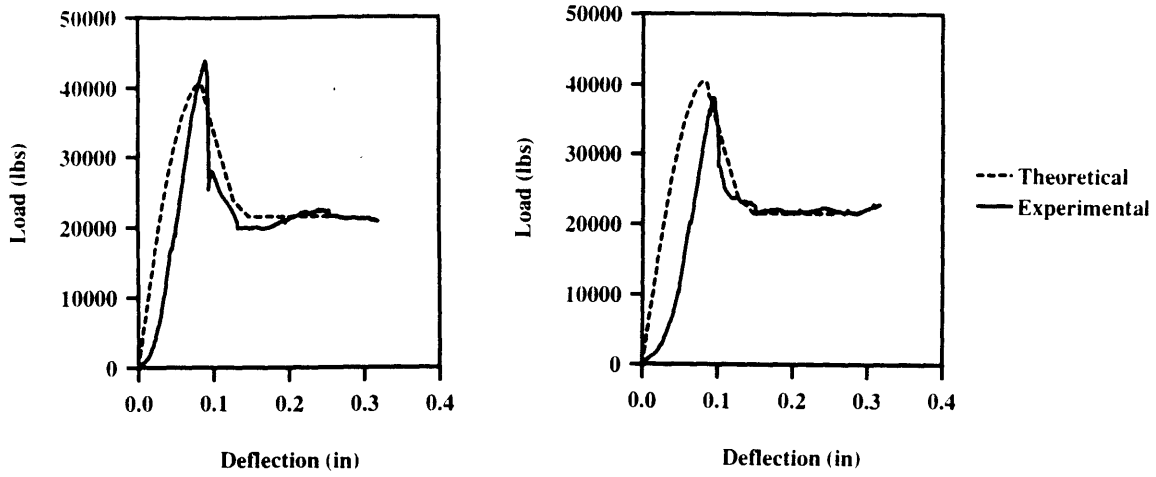

Figure 6-3: Model comparison for $V_f = 0.4\%$

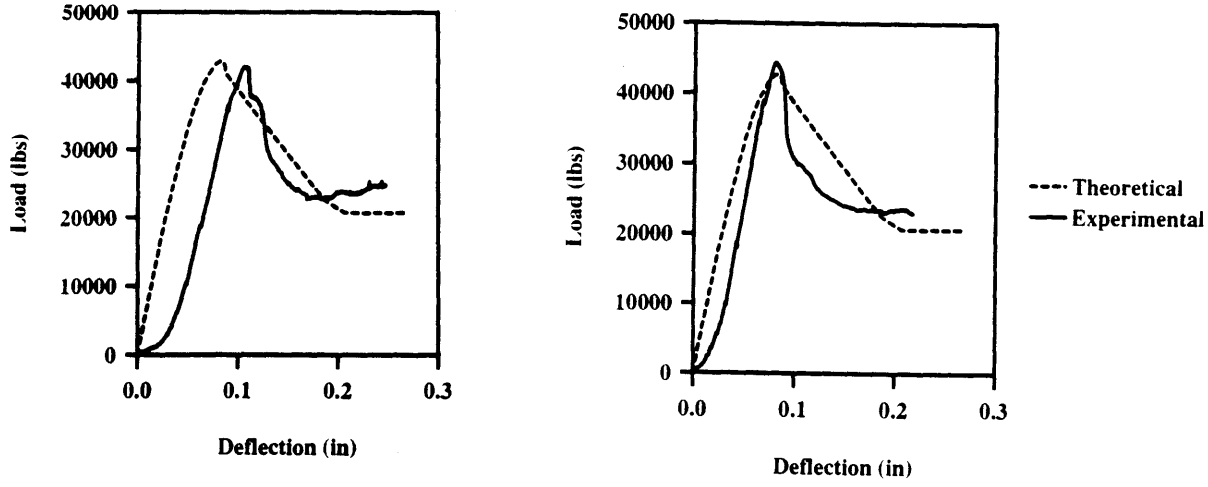

Figure 6-4: Model comparison for $V_f = 0.8\%$

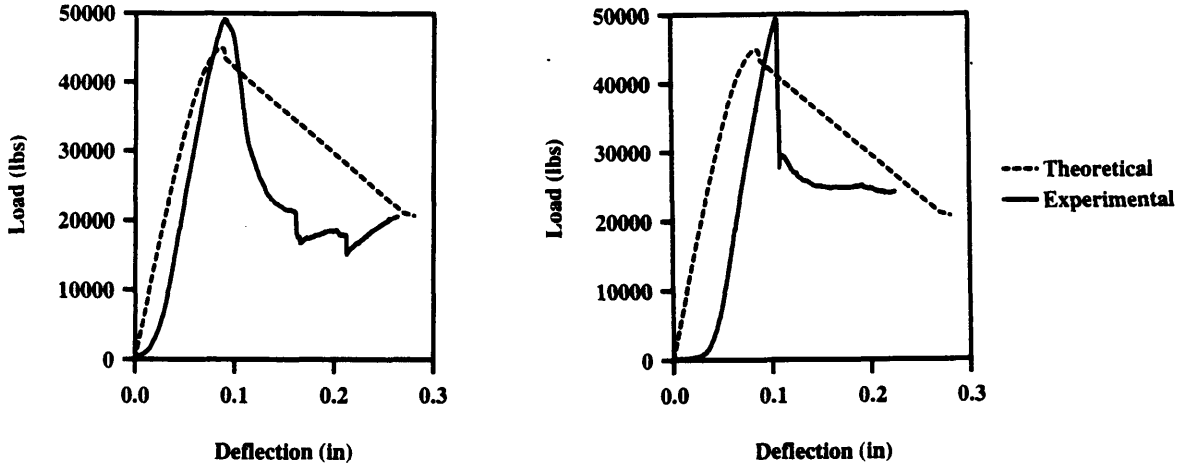

Figure 6-5: Model comparison for $V_f = 1.2\%$

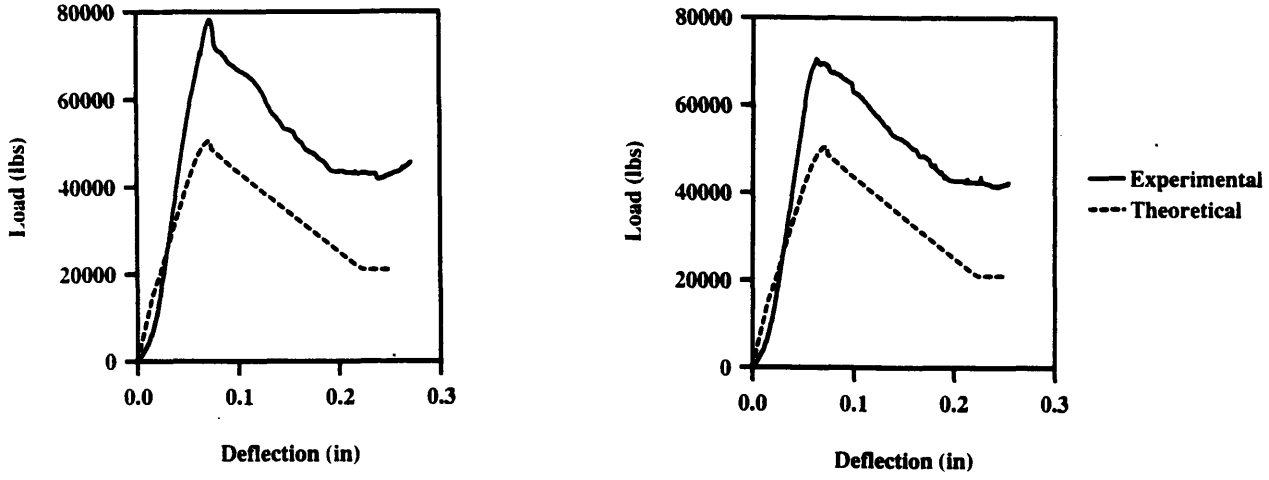

Figure 6-6: Model comparison for $a/d = 0.88$

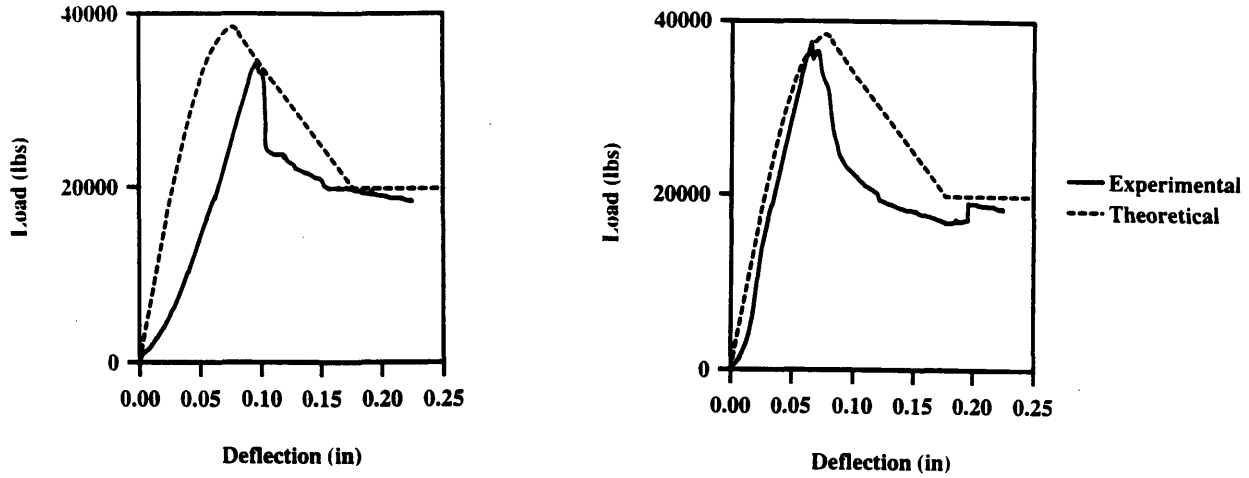

Figure 6-7: Model comparison for $a/d = 1.73$

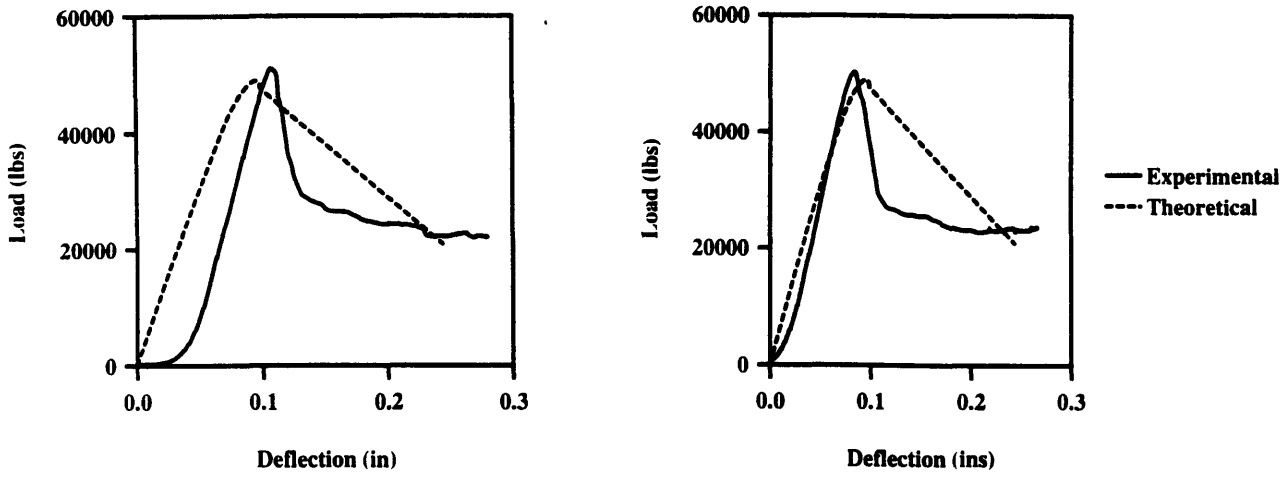

Figure 6-8: Model comparison for hooked end fibers

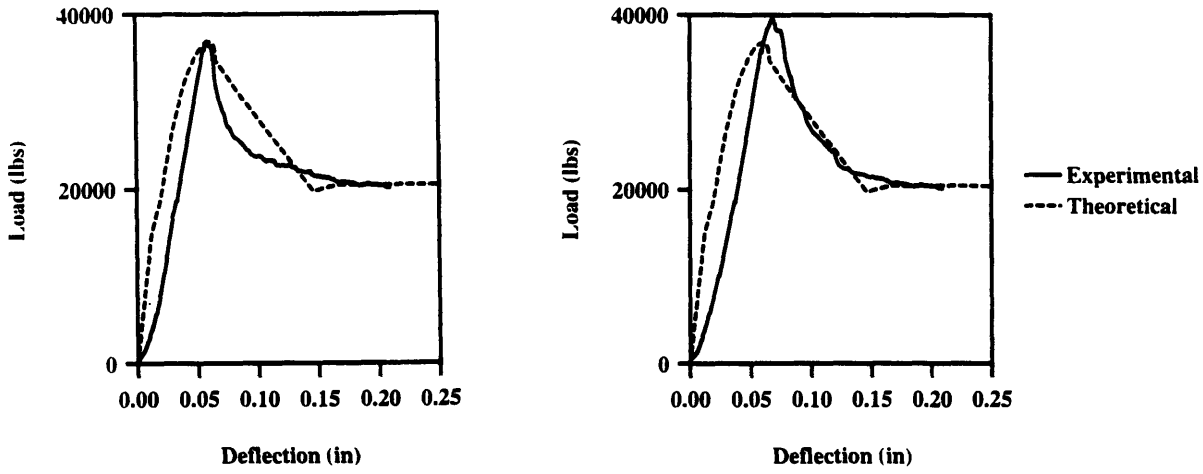

Figure 6-9: Model comparison for straight fibers

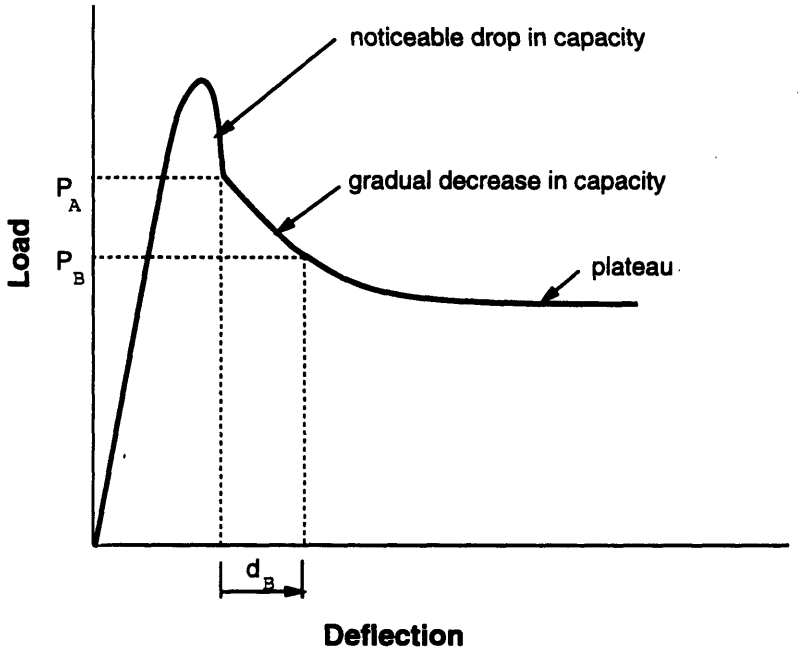

Figure 6-10: Generalised post-peak behavior of specimens

As seen in Figure 6-10, the fiber contribution to the improved post-peak behavior was obtained by subtracting the (approximate) residual dowel capacity from the load at which the post-peak ductility comes into effect . The gradient of the post-peak portion for the various volume fractions was then obtained, and a simple linear formula was used to fit these results for the particular steel fiber type used in this study, of the form (Figure 6-10) :

$$P_B = P_A - 183333.3 \times d_B \times 0.008/V_f$$

This modification to the post-peak behavior of the model was necessary as the model predictions, when this modification was not included, did not correspond to the observed behavior for the post peak portion .

It should, however, be noted that the main purpose of this study was not to study the post-peak behavior of the specimens, but to predict the ultimate capacities of the specimens .

The drop in capacity at peak load, followed by a gradual decrease in capacity, probably arises because the combination of arch, fiber and dowel action are active up to the maximum load, however, on exceeding the corresponding strain, the arch mechanism is no longer active and so the load can only then be supported by the combined dowel and fiber supporting action .

Hence, as the capacity of these two mechanisms is not as great as when the arch action is also present, in a displacement controlled system, it is expected that a drop in capacity will be exhibited, until the residual load can be supported, as observed .

The gradual gradient then results from a combination of further fiber yield and rupture, and pullout of fibers (which will occur for some fibers before the yield strength is reached, even though the bond strength has been improved), and dowel action .

This sudden drop in capacity at peak load was also evident in the tests performed by Shahbazker[24] and Ashour[23] .

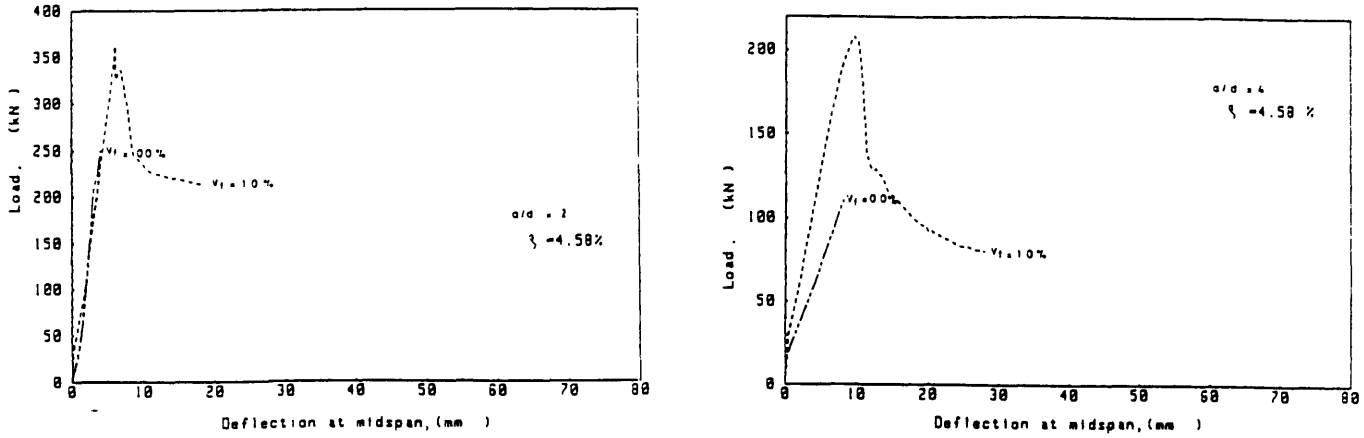

Figure 6-11: Beam tests by Ashour[23]

Indeed, Ashour[23] noted this fact and remarked that "HSFRC beams with low fiber content failed in shear and *exhibited sudden failure at the ultimate stages* " . Beam tests performed by Ashour[23], and illustrative of this behavior, are shown in Figure 6-11 .

Thus the behavior observed in this research program is consistent with the results from past studies .

Valle[8], however, observed noticeable increases in the ductility of push-off specimens at $V_f = 1.0\%$.

This may be explained by the fact that the experimental variable in Valle's push-off tests was the shear strain .

In the beam tests, however, central span deflection results from a combination of shear and flexural strains . Thus, on exceeding the peak load, at a load level below that of the ultimate capacity, while the shear deflection might be increasing, there is a decrease in flexural deflection and, thus, the overall deflection is less than if shear strains were the only contributing factor to the beam deflection (which is essentially

the situation with Valle's tests) .

Comparing the results for the beam tests with different volume fractions of fibers (Figure 6-12 and Figure 6-13), it is seen that as the volume fraction of fibers increases, there is, indeed, a trend of increase in the ductility of the specimens, in terms of the area below the curves .

Most notably, addition of fibers raises the load at which the plateau occurs, thus indicating that, for this portion of the post-peak behavior, both fibers and dowel action are active .

The plateau therefore results from a combination of dowel steel yielding and fiber yielding/pullout, and contributes greatly to an increase in ductility, with reference to the specimen without any fibers .

Also note that the dowel steel ratio is $\rho = 7.08\%$, which is a very high prcentage .

Thus, if we assume that, in a practical specimen, the steel ratio might only be half of this value, then the ultimate dowel capacity would be reduced from approximately 16000 *lbs* at $V_f = 0.0\%$ in Figure 6-12, to approximately 8000 *lbs* .

Therefore, for the specimen with $V_f = 0.4\%$, the increase in plateau load, and hence ductility, would be 50%, as opposed to the current value of approximately 30% (Figure 6-12), thus showing the significant improvement in ductility on the addition of fibers .

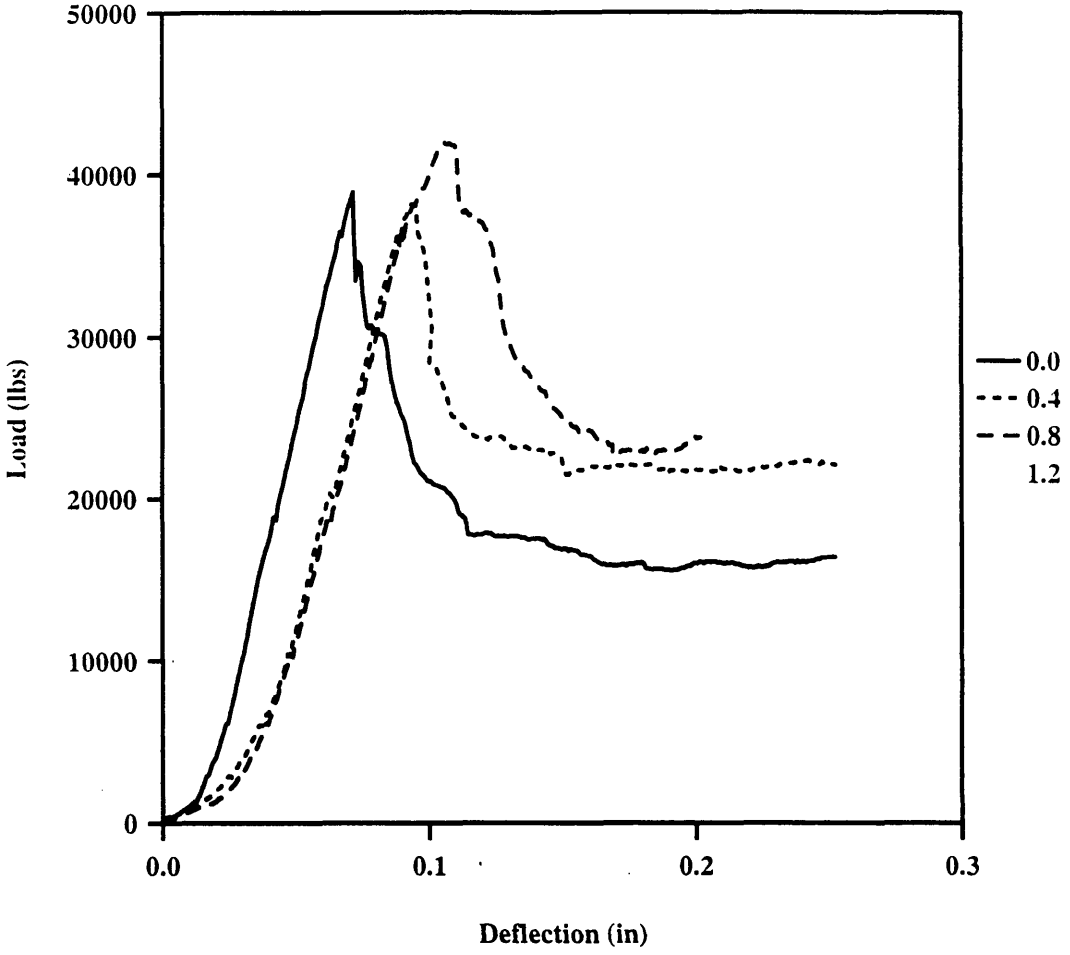

Figure 6-12: Comparison of load-deflection plots for various V_f

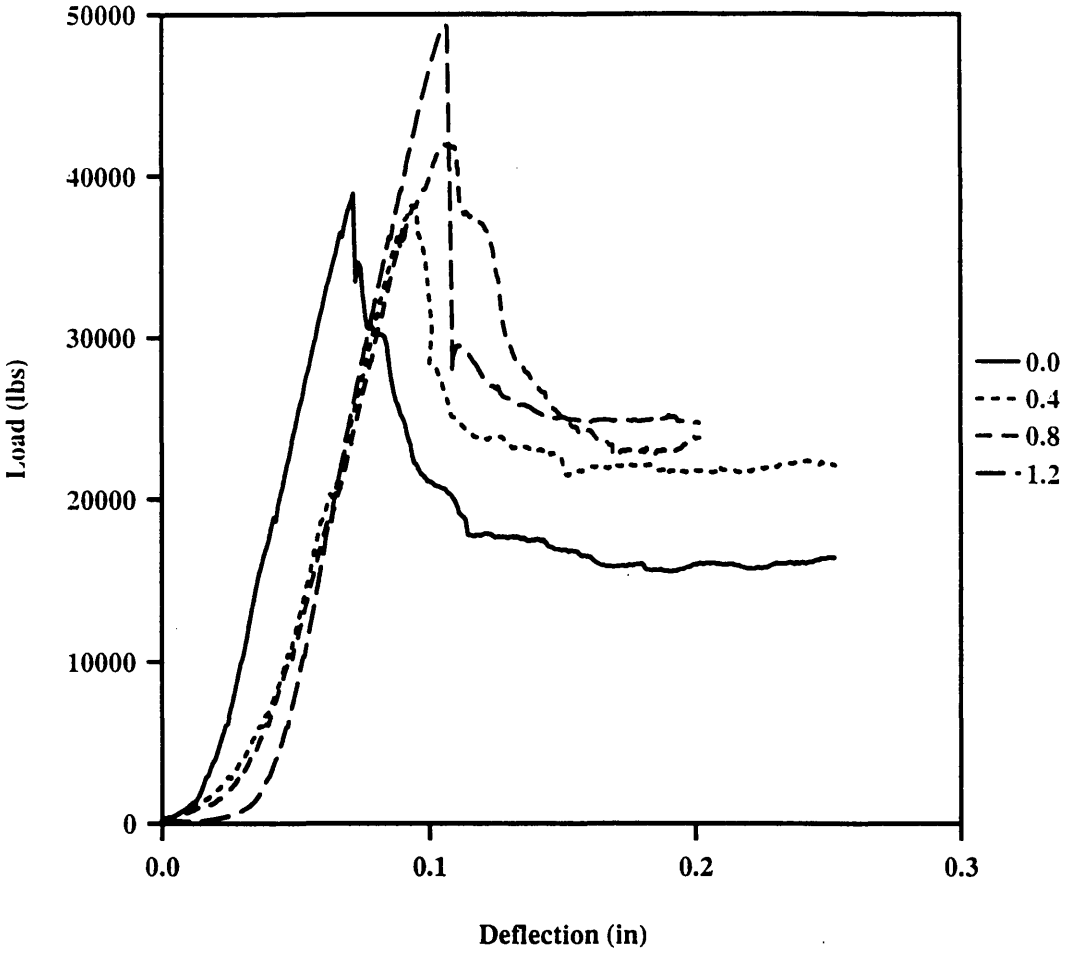

Figure 6-13: Comparison of load-deflection plots for various V_f

Specimen	Observed (lbs)	Predicted (lbs)	As (in^2)
0.0-0	38200	40764	0.000
0.0-1	45200	43922	0.000
0.0-2	48168	47584	0.000
0.4-0	45200	44065	0.029
0.4-1	50072	52207	0.029
0.4-2	52356	54073	0.029
0.8-0	48400	47863	0.065
0.8-1	54832	55438	0.065
0.8-2	57138	57155	0.065

Table 6.2: Application of model to the results from Shahbazker[23]

It should also be noted that when comparing the plots for the theoretical and observed results, the peak loads do not match .

This is because each of the plots only makes a comparison to a single test specimen, and Table 6.1 shows that the results from the model actually offer a satisfactory fit to the average of the two test data obtained for each case .

The predicted peak load deflections also do not correspond in all cases to the observed deflections, and this primarily arises because of the settling in deflection which is incurred in the experimental tests .

A further discussion of the value of ρ_y used will be provided in the following section .

Table 6.2 (first column indicates the V_f as well as the number of stirrups) indicates that the model predictions correlate quite well to the data from other tests, although, Table 6.3 shows that the results for the tests performed by Ashour[38] tend to be overestimated, the exact reason for this not being certain . This suggests the need for a much greater database of results in order to further test the applicability of this model .

a/d	V_f	ρ	Observed (lbs)	Predicted (lbs)
1	0.5	2.84	110984	158413
2	0.5	2.84	58847	103106
1	1.0	2.84	155427	162300
2	1.0	2.84	73987	103556

Table 6.3: Application of model to the results from Ashour[23]

6.2 Discussion of proposed equation for shear strength prediction

While the use of a computer model gives useful insight into the behavior of the deep beam specimens, nevertheless, the development of a design equation would provide a more versatile means of strength prediction to the practising engineer .

Therefore, specific emphasis has been placed in this research program on modifying a practical formula which can readily be used for strength predictions .

6.2.1 Choice of shear equation

In examining the available procedures for shear strength estimation, the formula which appears to offer the best results was proposed by Bazant[26] :

$$v_c = 6.5\,\rho^{1/3}(\sqrt{f'_c} + 3000\,\sqrt{\rho/(a/d)^5})\,\frac{(1+\sqrt{0.2/d_a})}{\sqrt{1+d/25d_a}}$$

$$\begin{aligned} \rho &= \text{longitudinal steel ratio,} \\ d_a &= \text{maximum aggregate size,} \\ \rho_v &= \text{stirrup reinforcement ratio,} \\ 1/\rho_0 &= 400\,(1+\tanh(2\,(a/d-2.8)))\ , \end{aligned}$$

This formula is a modified version of the formula proposed by the same researcher in 1984[25], and is more powerful because it takes into account :

1. not just the size effect of the specimen, but also the effect of the maximum aggregate size,

2. the effect of stirrup action in improving the concrete shear capacity, due to the application of a confining effect on the concrete, and also by offering support to the rebars and thereby improving the dowel contribution .

It should perhaps at this stage be noted that the specimen size effect arises principally because of a release of strain energy from the beam into the cracking zone, as it extends . Thus, as the size of the structure increases, the greater is the energy release into the this zone .

The area of the cracking zone is assumed to be proportional to the maximum aggregate size in this treatment .

The obvious advantage of this formulation is therefore the consideration of the size effect, for even though the formula proposed by Zsuttty and used in practise offers satisfactory predictions, it nevertheless does not account for the size effect .

Therefore, in Zsutty's formulation, as well as in the ACI formulation, as the size of the structure increases, the margin of safety between the predicted and actual failure load decreases, i.e. the factor of safety is not uniform .

Comparison of Bazant's formula to others available for shear strength estimation, confirms its applicability, as shown in Figure 6-14 .

Bazant's formula is also attractive for practical applications because it has been derived largely from theoretical considerations (though some emperical analysis has been utilised), and therefore actual material behavior has been utilised in effecting its derivation .

To implement the equation in design practise, Bazant suggests using a coefficient of 4.5 instead of 6.5, as this leads to a lower bound estimate of the beam shear capacity .

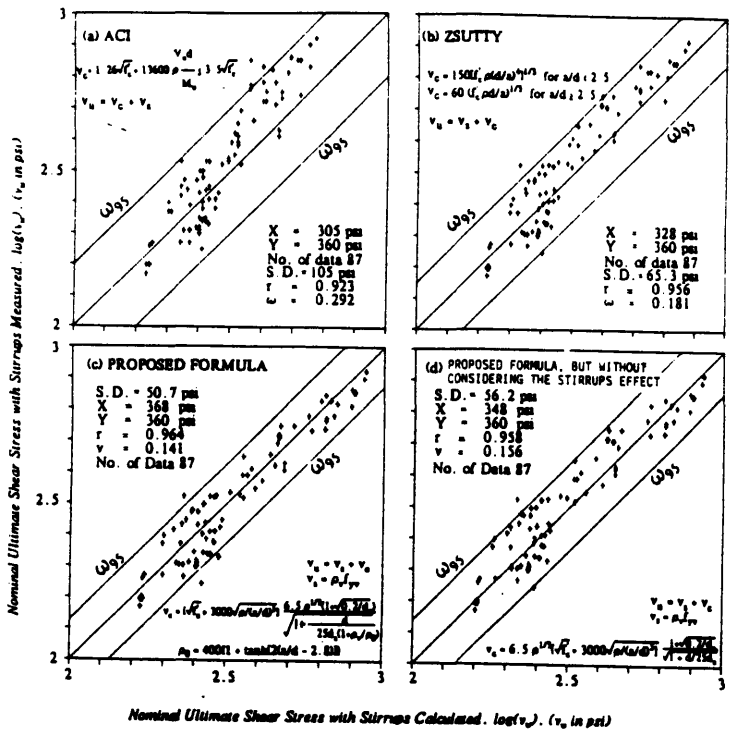

Figure 6-11: Comparison of strength predictions using different formulae[26]

6.2.2 Verification of the applicability of Bazant's formula to HSC deep beams

As mentioned in the previous section, the correlation between Bazant's formula and experimentally observed data is very good, however, the data-base used for the comparison was generally based on normal strength concrete, with $f_c' < 7\,000$ psi .

Therefore, before modifying this formula to account for the beneficial contribution from fibers, it was necessary to validate its applicability to HSC deep beams .

Now, as there is not a large database of results for HSC, the procedure adopted was to use the existing formula to see whether it offerred satisfactory predictions i.e. whether the constants of the equation were adequate .

This was achieved by utilising the deep beam results from tests performed by Ahmad[21] , in which the behavior of HSC beams, with $f_c' = 10\,000$ psi, were investigated .

As seen from Figure 6-12, Figure 6-13, Figure 6-14, Figure 6-15, and from Ta-

Specimen	a/d	ρ	Observed (psi)	Bazant (psi)	Method II
A4	2.3	0.0393	525	485	497
A5	2.0	0.0393	938	572	587
A6	1.0	0.0393	2250	1951	2001
A10	2.3	0.0177	452	317	326
A11	2.0	0.0177	305	362	371
A12	1.0	0.0177	1221	1068	1096
B4	2.3	0.0504	811	572	587
B5	2.0	0.0504	605	680	697
B10	2.3	0.0225	352	370	379
B11	2.0	0.0225	672	424	435
B12	1.0	0.0225	1172	1287	1320
C4	2.3	0.0664	552	674	690
C5	2.0	0.0664	1531	811	832
C10	2.3	0.0326	315	444	455
C11	2.0	0.0326	590	518	532
C12	1.0	0.0326	1353	1695	1738

Table 6.4: Results from tests by Ahmad[21] and predicted strengths (Method II discussed in Section 6.2.3)

ble 6.4, comparison of the observed and predicted results indicate that the formula offers a satisfactory means of prediction for the shear strengths of HSC deep beams .

The results from Elzanaty[22] with $f_c' = 10000$ psi also indicate the capacity of this equation to predict the shear failure loads for deep beams as shown in Table 6.5.

In addressing the issue of why, as the equation implies, the only factor which really determines the ultimate strength of the specimens, when changing from NC to HSC, is f_c', it must be realised that the principal method of shear transfer is through the arch mechanism, the effectiveness of which will ultimately depend on the strength of the concrete, f_c' .

6.2.3 Modification of Bazant's formula

As Bazant's formula has been shown to be valid for application to HC deep beam shear behavior, it is therefore necessary to modify this formula to enable the increase

a/d	ρ	Observed (lbs)	Predicted-Bazant (lbs)	Predicted-Bazant(coef.=4.5) (lbs)
2.0	0.012	35447	41524	28748
2.0	0.025	49281	60382	41803

Table 6.5: Results from tests by Elzanaty[22] (f'_c = 10000 psi)

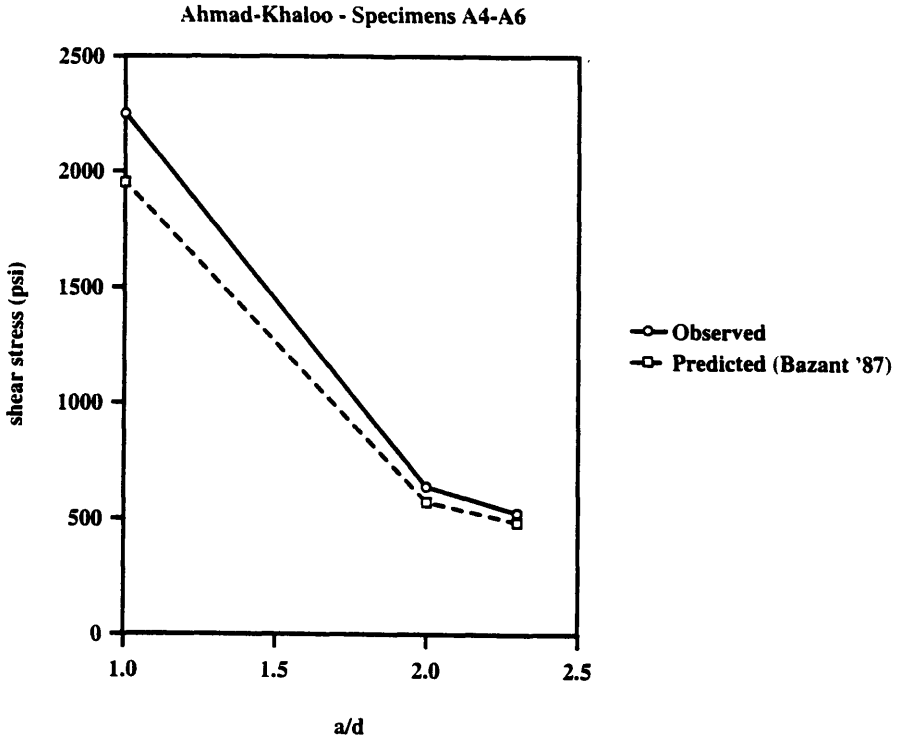

Figure 6-12: Comparison of Bazant's predictions to Ahmad's results

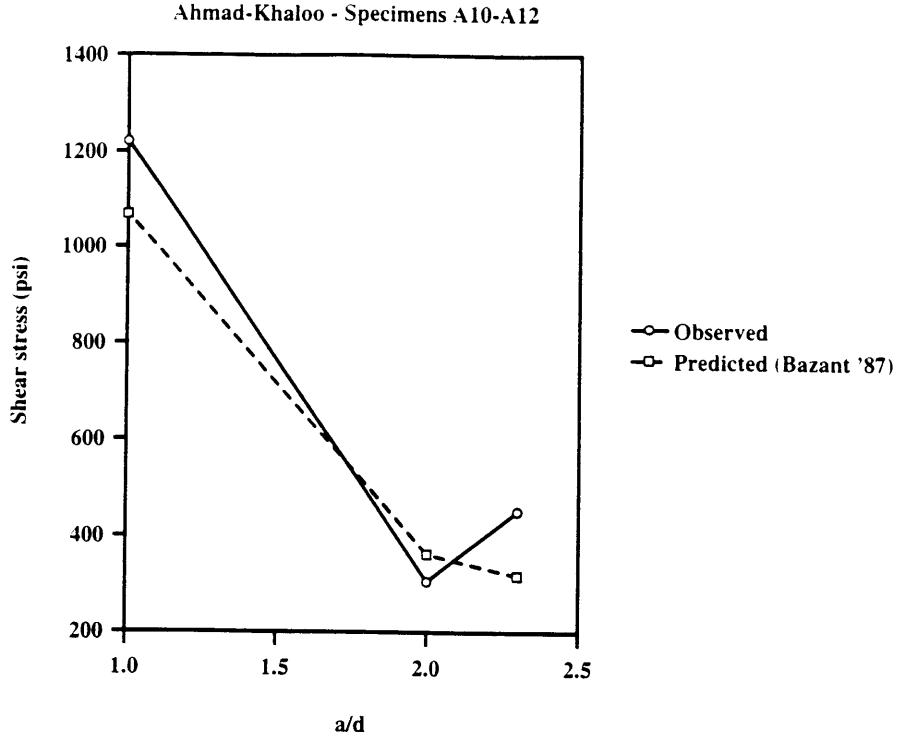

Figure 6-13: Comparison of Bazant's to Ahmad's results

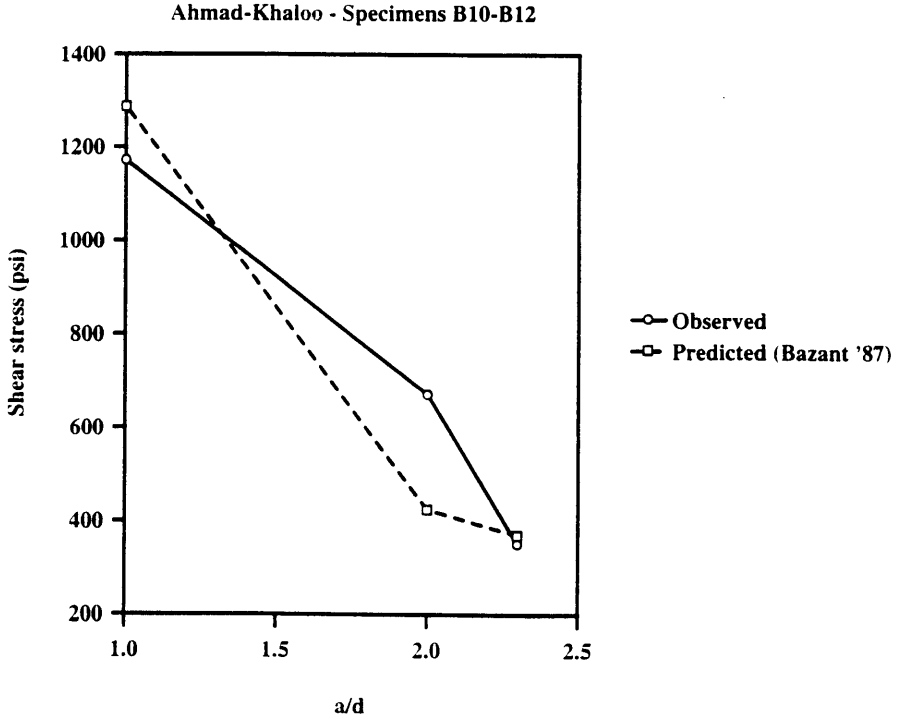

Figure 6-14: Comparison of Bazant's to Ahmad's results

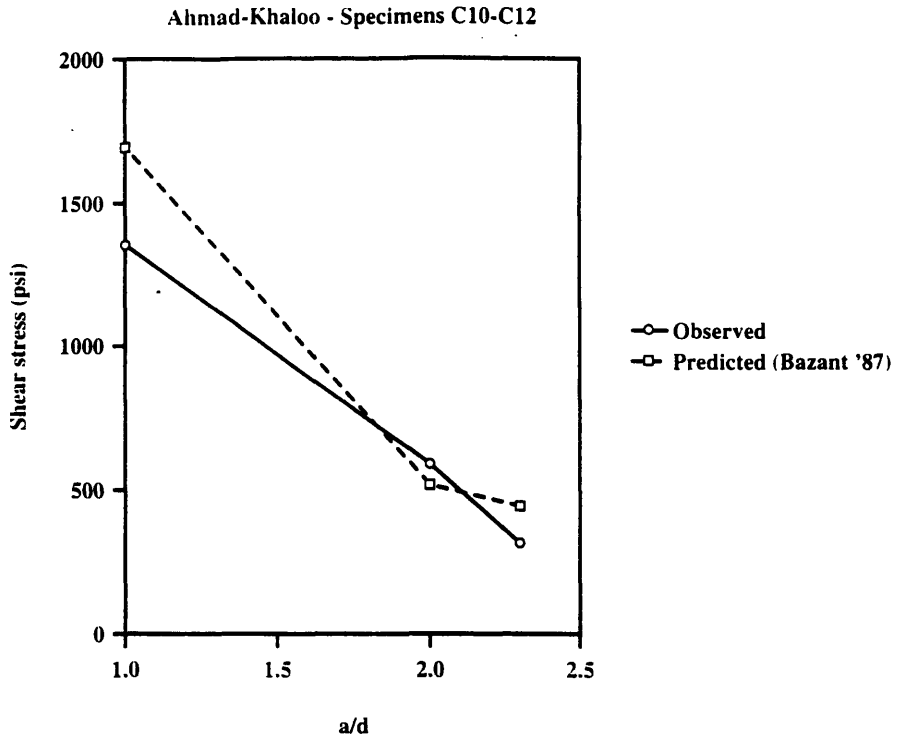

Figure 6-15: Comparison of Bazant's to Ahmad's results

in strength, through the addition of fibers, to be satisfactorily predicted .

In applying Bazant's formula, it is necessary to note that the d_a term in $\sqrt{1 + d/25d_a}$ is actually included to effect the nondimensionalisation of the ratio d/d_a .

Bazant[26] argues that every physically correct formula must be reduceable to a nondimensional form . As the maximum aggregate size, d_a, is the only nondimensionalising constant which is easily defined, it was therefore used for this purpose in the derivation .

The question then arises as to the effect of the maximum aggregate size variation on beams of equivalent depth, since $\sqrt{1 + d/25d_a}$ is meant to only account for the actual specimen size variation .

To account for this effect, Bazant[26] added the modifying term $(1 + \sqrt{0.2/d_a})$ based on a study of the spread of cracks in the contact area wit aggregates, to account for the actual effect of the aggregate size on the specimen behavior .

Now, accepting the modifying term $\sqrt{1 + d/25d_a}$ as being representative of the specimen size effect, the use of the term $(1 + \sqrt{0.2/d_a})$ would not seem applicable to

HSC as the aggregate size is not expected to have any significant effect on the material behavior , as cracks generally propagate directly through the aggregate (Figure 2-6).

For the case of NC, the use of $(1 + \sqrt{0.2/d_a})$ is acceptable as the fracture process zone (concrete is a brittle material characterised by brittle fracture - the tip of a crack is blunted by a zone of micro-cracking that lies ahead of the crack tip) is essentially determined by the material inhomogenieties, but this is not the case for HSC, which is a much more homogeneous material than NC .

If this term is then excluded for HSC, there is also a need to eliminate the introduction of d_a in the expression $\sqrt{1 + d/25d_a}$, as not only would HSC be expected to have a much smaller fracture process zone than NC (and of more constant size as the material is more homogeneous), but also, as previously discussed, the actual aggregate size variation should not have an effect on the strength of the specimens .

Thus, in terms of utilising an expression for predicting the shear response of HSC specimens, there are two options available :

1. Utilise Bazant's 1987 formula, noting that though the theory behind its derivation is not necessarily applicable to HSC, the term $(1 + \sqrt{0.2/d_a})$ offsets the d_a term in $\sqrt{1 + d/25d_a}$, and thereby makes the expression provide more constant results for maximum aggregate size variation at any particular depth - method I .

   In practise, the maximum aggregate size will only vary within a very narrow range of typically 0.75-1.0 in., and therefore this is a satisfactory assumption . Table 6.6 indicates how small an effect the aggregate size variation would have on typical practical specimens of HSC using the 1987 formula (and the formula from method II - see later).

2. Modify the 1987 formula to allow for a constant nondimensionalising term to be used which is not reflective of the maximum aggregate size - method II.

   This is because even if the fracture process zone ahead of the crack tip is treated as a line, a certain characteristic length must be introduced for this zone, if the idea of nondimensionality is adhered to .

a/d	$d_a = 0.5$ in	$d_a = 0.75$ in	$d_a = 1.0$ in	Method II
1.5	423070	440360	449990	43576
2.0	274390	285590	291850	28261

Table 6.6: Predictions for practical sized specimens using 1987 formula and method II formula($\rho = 0.04, f_c' = 10000\ psi, d = 19.6$in.)

Method I - use of Bazant's 1987 formula

As previously mentioned, the contribution from the fibers can be assumed to be two-fold :

1. they cause an improvement in the inherent behavior of the concrete, and

2. they perform the role of stirrups .

Assumption 1 is generally expected (and verified by the values of f_c' and f_{st} etc.) on adding fibers to concrete, and the validity of assumption 2 is indicated in Figure 6-19 .

From the figure it is seen that there is a definite, almost linear, trend in shear strength as the volume fraction of fibers is increased .

While the fibers do contribute to the inherent strength increase of the concrete, this strength increase is not so dramatic as to create such a noticeable increase in the shear strength of the beams .

Therefore some other factor must account for this strength improvement, and this factor is taken to be the effective contribution from the fibers to the truss supporting action i.e. the fibers perform the role of transverse steel .

As $v_u = v_c + v_s$ then the proposed modification to the equation is of the form :

$$v_u = 6.5\,\rho^{1/3}(\sqrt{f_c'} + 3000\,\sqrt{\rho/(a/d)^5})\,\frac{1+\sqrt{0.2/d_a}}{\sqrt{1+\frac{d}{25d_a\,(1+(\rho_v+\rho_f)/\rho_0)}}} + (\rho_v + \rho_f)\,f_y$$

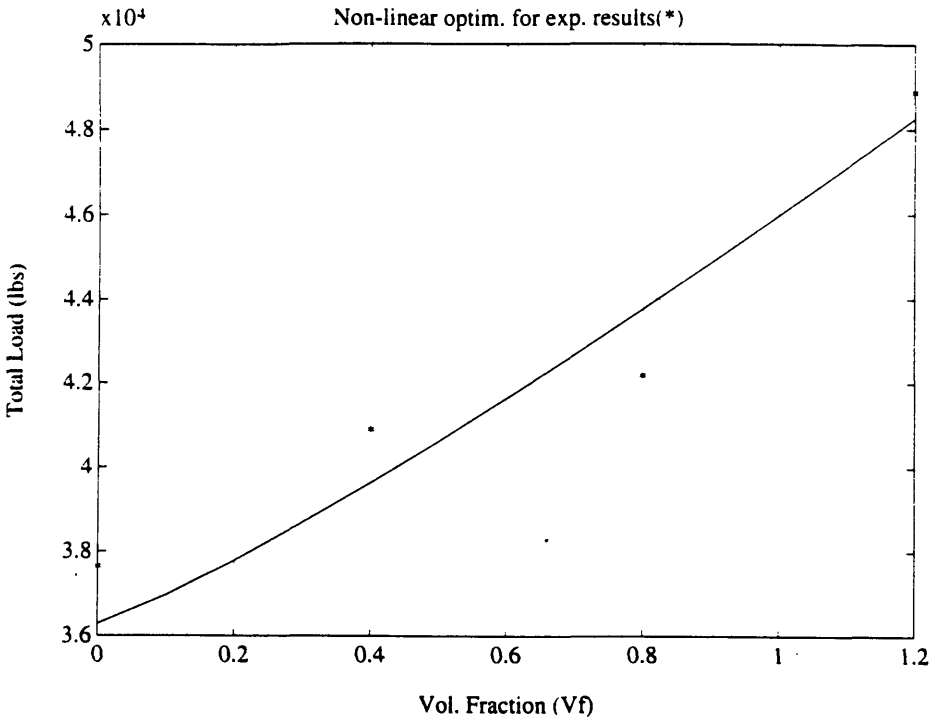

Figure 6-16: Normalised experimental results and non-linear optimal curve

v_u = ultimate shear stress capacity,

v_c = contribution from the concrete,

v_s = contribution from the stirrups,

ρ_f = equivalent transverse steel contribution from the fibers .

Figure 6-16 also shows the results of a non-linear optimization analysis, performed using the 'Matlab' matrix analysis package, to enable the unknown paramater ρ_f to be identified for the particular situation under study .

Analysis, treating V_f as the only variable, resulted in an expression for the unknown variable of the form :

$$\rho = C\, V_f$$

where the coefficient in the expression is actually a function of the fiber and specimen properties .

Therefore, the reason for the large number of variables in the experimental program is identified, for these variations, as well as the results from the studies by Shahbazber[24] and Ashour[23] , enable the variables which influence the value of ρ_f to be determined .

Examination of the results due to Shahbazker indicates that there is a trend of increased fiber contribution as the strength of the concrete increases .

This is taken to result from the fact that, as the strength of the concrete increases, it is expected that the fiber-matrix bond will correspondingly increase (within the strength range used of $f'_c < 15\,000$ psi), thus accounting for the term $\sqrt{\frac{f'_c}{10\,000}}$.

Study of the results for the other variables affecting the behavior of the fibers has led to an expression of the form :

$$\rho_f = \frac{\sqrt{b.s}}{b.d} \left(\frac{l_f}{d_f} F\right)^{0.2} V_f \sqrt{\frac{f'_c}{10\,000}}$$

$$\begin{aligned} s &= a \quad for\ a >= d, \\ s &= d \quad for\ a < d \end{aligned}$$

Valid for $V_f \leq 1.2\%$ and $f'_c < 15\,000$ psi

The fiber effectiveness is given by the term F, and is equal to 1.0 for crimped/hooked end fibers, and 0.5 for smooth-straight fibers .

The term $(\frac{l}{d})^{0.2}$ expresses the influence of the aspect ratio of the fiber on the overall strength increase of the specimens . The small value of the index indicates that the pullout mechanism is not as major a contributing factor to the fiber behavior as in NC .

The term $\sqrt{b.s}$ is essentially related to the overall size of the specimen . It is used to account for the fact that as the size of the specimen increases, so the quantity of fiber 'transverse' reinforcement on the shear plane will correspondingly increase .

The square root reflects the fact that all the fibers are not effective at any one cross section i.e. it includes the contribution from an orientation factor, and as well, as

Specimen	Observed (lbs)	Predicted-6.5 (lbs)	Predicted-4.5 (lbs)	$A_f\ (in^2)$
a1	37585.5	35850	24819	0.000
a2	40993.4	39927	28820	0.032
a3	42377.8	43998	32843	0.065
a4	49225.7	48308	37085	0.099
b1	74443.6	98362	69871	0.048
b2	35953.9	35282	27001	0.070
c1	50691.1	46443	35111	0.080
c2	38237.1	38802	28026	0.031
d1	40379.1	44234	32913	0.061
d2	30980.6	41124	30449	0.054

Table 6.7: Comparison of observed and predicted shear capacities using the modified equation

the beam size increases, the fibers are less likely to be evenly distributed and bonded (as the size of the specimen increases, specimen quality generally decreases), and therefore it helps to account for this size effect . In addition, as all the fibers along the failure plane do not yield at the peak load, it therefore also reflects the equvalent area of failure plane on which yielding occurs .

Table 6.7 (see also Table 4.1) provides the results obtained using this equation (as well as the results obtained using a design coefficient of 4.5 instead of 6.5) .

Comparison of the observed results for the aspect ratio and fiber effectiveness with the predicted results shows that the behavioral trend is correctly captured by this modified version of Bazant's equation (Figure 6-20) .

It should, however, be noted that as the aggregate size was decreased, the strength tended to drop, and not increase, as predicted by the equation . This might result from the fact that, on decreasing the size of the aggregate, the workability of the mix also decreased, consequently affecting the overall shear strength of the specimens . It should also be noted that the observed strength of specimen d0.09 (see Table 6.7) is far below the predicted value, and this is because the decrease in workability when using such small aggregate (of size equivalent to that of sand) was so distinct as to cause a dramatic reduction in strength .

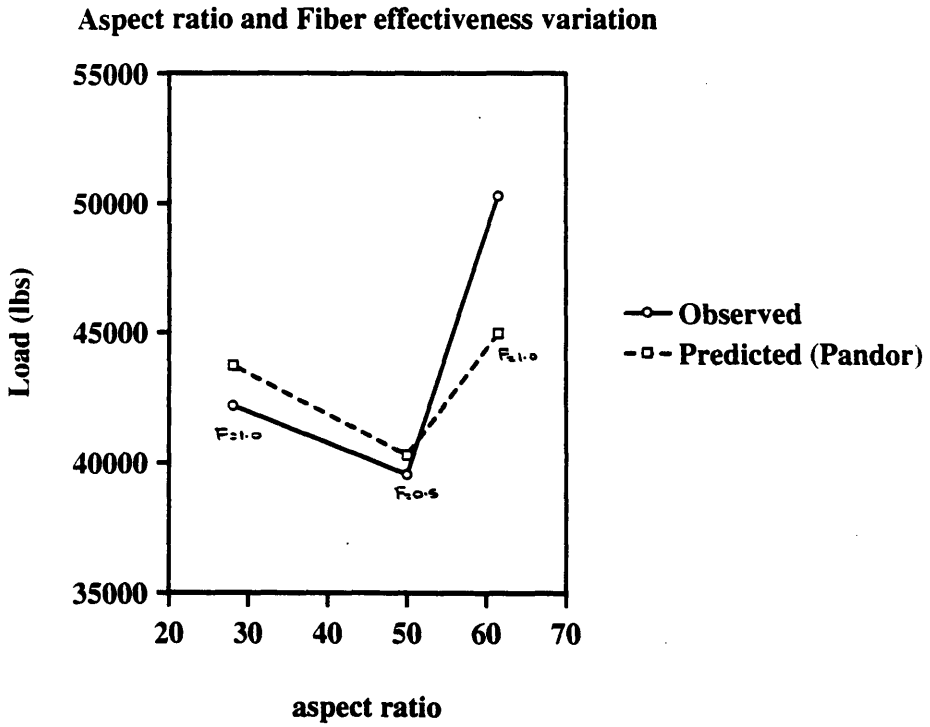

Figure 6-17: Predictions for the fiber aspect ratio and effectiveness variation

The result for specimen d0.25, with only a small drop in strength, might, however, indicate that, as previously discussed, the aggregate size effect is not necessarily significant for HSC, as the cracks pass directly through the aggregate particles . This would therefore indicate that the inclusion of an aggregate size effect term is not necessary in the modified equation, however, as also previously mentioned, further tests would need to be performed in order to confirm this .

Comparison of the predictions to the results obtained by Shahbazker (Figure 6-18, Figure 6-19, Figure 6-20, and Figure 6-21) indicate that the modified equation again allows for satisfactory correlation to the observed trends .These results are also provided in Table 6.8 .

With two stirrups, however, it is seen that the equation tends to overpredict slightly the observed strength of the specimens .

This probably results from the fact that in practise, Shahbazker[24] observed that in these cases the stirrups had not yielded at failure, wheras, in applying the modified equation, it is assumed that the stirrups have yielded .

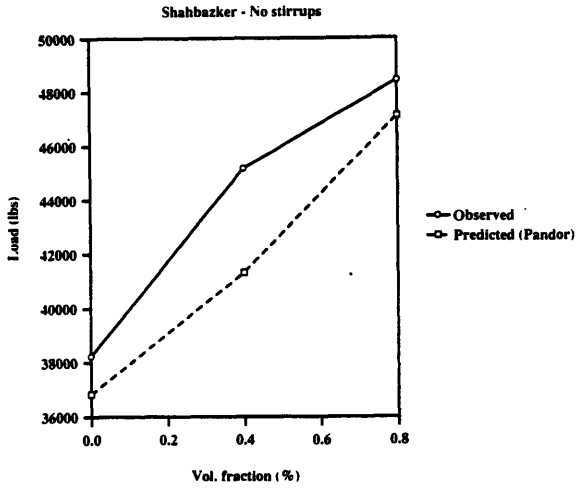

Figure 6-18: Application of modified equation to tests performed by Shahbazker for volume fraction variation

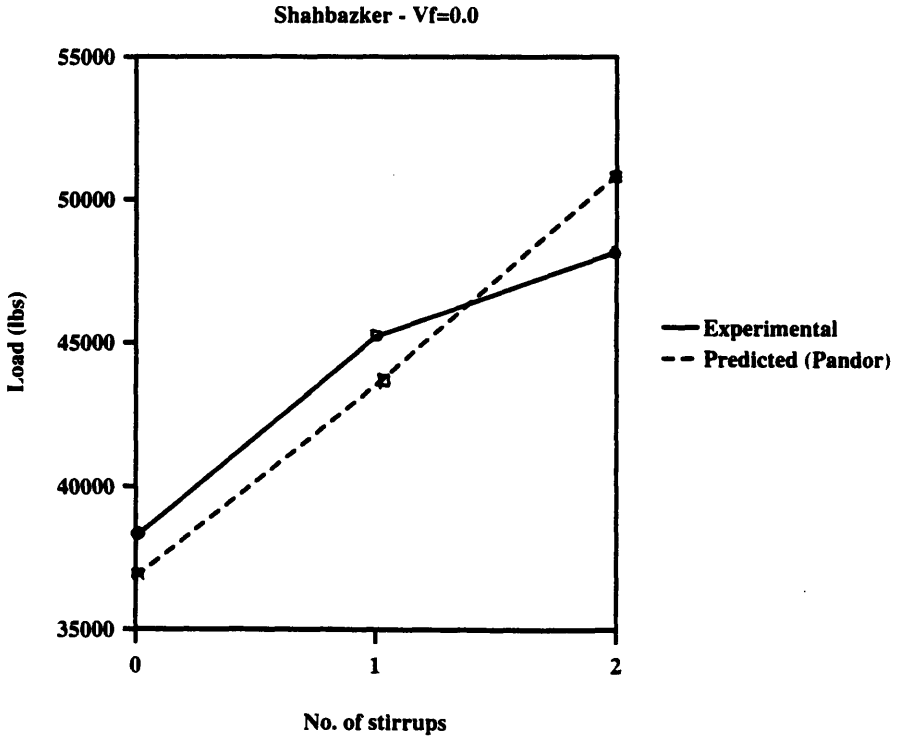

Figure 6-19: Application of modified equation to tests performed by Shahbazker for $V_f = 0.0\%$

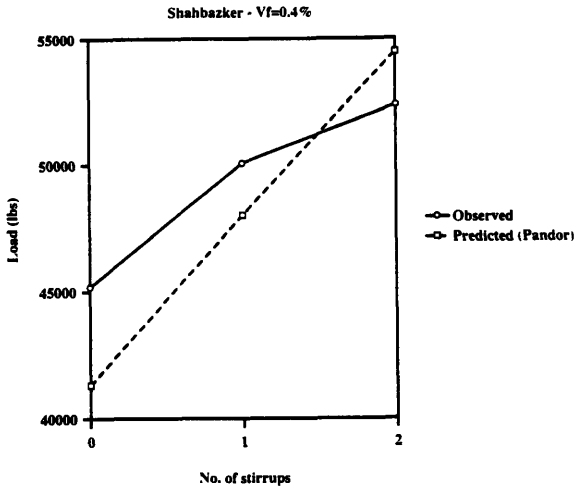

Figure 6-20: Application of modified equation to tests performed by Shahbazker for $V_f = 0.4\%$

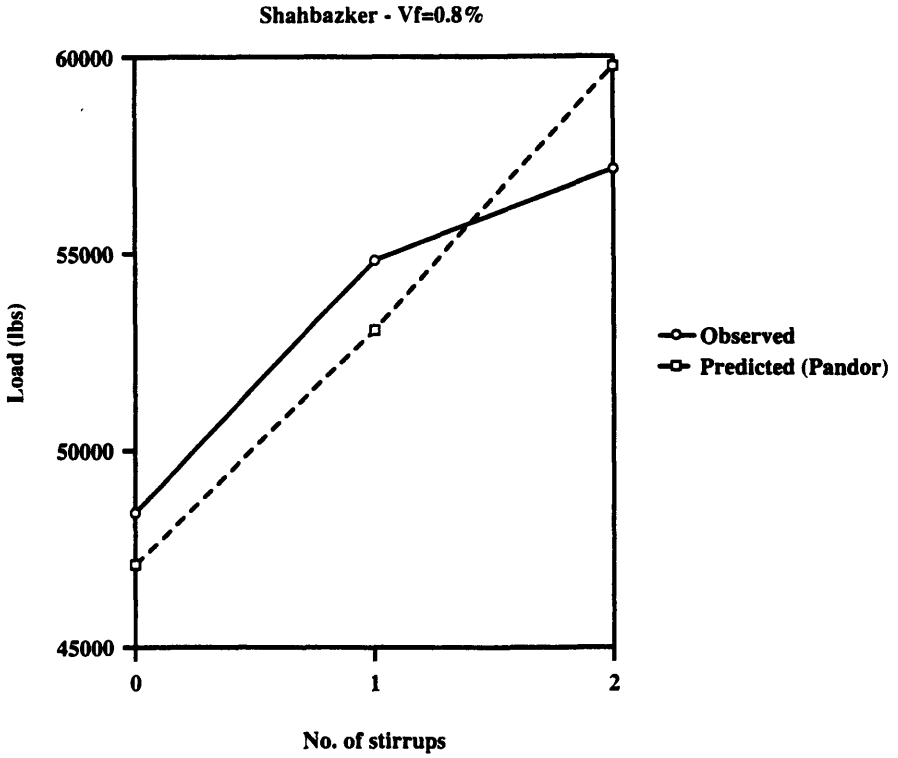

Figure 6-21: Application of modified equation to tests performed by Shahbazker for $V_f = 0.8\%$

Specimen type	Observed (lbs)	Method I	Method II
HB-0.0-0	38200	36827	36862
HB-0.0-1	45200	43522	43537
HB-0.0-2	48168	50848	50843
HB-0.4-0	45200	41319	41306
HB-0.4-1	50072	48013	47980
HB-0.4-2	52356	54465	54413
HB-0.8-0	48400	47119	47050
HB-0.8-1	54832	53063	52979
HB-0.8-2	57138	59753	59649

Table 6.8: Shahbazker's test results and modified equation predictions

a/d	V_f	ρ	Observed (lbs)	Method I	Method II
1	0.5	0.0284	110984	143020	147880
2	0.5	0.0284	58847	60413	62092
1	1.0	0.0284	155427	154020	158070
2	1.0	0.0284	73987	75405	77307
2	1.0	0.0458	82171	89017	91680

Table 6.9: Ashour's test results and modified equation predictions

Applying the modified equation to the test specimens used by Ashour[23] provides the results shown in Table 6.9 .

It is again seen that the correlation between experimental and observed values is excellent, and this is shown graphically in Figure 6-25 .

The proposed equation therefore satisfies the available test data for HSFRC specimens .

Method II - Replacement of d_a term

In this method, it will be attempted to replace the d_a term in the 1987 equation (Bazant[26]) with a constant which reflects the fracture process zone length for HSC beams .

Bazant[39] arrived at a value for a term d_0, which is related to the length of the fracture process zone (and the specimen geometry) at $f'_c = 12400$ psi . While it

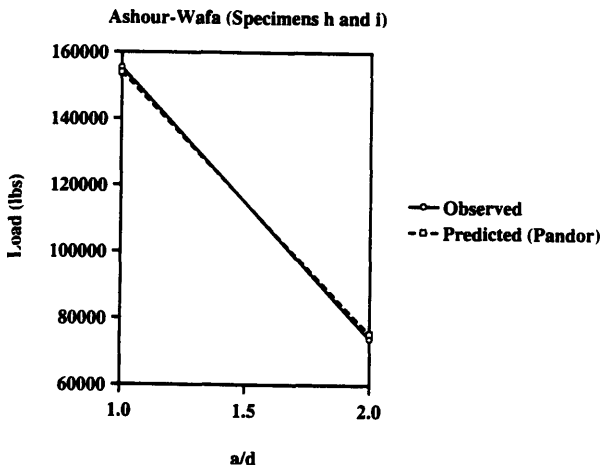

Figure 6-22: Application of modified equation to tests performed by Ashour

would be expected that this value would decrease as the strength of the concrete increases, and therefore the concrete becomes more brittle, it is not expected that this decrease would become too dramatic, and therefore this term will be used as the constant in the size effect expression .

It is also noted that the magnitude of d_0 (0.52 in) is of the same order of magnitude as the maximum aggregate size .

This implies that the other constants will not be dramatically affected by the replacement of the d_a term by d_0 in order to arrive at a reasonable correlation between the experimental readings and the predicted values .

As the trend of strength increase on inclusion of fibers will be the same for either method I or method II, then the contribution from the fibers to the strength of the specimens will be the same using either method, and so ρ_f does not change .

Therefore the modified equation by method II is of the form :

$$v_u = \frac{10.8}{\sqrt{1 + \frac{d}{25 d_0 \, (1+(\rho_v+\rho_f)/\rho_0)}}} \rho^{1/3}(\sqrt{f'_c} + 3000 \sqrt{\rho/(a/d)^5}) + (\rho_v + \rho_f) f_y$$

Comparison of the predictions of this formula to the observed data (Table 6.10, Table 6.9, Table 6.4 and Table 6.8) indicate that the correlation between the results

Specimen	Observed (lbs)	Predicted-Method II (lbs)
a0.0	37585.5	35885
a0.4	40993.4	39950
a0.8	42377.8	44009
a1.2	49225.7	48307
b0.93	74443.6	98406
b1.73	35953.9	35289
c61.5	50691.1	46449
c50.0	38237.1	38825
d0.25	40379.1	43346
d0.09	30980.6	41139

Table 6.10: Comparison of observed and predicted shear capacities using method II

is very satisfactory and the predictions are indeed extremely close to those using method I (typical graphs to illustrate the closeness of fit for method II were not plotted for this reason .) .

Returning to the model used, and examining the value for ρ_y used in trying to fit the observed data to the predictions, it is seen, by comparing Table 6.1 to Table 6.7, that the expression for ρ_y could be of the form :

$$\rho_y = 0.82 \frac{\sqrt{b.s}}{b.d} (\frac{l_f}{d_f} F)^{0.2} V_f \sqrt{\frac{f'_c}{10\,000}}$$

Thus, while the values of ρ_y and ρ_f do not exactly correspond, they are nevertheless very close in magnitude, and this further tends to support the use of the expression for ρ_f in the modification to Bazant's equation .

The use of a coefficient of 4.5 instead of 6.5 (Table 6.7) in method I allows for a higher degree of safety when applied to actual design practise . Indeed the predicted results were all on the conservative side when compared to the experimental observations, even for the cases with two stirrups .

The application of the same safety margin to method II would again yield consistent results .

Chapter 7

Summary, conclusions and recommendations for future work

7.1 Summary

In the experimental program of this research study, the behavior of HSFRC deep beams was studied when the experimental variables of a/d, V_f, l/d, and d_a were varied .

Overall 22 specimens were tested, with 4 concrete cylinders being tested under splitting tensile loading and direct compression for every 2 beams cast .

In the theoretical program, an existing shear truss model was modified in order to incorporate the effect of HSC, as opposed to NC, and also to include the contribution from the fibers to the specimen behavior .

An existing shear strength equation for NC was also modified to enable the shear strength of HSFRC deep beam specimens to be predicted .

7.2 Conclusions

7.2.1 Experimental

1. Some workability problems were incurred in trying to achieve a 28 day compres-

sive strength of $12000\,psi$, which necessitated the use of lower strength concrete of $f_c' = 10000\ psi$. This was thought to result mainly from the effectiveness of the mixer used in this study, which did not offer the advantage of a pressurised container, and relied on gravitational action for mixing .

At the water/cement used for this lower strength mix, satisfactory workability was, however, attained .

2. Compared to plain NC, the post-peak softening behavior of plain HSC is dramatically reduced .

   This was clearly observed in the compression tests, and in the actual beam shear tests, where nominal post-peak 'ductility' was observed . This primarily results from the less distributed cracking in HSC compared to NC, and to the ability of the cracks to pass directly through the aggregates, which are therefore unable to perform a crack-arresting role .

3. As noted above, the cracks in HSC were observed to pass directly through the aggregates when propagating, instead of around them . This therefore indicates an improved fracture toughness of the aggregate-mortar interface when compared to the fracture toughness of the aggregate .

4. A trend of increased compressive strength (approximately $200-300\,psi$ for every 0.4% of fibers added) was observed on adding fibers to the HSC .

   The splitting tensile strength also showed this trend of improved strength on addition of fibers, and a comparison of the f_{st} and f_c' values indicates that the ratio f_{st}/f_c' for the HSC is not as high as would be expected for NC . This indicates that though an improved tensile strength is observed for HSC, the increase in tensile strength does not occur at the same rate as the increase in the compressive strength .

5. The beams generally failed by the development of a crack at mid-depth, which eventually propagated to the supports, resulting in a loss in the supporting arch transfer mechanism .

Cracking began at approximately 20000 *lbs* for all the beams tested . As fiber action occurs mainly in the post-cracking region when the fibers bridge across cracks that have propagated within the matrix, this almost constant value of first cracking load is expected, as the fibers do not therefore have a significant influence on this load .

6. Addition of fibers to HSC causes a substantial increase in shear strength (for $V_f = 1.2\%$, shear strength increase = 30%), for the range of fiber volume fraction investigated in this testing program (It should be noted that Shahbazker[24] obtained only nominal improvements in shear strengths on adding fibers to NC) .

   This suggests an improved bonding of the fibers to the HSC matrix, and that the fibers are performing the role of pseudo-stirrups .

   The experiments also show that the hooked ended fibers, with the largest aspect ratio, are most effective in increasing the shear strengths of the beams .

   The aggregate size effect tests performed were inconclusive .

7. The post-peak behavior of the beams may be divided into three categories :

   - an initial drop in capacity as the arch mechanism terminates,
   - a gradual decreased capacity, during which period the fiber and dowel action are contributing to the load carrying capacity, and
   - a final plateau dominated by dowel yielding and fiber yielding/pullout .

8. Addition of fibers caused an improvement to the post-peak ductility of the beams, as more fibers were available to contribute to the load carrying capacity . This fact is of significance to construction in seismic regions, where the energy absorption capacity of a structure is very important .

9. The addition of fibers caused the specimens to maintain total integrity for the compression and splitting tensile tests . The same observation was made for the shear tests, and in addition , with fibers, the ultimate load was not characterised by a loud noise, as the capacity diminished .

7.2.2 Theoretical

From the discussion presented in Chapter 6, the following conclusions are drawn :

1. The modified shear truss model applied to HSFRC may be used successfully to investigate the behavior of these specimens, in terms of the prediction of the peak loads, and the corresponding central point deflections .

2. The equation proposed by Bazant[26], may be successfully modified to account for the behavior of HSFRC specimens .

   As the aggregate size effect has not been established for HSC, two formulae have been provided for this purpose .

   The first formula includes the aggregate size effect, but the presence of the aggregate variable in two sections of this equation, essentially leads to the effects balancing each other i.e. maximum aggregate size variation for the same specimen depth does not have a dramatic effect on the specimen strength .

   The second formula does not include the effect of maximum aggregate size variation, and this is achieved by the replacement of the maximum aggregate size term by a constant related to the length of the fracture process zone .

   The fracture process zone, in this treatment, is quantified as being constant in size because HSC is a much more homogeneous material than NC, and therefore, as the fracture zone is generally related to the inhomogenieties in the material, then it is not expected that the size of the fracture process zone will vary much for HSC specimens .

   In both the model and the proposed equations, the fiber behavior has been treated as leading to an inherent increase in the strength of the concrete, through a crack arresting mechanism, and also, as performing the role of stirrups across the shear plane, and the experimental program allowed for the equivalent area of transverse steel provided by the fibers to be quantified .

3. The experimental variations in a/d, l/d, F, d_a and V_f were performed in order to validate the model and the proposed equations . It is seen that the model and equations offer very satisfactory predictions for these various cases .

   It should, however, be noted that the model and equations do not provide good estimates for $a/d < 1$, and therefore should not be applied to these situations .

4. Application of the model and the proposed equations to the results from other studies on HSFRC deep beam behavior indicate that the model, and especially the proposed formulae, predict results which correlate very closely to the observed data .

   They therefore provide the basis for the use as tools in practical design applications .

7.3 Recommendations for further study

Several areas may be identified which need further study in order for a more complete understanding of the behavior of HSFRC beams to be attained :

- Aggregate sizes for larger specimen should be varied in order to verify the effect of aggregate size on specimen behavior .
- The V_f of fibers should be increased above 1.2% in order to determine the limit of applicability of the proposed formulae and to investigate any further change in the post-peak behavior of the specimens .
- The post-peak behavior of deep beam specimens needs to be modelled more accurately .
- A wider database of specimen test results is needed, as current data is very limited .
- Practically sized specimens need to be tested to verify the applicability of the proposed relationships, especially with respect to the specimen size effect .

- The behavior of test specimens with $f_c' \geq 14000$ psi must also be investigated as current tests have been limited to lower strengths .

- Research must be extended into the area of HSFRC slender beams ($a/d \geq 2.5$), as these are the members principally used in structural practise .

Appendix A

Computer model

C program model for the behavior of HSFRC .

```
#include<stdio.h>

#include<math.h>


main()

{

 FILE * fpo ;


 int m,n,check,k   ;

 double fc=9052.6,b=3.0,h=4.5,dv=2.52,stu,sqlamda,lamda,a1,a2  ;

 double ex,ey,er,ed,load,txy,fr,Ig,d=3.75,yt,Mcr,Ma,Mu,Icr,kd,Ie,delta,Ect;

 double Ec,fcr,v,e0=0.003,sd,sr,Be,ecr,fx,fy,prod  ;

 double Es = 29e6,sx,sy,rh,rhy,S,nbars=3,T,Vf ;

 double gxy,sum,K,a=3.5,ans1,ans2,load1,delta1,disp ;

 double db=0.583,fb,c,Kf=1e6,sqgdow,gdow,Du,totaldow,Su,D ;


 /* s=sigma a=alpha rh=area_steel gxy=shear_strain e=epsilon Be=par._beta

   db=ave._bar_diam. c=crushed_zone Du=ult._dow. Kf=conc._fndtn._mod.

   Su=peak_dow._defl. D=actual_dow._load*/


 /* note that used a positive e0 above - modify below, as tension +ve */


 /* note dv used */


 Vf = 0.8 ;
```

```
stu = 0.41*0.82*(Vf/100)*1*600/(2*4.42e-3);

Ec = 40000*sqrt(fc) + 1000000 ;

fcr = 7.5*sqrt(fc) ;

ecr = fcr/Ec;

K = dv/h*(h/a*(4/3-2/3*a/h)) ;

fy = 60000 ;

fr = 7.5*sqrt(fc) ;

Ig = b*h*h*h/12 ;

yt = d/2.0;

Mcr = fr*Ig/yt ;

Mu =  26000*5.5 ;              /* mom. capacity of section - check!! */

Ect =  0.4*(Ec*(100-Vf) + Es*Vf*0.41*0.82)/100.0  ;

sqgdow = sqrt(Es/(Kf*db)) ;

gdow = sqrt(sqgdow) ;

fb =154*sqrt(fc)/cbrt(db) ;

fb = 18434.5 ;

load1 = 0.0 ;

rh = 0.797/(b*d) ;

rhy = (0.053)/(b*d)*Vf/0.8 ;   /* note well !!!!!!!!!!!!!!*/


fpo = fopen("moda2.mat","w");

if(fpo == NULL)   /* check for opening error */
```

```
 {
  printf("File opening error\n");
  exit(-1);
  }

for(ed=-0.0002;ed>-0.0046;ed = ed - 0.0001)
 {
  ans2 = 1000000.0 ;

        for(er=0.00001 ; fabs(ans2) > 0.05 ; er = er + 0.00001)
         {
           printf("c\n");
           sqlamda = 0.7-er/ed;
           lamda = sqrt(sqlamda);

/* compute stress using stress-strain conditions -
    remember to use appropriate part of stress-strain curve */

           if(-ed < (e0/lamda) && ed < 0.0000)
   /* sd */    sd = -fc*(2*ed/-e0-lamda*ed*ed/(e0*e0));

   /* tension +ve,  so fc -ve */

           if(-ed > (e0/lamda) && ed < 0.0000)  /* post peak */
```

```
        sd = -fc/lamda*(1-(ed/-e0-1/lamda)*(ed/-e0-1/
                lamda)/((2-1/lamda)*(2-1/lamda)));

      if(ed < ecr && ed > 0.0000 )
        sd = ed*Ec ;

      if(ed > ecr && ed > 0.0000 )  /* post peak */
      {
       Be = sqrt((ed-ecr)/0.005) ;
       sd = (fcr+Be*stu)/(1+Be);
          }

      if(er < ecr && er > 0.0000 )
/* sr */  sr = er*Ec ;

      if(er > ecr && er > 0.0000 )  /* post peak */
      {
       Be = sqrt((er-ecr)/0.005) ;
       sr =0.2*(fcr+Be*stu)/(1+Be);
          }

      if(-er < (e0/lamda) && er < 0.0000)
        sr = -fc*(2*er/-e0-lamda*er*er/(e0*e0)) ;
```

```
if(-er > (e0/lamda) && er < 0.0000)  /* post peak */
  sr = -fc/lamda*(1-(er/-e0-1/lamda)*(er/-e0-1/
            lamda)/((2-1/lamda)*(2-1/lamda)));


  a1=acos(sqrt((sr+rh*Es*er)/(sr-sd+rh*Es*(er-ed)))) ;
  ex =  ed*cos(a1)*cos(a1)+er*sin(a1)*sin(a1);
  ey = ed*sin(a1)*sin(a1)+er*cos(a1)*cos(a1);

   if(fabs(ex) > fy/Es )
      a1 = acos(sqrt((sr+rh*fy)/(sr-sd))) ;

   ans1=(sd*(K*sin(a1)*cos(a1)-sin(a1)*sin(a1))-rhy*Es*ey)/
         (K*sin(a1)*cos(a1)+ cos(a1)*cos(a1)) ;

   if( fabs(ey) > fy/Es )
      ans1=(sd*(K*sin(a1)*cos(a1)-sin(a1)*sin(a1))-rhy*fy)/
         (K*sin(a1)*cos(a1)+ cos(a1)*cos(a1)) ;

ans2 =  (sr - ans1)/sr ;

printf("fb %lf  er %lf  ed %lf\n",fb,er,ed) ;
```

```
}

if( fabs(ey) < fy/Es )
  prod = Es*ey ;
else
  prod = fy ;

sy=sd*sin(a1)*sin(a1)+sr*cos(a1)*cos(a1)+rhy*prod ;
gxy = 2*(ed-er)*sin(a1)*cos(a1);
txy = sy/K ;
load = -txy*b*dv ;

/* dowel calcs. */
c = 0.05*fy*db*sin(a1)/fc ;
T = Ma/(dv*rh*b*d) /* Ma/Mu*60000*/ ;
/* tension in each bar*/
Du = 2*nbars*(0.5*fb*(0.37*gdow*db-c)*(0.37*gdow*db-c)
      + 0.45*fy*db*db*(1-T*T/(fy*fy))/gdow) ;
/* Du is 2*load for one section */

Su = 4.26/1e6*Du/2.0 + 0.00945 ;
S = -gxy*dv ;
```

```
            if( S < Su )
              D = Du*sqrt(S/Su) ;
            else
            {
              D = Du-Du*(S-Su)/(0.4/db-Su) ;
              if( D < 0.4*Du )
                D = 0.7*Du ;
                  }

            totaldow = D ;

            load = 2*load + totaldow ;

/* deflection */ Ma = a*load/2.0 ;
            kd = fy*rh*b*d/(b*fc) ;
            Icr = Mu*kd/fc ;

            if( Ma < Mcr)
              Ie = Ig ;
            else
              Ie = (Mcr/Ma)*(Mcr/Ma)*(Mcr/Ma)*Ig +
                   (1 - (Mcr/Ma)*(Mcr/Ma)*(Mcr/Ma))*Icr ;
```

```
if(load1 > load)
  Ie = Icr ;    /* for large deflections */

load1 = load;   /* update this check */


delta = 601.59*(load/2.0)/(6*Ect*Ie) + - gxy*dv ;

if(delta1 < delta )
        {
fprintf(fpo,"%lf  %lf   %lf   %lf   %lf   %lf\n",
           Du,Su,D,load,delta,gxy);
        }


if(delta1 > delta || ed == -0.0046 )
 {
  for(disp = 0.02; load > D; disp = disp + 0.02)
   {
    load = -183333.3*disp*0.8/Vf + load1 ;
    delta = delta1 + disp ;
    Ma = a*load/2.0 ;
    T = Ma/(dv*rh*b*d) /* Ma/Mu*60000*/ ;
    Du = 2*nbars*(0.5*fb*(0.37*gdow*db-c)*(0.37*gdow*db-c)
        + 0.45*fy*db*db*(1-T*T/(fy*fy))/gdow) ;
```

```
                D = 0.7*Du ;

fprintf(fpo,"%lf  %lf  %lf  %lf  %lf  %lf\n",
                    Du,Su,D,load,delta,gxy);

                }
                ed = -0.0051 ; /* to terminate loop */
                continue ;
                }


              delta1 = delta ;

    printf("total load %lf  gxy  %lf  %lf %lf\n",load,gxy,fb,c) ;

   }

 fclose(fpo);
}
```

Bibliography

[1] Webb, J., *High-Strength Concrete: Economics, Design and Ductility*, Concrete International, Jan. 1993 .

[2] Neville, A. and Aitchin, P.A., *High-Performance Concrete Demystified*, Concrete International, Jan. 1993 .

[3] Green, E.C., *Behavior of Fiber Reinforced Concrete*, M.S. Thesis, Department of Civil Engineering, Massachusetts Institute of Technology, 1989 .

[4] Sarker, S.L., *Performance of High Strength Field Concrete at 7 years*, Concrete International, Jan. 1993 .

[5] Park, R. and Paulay, T., *Reinforced Concrete Structures*, John Wiley & Sons Inc., 1975 .

[6] Kani, G.N.J., *Basic Facts Concerning Shear Failure*, ACI Journal, Vol. 63, No. 6, June 1966, pp. 675-691 .

[7] Mindess, S. and Bentur, A., *Fibre Reinforced Cementitious Composites*, Elsevier Applied Sciences, London, 1990 .

[8] Valle, M.O., *Shear Transfer in Fiber Reinforced Concrete*, M.S. Thesis, Department of Civil Engineering, Massachusetts Institute of Technology, 1991 .

[9] Swamy, R.N. and Bahia, H.M., *The Effectiveness of Steel Fibers as Shear Reinforcement*, Concrete International : Design and Construction, Vol. 7, 1985, pp. 35-40 .

[10] Swamy, R.N., Jones, R. and Chiam, T., *Shear Transfer in Steel Fiber Reinforcde Concrete*, Fiber Reinforced Concrete - Properties and Applications, ACI SP 105-29, Detroit, 1987, pp. 565-592 .

[11] Narayanan, R. and Darwish, I.Y.S., *Use of Steel Fibers as Shear Reinforcement*, ACI Structural Journal, Vol. 84, No. 3, March 1983, pp. 216-227 .

[12] Ward, R., Li, C. and Hamza, A.M., *Steel and Synthetic Fibers as Shear Reinforcement*, ACI Materials Journal, Vol. 5, Sept.-Oct. 1992, pp. 499-509 .

[13] Sharma, A.K., *Shear Strength of Steel Fiber Reinforced Concrete Beams*, ACI Journal, Vol. 83, 1986, pp. 624-628 .

[14] Batson, G.B., *Use of Steel Fibers for Shear Reinforcement and Ductility*, Steel Fiber Concrete U.S.-Sweden joint seminar, Stockholm, 1985, pp. 377-383 .

[15] Swamy, R.N. and Bahia, H.M., *Influence of Fiber Reinforcement on the Dowel Resistance to Shear*, ACI Journal, Proceedings, Vol. 76, No. 2, Feb. 1979, pp. 327-355 .

[16] Ezeldin, A.S. and Balaguru, P.N., *Bond Behavior of Normal and High Strength Fiber Reinforced Concrete*, ACI Materials Journal, Vol. 86, No. 5, pp. 515-524 .

[17] ACI Committee 544, *Design Considerations for Steel Fiber Reinforced Concrete*, ACI 544.5R, ACI Structural Journal, 1988, pp. 563-580 .

[18] ACI Committee 363, *Research Needs for High Strength Concrete*, ACI Materials Journal, Vol. 84, No. 6, Nov.-Dec. 1987 .

[19] Naaman, A.E. and Homrich, J.R., *Properties of High-Strength Fiber reinforced Concrete*, High Strength Concrete, ACI SP-87, 1985, pp. 110-146 .

[20] Wafa, F.F. and Ashour, S., *Mechanical Properties of High Strength Fiber Reinforced Concrete*, ACI Materials Journal, Vol. 5, 1992, pp. 449-456 .

[21] Ahmad, S.H., Khaloo, A.R. and Poveda, A., *Shear Capacity of Reinforced High-Strength Concrete Beams*, ACI JOurnal, Vol. 83, 1986, pp. 297-305 .

[22] Elzanaty, E.H., Nilson, A.H. and Slate, F.O., *Shear Capacity of Reinforced Concrete Beams using High Strength Concrete*, ACI Journal, Vol. 86, No. 3, March-April 1986 .

[23] Ashour, S., Hasanain, G.S. and Wafa, F.F., *Shear Behavior of High Strength Fiber Reinforced Concrete Beams*, ACI Structural Journal, Vol. 89, No. 2, March-April 1992, pp. 176-184 .

[24] Shahbazker, A., *Shear Behavior of Fiber Reinforced High Strength Concrete Beams*, M.S. Thesis, Department of Civil and Environmental Engineering, Massachusetts Institute of Technology, 1993 .

[25] Bazant, Z. and Kim, J., *Size effect in Shear Failure of Longitudinally Reinforced Beams*, ACI Journal, Title no. 81-38, Sept.-Oct. 1984, pp. 456-468 .

[26] Bazant, Z. and Sun, H.H., *Size Effect in Diagonal Shear Failure: Influence of Aggregate Size and Stirrups*, ACI Materials Journal, Title no. 84-M27, July-Aug. 1987, pp. 259-272 .

[27] Hsu, T.T.C., and Mau, S.T., *Shear Strength Prediction for Deep Beams with Web Reinforcement*, ACI Structural Journal, Title no. 84-S53, Nov.-Dec. 1987, pp. 513-523 .

[28] Tan, K.H. and Mansur, M.A., *Shear Transfer in Reinforced Fiber Concrete*, ASCE Journal of Materials in Civ. Eng., Vol. 2, No. 4, Nov. 1990, pp. 202-214 .

[29] Hsu, T.T.C, Mau, S.T. and Chen, C., *Theory of Shear Transfer Strength of Reinforced Concrete*, ACI Structural Journal, Title no. 84-S16, March-April 1987, pp. 149-160 .

[30] Mansur, M.A. and Ong, K.C.G., *Behavior of Reinforced Fiber Concrete Deep Beams in Shear*, ACI Structural Journal, Title no. 88-S13, Jan.-Feb. 1991, pp. 98-105 .

[31] Vecchio, F.J. and Collins, M.P., *Modified Compression Field Theory for Reinforced Concrete in Pure Shear*, ACI Journal, Proceedings Vol. 85, No. 3, March-April 1986, pp. 219-231 .

[32] Vecchio, F.J. and Collins, M.P., *Predicting the Response of Reinforced Concrete Beams Sublected to Shear, Using the Modified Com,pression Field Theory*, ACI Structural Journal, Vol. 85, No. 3, May-June 1988, pp. 258-268 .

[33] Soroushian, P., Obaseki, K., Rojas, M.C. and Sim, J., *Analysis of Dowel Bars Acting Against Concrete Core*, ACI Journal, Title no. 83-59, July-August 1986, pp. 642-649 .

[34] Henager, C.H. and Doherty, T.J., *Analysis of Reinforced Fibrous Concrete Beams*, ASCE, Journal of the Structural Division, Proceedings, Vol. 102, No. ST1, Jan. 1976 .

[35] ACI Committee 363, *State-of-the-Art Report on High-Strength Concrete*, Title no. 81-34, ACI 363R-84, July-August 1984, pp. 364-410 .

[36] ACI, *Building Code Requirements for Reinforced Concrete and Commentary*, ACI 318-89, pp. 156-165 .

[37] ACI Committee 544, *Guide for Specifying, Proportioning, Mixing, Placing and Finishing Steel Fiber Reinforced Concrete*, ACI Materials Journal, Vol. 90, No. 1, 1992, pp. 94-102 .

[38] Ashour, S.A. and Wafa, F.F., *Flexural Behavior of High-Strength Fiber Reinforced Concrete Beams*, ACI Structural Journal, Vol. 90, Title no. 90-s29, May-June 1993, pp. 279-287 .

[39] Bazant, Z.P., Gettu, R. and Kerr, M.E., *Fracture Properties and Brittleness of Hish-Strength Concrete*, ACI Materials Journal, Vol. 88, Title no. 87-m66, Nov.-Dec. 1990, pp. 608-618 .

[40] Valle, M. and Buyukozturk, O., *Behavior of Fiber reinforced High Strength Concrete under Direct Shear*, ACI Materials Journal, Vol. 90, Title no. 90-m13, March-April 1993, pp. 122-133 .